

INTENSITY AND SPECTRUM OF LIGHT
SCATTERED FROM A FLUID NEAR
ITS CRITICAL POINT

by

GILBERT T. FEKE

B.S., John Carroll University

1967

M.S., John Carroll University

1969

SUBMITTED IN PARTIAL FULFILLMENT

OF THE REQUIREMENTS FOR THE

DEGREE OF DOCTOR OF

PHILOSOPHY

at the

MASSACHUSETTS INSTITUTE OF

TECHNOLOGY

January, 1974

Signature of Author

Department of Physics, January 16, 1974

Certified by.....
Thesis Supervisor

Accepted by.....
Chairman, Department Committee on
Graduate Students

Archives



INTENSITY AND SPECTRUM OF LIGHT SCATTERED
FROM A FLUID NEAR ITS CRITICAL POINT

by

GILBERT T. FEKE

Submitted to the Department of Physics on January 16, 1974 in partial fulfillment of the requirements for the degree of Doctor of Philosophy.

Abstract

This thesis reports measurements of the intensity and spectrum of light scattered from sulfur hexafluoride, SF_6 , near its liquid-vapor critical point. These measurements were carried out along the critical isochore over the temperature range $0.048^\circ\text{K} < (T - T_C) < 2.4^\circ\text{K}$, and along the coexistence curve over the temperature range $0.021^\circ\text{K} < (T_C - T) < 1.027^\circ\text{K}$.

Using the techniques of optical mixing spectroscopy, measurements were made of the photocurrent power spectrum and the photocurrent correlation function arising from the light scattered quasielastically from thermally excited entropy fluctuations in SF_6 . These measurements are analyzed in order to determine the magnitude and temperature dependence of the critical part of the thermal diffusivity, D_C . The results are discussed in terms of the Kadanoff-Swift-Kawasaki mode-mode coupling theory.

Measurements of the intensity of the scattered light are analyzed in order to determine the magnitude and temperature dependence of the isothermal compressibility, κ_T . It is found that along the critical isochore, $\kappa_T = 1.26 \times 10^{-9} (T/T_C - 1)^{-1.235 \pm 0.015} \text{ cm}^2/\text{dyne}$ and that along the liquid side of the coexistence curve, the reduced compressibility is given by $(\frac{\partial \rho}{\partial \mu})_T = 1.67 \times 10^{-10} (1 - T/T_C)^{-1.225 \pm 0.015} \text{ g}^2 \text{ erg}^{-1} \text{ cm}^{-3}$. These results are discussed in terms of the predictions of the scaling law equations of state.

Finally, from measurements of the pressure, accurate values have been obtained for the slope of the vapor pressure curve, $(\partial P/\partial T)_{\ell v}$, close to T_C and for the slope of the extension of the vapor pressure curve above T_C , $(\partial P/\partial T)_v$. These quantities play an important role in the analysis leading to the determination of D_C from the experimental data.

Thesis Supervisor: George B. Benedek

Title: Professor of Physics

Table of Contents

Chapter I	Introduction	11
Chapter II	Liquid-Vapor Critical Point Phenomena and the Use of Light Scattering to Measure Properties of the System	
	A. Introduction to Critical Point Phenomena	20
	B. Theoretical Predictions for the Behavior of the Static Properties of a Fluid near its Critical Point	27
	1. Relationship between the Magnitude of the Density Fluctuations and the Isothermal Compressibility	27
	2. Relationship between the Spatial Range of the Density Fluctuations and the Isothermal Compressibility	30
	3. Ornstein-Zernike Relation between the Isothermal Compressibility, κ_T , and the Long Range Correlation Length, ξ	33
	4. Explicit Predictions for the Behavior of the Static Properties of a Fluid near its Critical Point	37
	C. Derivation of the Einstein-Ornstein-Zernike Equation Relating the Intensity of Light Scattered from a Fluid near its Critical Point to κ_T and to ξ	45
	D. Relationship between the Time Dependence of the Light Scattered from a Fluid near its Critical Point and the Time Dependence of the Isobaric Entropy Fluctuations in the Fluid	56
	E. Theoretical Predictions for the Behavior of the Dynamic Properties of a Fluid near its Critical Point by Application of the Physical Ideas Embodied in the Mode-Mode Coupling Theory	66

		5
	1. The Basic Physical Idea of Fixman	66
	2. The First Quantitative Expression of the Mode-Mode Coupling Theory due to Kawasaki	67
	3. The Specific Predictions of Kadanoff and Swift for the Temperature Dependence of Transport Coefficients of a Fluid near its Critical Point	71
	4. Explicit Predictions for the Magnitude and Temperature Dependence of the Critical Part of the Thermal Diffusivity of a Fluid near its Critical Point	89
Chapter III	Experimental Apparatus and Methods	
	A. Introduction	100
	B. The Sample	100
	C. The Sample Chamber	101
	D. Control and Measurements of the Sample Temperature	105
	1. Temperature Control	105
	2. Temperature Measurement	110
	E. Measurement of the Sample Pressure	112
	F. Measurement of the Sample Density	113
	1. Optical Measurement of the Absolute Density	114
	2. Measurement of the Density Relative to ρ_C by Meniscus Height Observations	119
	3. The Question of Density Gradients	122

		6
G.	The Optical System	128
1.	Description of the Components	128
2.	Alignment of the Optics and the Determination of the Scattering Vector	132
H.	The Electronic Detection System	137
1.	Measurement of P_S/P_I	139
2.	Measurement of $S_i(\nu)$	141
3.	Measurement of $R_i(\tau)$	145
Chapter IV	Experimental Results, Analysis, and Discussion	
A.	Introduction	150
B.	The Critical Isochore	150
1.	Measurements of Pressure	151
2.	Measurements of κ_T	153
3.	Measurements of Γ/q^2	155
4.	Analysis of Γ/q^2 Measurements	161
5.	Discussion of the Results in Terms of the Mode-Mode Coupling Theory	166
C.	The Coexistence Curve	171
1.	Measurements of Pressure	171
2.	Measurements of $(\partial\rho/\partial\mu)_T$	173
3.	Measurements of Γ/q^2	179
4.	Analysis of Γ/q^2 Measurements	184
5.	Discussion of the Results in Terms of the Mode-Mode Coupling Theory	186

		7
Appendix A	3 Parameter Single Lorentzian Fitting Program	200
Appendix B	3 Parameter Single Exponential Decay Fitting Program	205
Biographical Note		207
Acknowledgments		208

List of Illustrations

<u>Figure Number</u>	<u>Title</u>	<u>Page</u>
2.1	Schematic P-T Phase Diagram	21
2.2	Schematic P- ρ Phase Diagram	23
2.3	Schematic ρ -T Phase Diagram	25
2.4a	Experimental Situation for Light Scattering	47
2.4b	Geometric Representation of the Scattering Process	47
3.1	Schematic Top View of the Sample Chamber	102
3.2	Schematic End View of the Sample Chamber	103
3.3	Schematic Diagram of the Temperature Control System	106
3.4	Temperature Control Feedback Circuit	108
3.5	Optical Measurement of the SF ₆ Refractive Index	115
3.6	Current Ratio Bridge Circuit	118
3.7	SF ₆ Density-Height Profile: $\rho = \rho_C, T \geq T_C$	125
3.8	The Optical System	129
3.9	Optical Alignment of the Sample Chamber	134
3.10	The Electronic Detection System	138
4.1	Isothermal Compressibility, κ_T , along the Critical Isochore	156
4.2	Experimental Thermal Diffusivity and Calculated Background Contribution to the Thermal Diffusivity along the Critical Isochore	159

List of Illustrations (continued)

<u>Figure Number</u>	<u>Title</u>	<u>Page</u>
4.3	Comparison of Experimental Thermal Diffusivities along the Critical Isochore	160
4.4	Background Thermal Conductivity for SF ₆	164
4.5	Deduced Critical Part of the Thermal Diffusivity and Comparison with the Mode-Mode Coupling Theory along the Critical Isochore	168
4.6	Reduced Compressibility, $(\partial\rho/\partial\mu)_T$, along the Liquid Side of the Coexistence Curve	178
4.7	Experimental Thermal Diffusivity and Calculated Background Contribution to the Thermal Diffusivity along the Coexistence Curve	183
4.8	Comparison of Measured Thermal Diffusivity with Predictions of the Mode-Mode Coupling Theory along the Liquid Side of the Coexistence Curve	190
4.9	Comparison of Measured Thermal Diffusivity with Predictions of the Mode-Mode Coupling Theory along the Vapor Side of the Coexistence Curve	191
4.10	Deduced Critical Part of the Thermal Diffusivity and Comparison with the Mode-Mode Coupling Theory along the Liquid Side of the Coexistence Curve	192
4.11	Deduced Critical Part of the Thermal Diffusivity and Comparison with the Mode-Mode Coupling Theory along the Vapor Side of the Coexistence Curve	193

List of Tables

<u>Table Number</u>	<u>Title</u>	<u>Page</u>
2.1	The Eigenvalue Matrix for Dissipative Phenomena near the Critical Point	78
4.1	Variation of Pressure with Temperature along the Critical Isochore	152
4.2	Isothermal Compressibility, κ_T , along the Critical Isochore	154
4.3	Γ/q^2 along the Critical Isochore	158
4.4	Experimental Thermal Diffusivity, Calculated Background Thermal Diffusivity, and Deduced Critical Part of the Thermal Diffusivity along the Critical Isochore	167
4.5	Variation of Pressure with Temperature along the Vapor Pressure Curve	172
4.6	Reduced Compressibility $(\partial\rho/\partial\mu)_T$, along the Liquid Side of the Coexistence Curve	176
4.7	Γ/q^2 along the Coexistence Curve	181
4.8	Experimental Thermal Diffusivity, Calculated Background Thermal Diffusivity, and Deduced Critical Part of the Thermal Diffusivity along the Coexistence Curve	187

Chapter I

INTRODUCTION

This thesis reports measurements of the intensity and spectrum of light scattered from sulfur hexafluoride near its liquid-vapor critical point. In this introduction we shall present the highlights of the historical development of the experimental and theoretical studies out of which grew the motivation for the study undertaken in this thesis.

The study of critical point phenomena began in 1869 when Andrews⁽¹⁾ experimentally discovered the existence of the critical point in carbon dioxide. Shortly afterward, Van der Waals⁽²⁾ published a theoretical description of the critical region of a liquid-gas system, based on his now famous equation of state, which to this day provides good qualitative predictions for the behavior of some of the properties of a fluid near its critical point.

In the course of his studies of the critical point behavior of CO_2 Andrews observed an anomalous increase in the scattering of light, the phenomenon now known as critical opalescence. Andrews explained this phenomenon qualitatively by arguing that the density inhomogeneities that cause light scattering increase tremendously as the critical point is approached.

The first quantitative treatment of light scattering was presented by Lord Rayleigh⁽³⁾ who solved the problem of light scattered by a gas of particles of sufficiently low density such that the interparticle spacing was larger than the wavelength of the light. He did not include the interactions between the particles of the gas in his calculations.

With his famous result that the time average intensity of the scattered light is inversely proportional to the fourth power of the incident radiation, he was able to explain a variety of basic phenomena, including the blue color of the sky. Rayleigh's theory failed, however, to account for the scattering from media whose particles interacted and whose interparticle separation is of the order of the wavelength of light. In particular, it could not account for critical opalescence.

Four decades later von Smoluchowski⁽⁴⁾ and Einstein⁽⁵⁾ presented a quantitative treatment of critical opalescence. In particular, Einstein was able to show that light which has been scattered through an angle θ has in fact been scattered by one particular spatial Fourier component of the density fluctuations, namely that component whose wavevector \underline{q} is related to the wavevectors of the scattered and incident light, \underline{k}_s and \underline{k}_0 by $\underline{q} = \underline{k}_s - \underline{k}_0$.

The Einstein-Smoluchowski theory of critical opalescence assumed that density fluctuations in neighboring volume elements are uncorrelated. This led to the prediction that the scattered light intensity is independent of angle and approaches infinity as the critical point is approached. Later, Ornstein and Zernike⁽⁶⁾ considered the effect of correlations between neighboring volume elements. They predicted that the scattered intensity exhibits an angular dependence and that the intensity approaches a finite value (except for forward scattering) as the critical point is approached. Aside from minor modifications, the Ornstein-Zernike theory still stands as the means by which measurements of the time average intensity of the scattered light are related to the behavior of the time-independent properties of a fluid near its critical point.

Since the Ornstein-Zernike theory was concerned only with the mean squared amplitude and the spatial extent of the density fluctuations, it could not predict the spectral distribution of the light scattered by the medium which depends upon the manner in which the density fluctuations evolve in time. Debye⁽⁷⁾ argued that the thermal content of a fluid could be considered to consist of adiabatically propagating pressure fluctuations; that is, sound waves. Brillouin⁽⁸⁾ and, independently, Mandel'shtam⁽⁹⁾ realized that the frequency of the light scattered from these fluctuations should differ from that of the incident light by an amount equal to the frequency of a sound wave whose wave vector is equal to the difference in wave vectors of the incident and scattered light.

The first experimental observation of the Brillouin-Mandel'shtam doublet was made by Gross⁽¹⁰⁾ who was able to resolve the doublet lines at $\theta = 90^\circ$ in seven liquids and show that the results agreed with the predicted splittings.

Gross also found that, in addition to the doublet, there was light scattered without a noticeable frequency shift in all seven liquids. This central, unshifted line was explained soon afterward by Landau and Placzek⁽¹¹⁾ who proposed that the density fluctuations producing the scattering can be described in terms of adiabatic pressure fluctuations and isobaric entropy fluctuations. The pressure fluctuations propagate giving rise to the Brillouin-Mandel'shtam doublet; the entropy fluctuations, however, obey the heat flow equation and decay away by diffusion thus giving rise to the unshifted, central component. According to Landau and Placzek the central component of the scattered light

should be a Lorentzian whose half-width at half maximum, Γ , is given by $\Gamma = Dq^2$ where q is the scattering vector and D is the thermal diffusivity; $D = \Lambda/\rho C_p$, where Λ is the thermal conductivity of the scattering medium, ρ is the density, and C_p is the specific heat per unit mass at constant pressure.

The experimental situation regarding measurements of the spectrum of light scattered from fluids remained essentially stagnant until 1964 when the dual problem of the lack of intense monochromatic light sources and the lack of sufficiently high resolution spectrometers was overcome with the availability of helium-neon lasers which could be used in conjunction with the technique of optical mixing spectroscopy.

The first measurements of the central component of the light scattered by a pure fluid near its liquid-vapor critical point were obtained by Ford and Benedek⁽¹²⁾ in 1965. They were able to determine the thermal diffusivity for several temperatures along the critical isochore of SF_6 and interpreted their results in terms of the Landau-Placzek theory. Shortly afterward, an extensive systematic study of the behavior of the width of the central component of the light scattered from SF_6 at a number of temperatures above T_C along the critical isochore and along six near-critical isochores, and at temperatures below T_C along the gas and liquid sides of the coexistence curve, was undertaken by Saxman and Benedek. They found⁽¹³⁾ a marked asymmetry in the temperature dependence of the thermal diffusivity above and below T_C . In particular, their results seemed to indicate that while the thermal conductivity diverged as $T \rightarrow T_C$ from below, Λ did not diverge as $T \rightarrow T_C$ from above. Their results were unusual and puzzling.

Shortly afterward, Swinney and Cummins⁽¹⁴⁾ obtained measurements of the thermal diffusivity of CO_2 along the critical isochore and along the coexistence curve. Their results indicated that the thermal conductivity diverges with approximately the same temperature dependence above and below T_C .

Motivated by the fundamental differences between the results obtained for SF_6 and those obtained for CO_2 , Lastovka and Benedek initiated an ambitious study whose goal was not only to re-measure the thermal diffusivity of SF_6 along various paths in the region of the critical point, but also to measure the behavior of the isothermal compressibility as deduced from measurements of the intensity of the scattered light. These measurements were to be supplemented with direct measurements of the density and the pressure as a function of temperature in the critical region. The initial results of this study, in which the author participated, have been reported.⁽¹⁵⁾

As the experimental investigations of the behavior of the thermal diffusivity of pure fluids in the critical region intensified, dramatic progress was made as well in a number of theoretical studies. Following a concept introduced by Fixman,⁽¹⁶⁾ Kadanoff and Swift⁽¹⁷⁾ developed what has become known as the mode-mode coupling theory. Their's is a general dynamical theory, not restricted to regions where hydrodynamics applies, which predicts the temperature dependences of the critical points of the transport coefficients of a pure fluid near its critical point. Their more general theory supplants the Landau-Placzek expression for the decay rate of entropy fluctuations which retains its validity only

when hydrodynamics applies. Subsequently, Kawasaki^{(18),(19)} extended the mode-mode coupling concept and derived a general expression which provides an explicit prediction for the magnitude and temperature dependence of the critical part of the thermal diffusivity of a fluid near its critical point. The theory has been further extended by Kawasaki and Lo⁽²⁰⁾ with the resulting prediction that in the hydrodynamic region (defined as the case when $q^2 \xi^2 \ll 1$, where ξ is the spatial range over which density fluctuations are correlated) the critical part of the thermal diffusivity is given by $(\frac{\Lambda}{\rho C_p})_C = \frac{k_B T}{6\pi\eta\xi}$ (1.055), where k_B is Boltzmann's constant and η is the shear viscosity.

This result may be interpreted physically if one considers that the diffusion of heat takes place by the spatial diffusion of regions of size ξ . If this is the case, then from the Stokes-Einstein relation it is known that the diffusion constant of spheres of radius ξ is given by $D = k_B T / 6\pi\eta\xi$.

It was in the wake of these theoretical advances and as an outgrowth of the experimental study initiated by Lastovka and Benedek that the work described in this thesis originated. The results described in this thesis have been previously reported.^{(21),(22)} These results together with the study of Lim et al.⁽²³⁾ have satisfactorily resolved the experimental question regarding the behavior of SF_6 near its critical point. Excellent agreement is obtained between the results of the experiments and the predictions of the mode-mode coupling theories along the critical isochore where independent data exist allowing proper analysis. Independent measurements of the correlation range, ξ , and

the shear viscosity, η , are required along the gas and liquid sides of the SF₆ coexistence curve before accurate comparisons between the experimental results and the predictions of the theory can be made.

References For Chapter I

1. T. Andrews, Phil. Trans. R. Soc. 159, 575 (1869).
2. J. D. Van der Waals, Ph. D. Thesis, University of Leiden, (1873).
3. Lord Rayleigh, Phil. Mag., 41, 107, 274, 447 (1871).
4. M. von Smoluchowski, Ann. Physik 25, 205 (1908).
5. A. Einstein, Ann. Physik 33, 1275 (1910).
6. L. S. Ornstein and F. Zernike, Proc. Acad. Sci. Amsterdam 17, 793 (1914); Physik Z. 19, 134 (1918).
7. P. J. W. Debye, Annln. Phys. 39, 789 (1912).
8. L. Brillouin, Ann. de Physique 17, 88 (1922).
9. L. I. Mandel'shtam, Zhurnal Russkogo Fiziko Khimicheskogo Obshchestva 58, 381 (1926).
10. E. F. Gross, Nature 126, 201, 400, 603 (1930).
11. L. Landau and G. Placzek, Physik Z. Sowjetunion 5, 172 (1934).
12. N. C. Ford, Jr. and G. B. Benedek, Phys. Rev. Lett. 15, 649 (1965).
13. G. B. Benedek, in Statistical Physics, Phase Transitions and Superfluidity, edited by M. Chretien et al. (Gordon and Breach, New York, 1968) Vol. 2, p. 1.
14. H. L. Swinney and H. Z. Cummins, Phys. Rev. 171, 152 (1968).
15. G. B. Benedek, J. B. Lastovka, M. Giglio, and D. Cannell, in Critical Phenomena, edited by R. E. Mills and R. I. Jaffee (McGraw-Hill, New York, 1971).
16. M. Fixman, J. Chem. Phys. 36, 310 (1962).
17. L. P. Kadanoff and J. Swift, Phys. Rev. 166, 89 (1968).
18. K. Kawasaki, Ann. Phys. 61, 1 (1970).
19. K. Kawasaki, Phys. Rev. A 1, 1750 (1970).

20. K. Kawasaki and S. Lo, Phys. Rev. Lett. 29, 48 (1972).
21. G. T. Feke, G. A. Hawkins, J. B. Lastovka, and G. B. Benedek, Phys. Rev. Lett. 27, 1780 (1971).
22. G. T. Feke, J. B. Lastovka, G. B. Benedek, K. H. Langley, and P. B. Elterman, Opt. Commun. 7, 13 (1973).
23. T. K. Lim, H. L. Swinney, K. H. Langley, and T. A. Kachnowski, Phys. Rev. Lett. 27, 1776 (1971).

Chapter II

LIQUID-VAPOR CRITICAL POINT PHENOMENA AND THE
USE OF LIGHT SCATTERING TO MEASURE
PROPERTIES OF THE SYSTEMA. Introduction to Critical Point Phenomena

We may begin our discussion of liquid-vapor critical point phenomena by identifying the critical point and the surrounding critical region in terms of elementary phase diagrams. We begin by recalling that every pure substance can be described by an equation of state which is a functional relationship of the form $f(P, \rho, T) = 0$. The equation of state defines a surface in a three-dimensional space whose coordinates are the pressure, P , the density, ρ , and the temperature, T , of the system. Each of the points on the surface corresponds to an equilibrium state of the system. In order to visualize the $P\rho T$ surface it is useful to consider its projections upon the PT , $P\rho$, and ρT planes. In Figure 2.1 we show a schematic PT phase diagram. From this diagram we see that the liquid and vapor phases coexist in equilibrium at pressures and temperatures which define the vapor pressure curve. The critical point is seen to be the end point of the vapor pressure curve. At temperatures greater than T_C there is no longer any distinction between the gaseous and liquid phases of the substance. In this region it is possible for the substance to exist in only one phase. At temperatures less than T_C compressing a gas sufficiently results in the formation of dropets of condensed liquid in the sample and so one has a physical separation into two phases. At temperatures greater than T_C the gas may be compressed without limit and yet there will be no physical separation of the substance into phases.

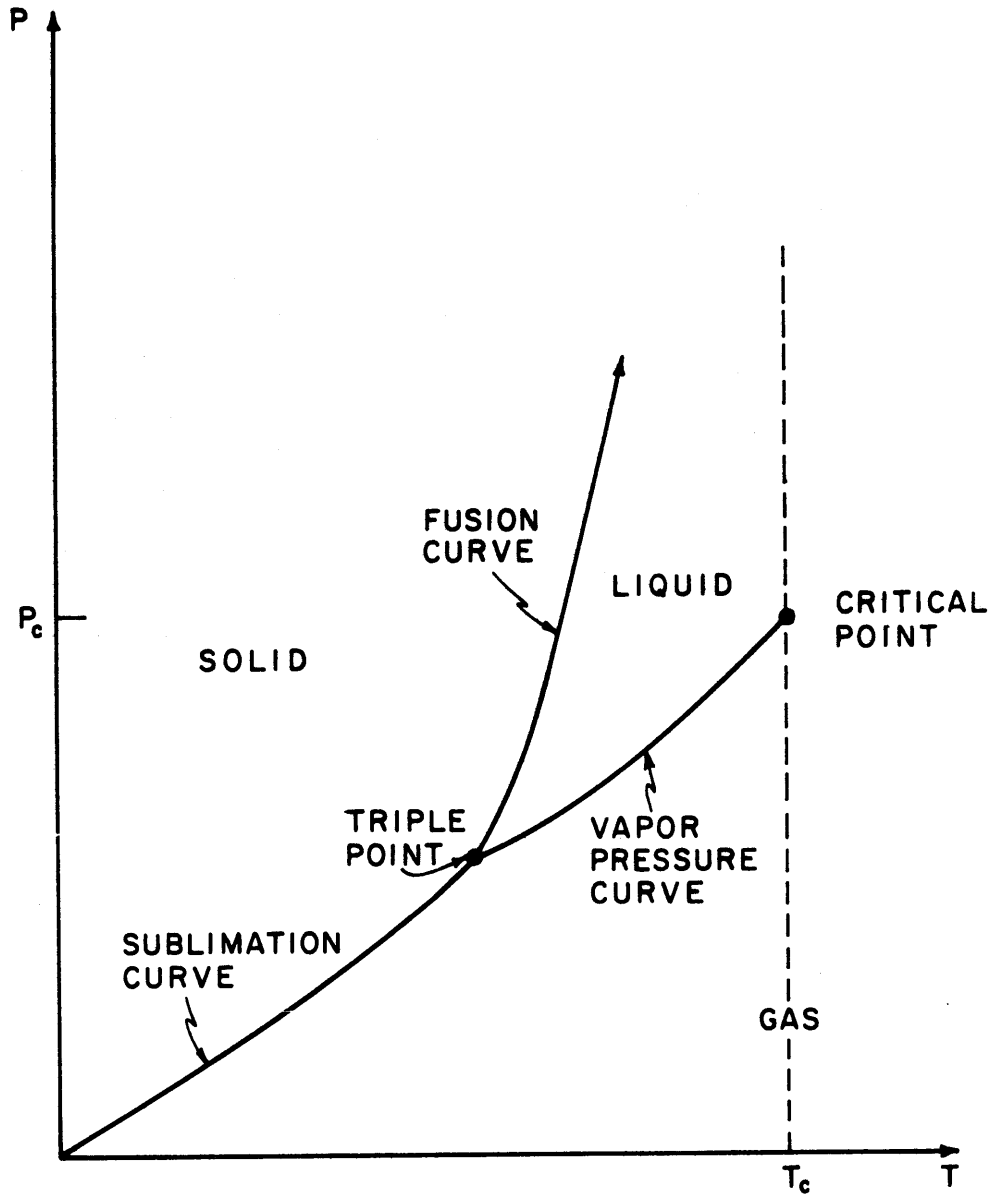
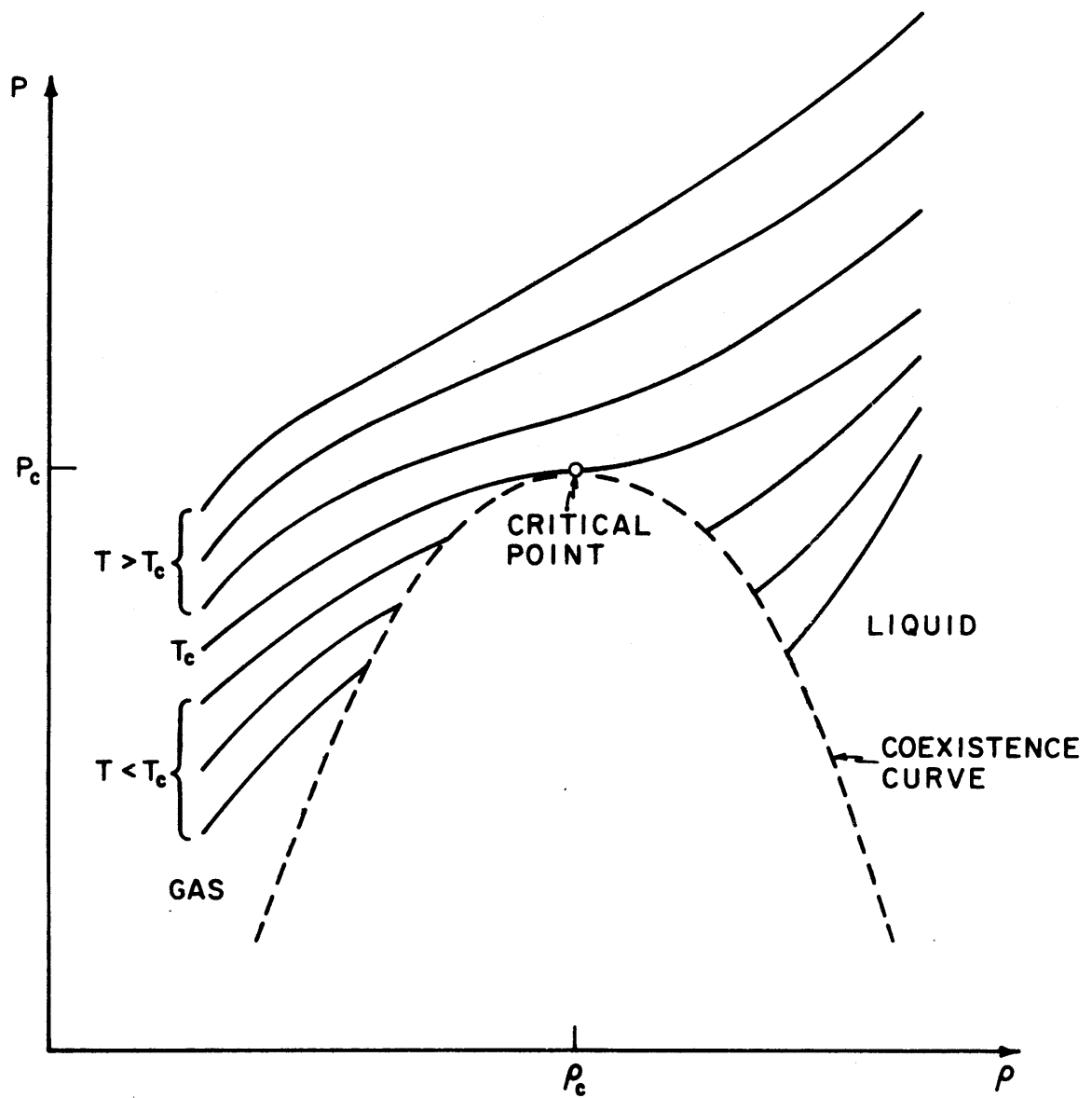


Fig. 2.1 Schematic P-T Phase Diagram

The critical temperature itself is seen to be the line of demarcation between the one phase and two phase states of the substance. It is to investigate the behavior of the physical properties of a substance when it is brought arbitrarily close to the critical temperature on an approach from the one phase region and on an approach from the two phase region that constitutes the motivation for studies of critical phenomena.

In Figure 2.2 we show a schematic $P\rho$ phase diagram on which are drawn supercritical and subcritical isotherms as well as the critical isotherm, T_C . We may consider an isothermal compression of a gaseous sample held at $T < T_C$ and beginning at low density. We will assume that the sample is held in a chamber at fixed volume and that the pressure is increased by introducing gas into the chamber. As gas is introduced both the pressure and the density of the sample increase until the density corresponding to the gas side of the coexistence curve is reached. As additional gas is introduced the pressure no longer increases. Instead, droplets of liquid at a density corresponding to the liquid side of the coexistence curve begin to condense in the chamber. As additional gas is introduced the pressure remains constant as the liquid volume (all at the liquid coexistence curve density) increases and the gas volume (all at the gas coexistence curve density) decreases. Finally, liquid fills the entire chamber and the average density of the sample is just the liquid coexistence curve density. As additional gas is introduced the pressure again increases and the liquid density also increases.

When the same procedure is carried out on a gaseous sample held at $T > T_C$, what is observed, as gas is continually added to the chamber, is

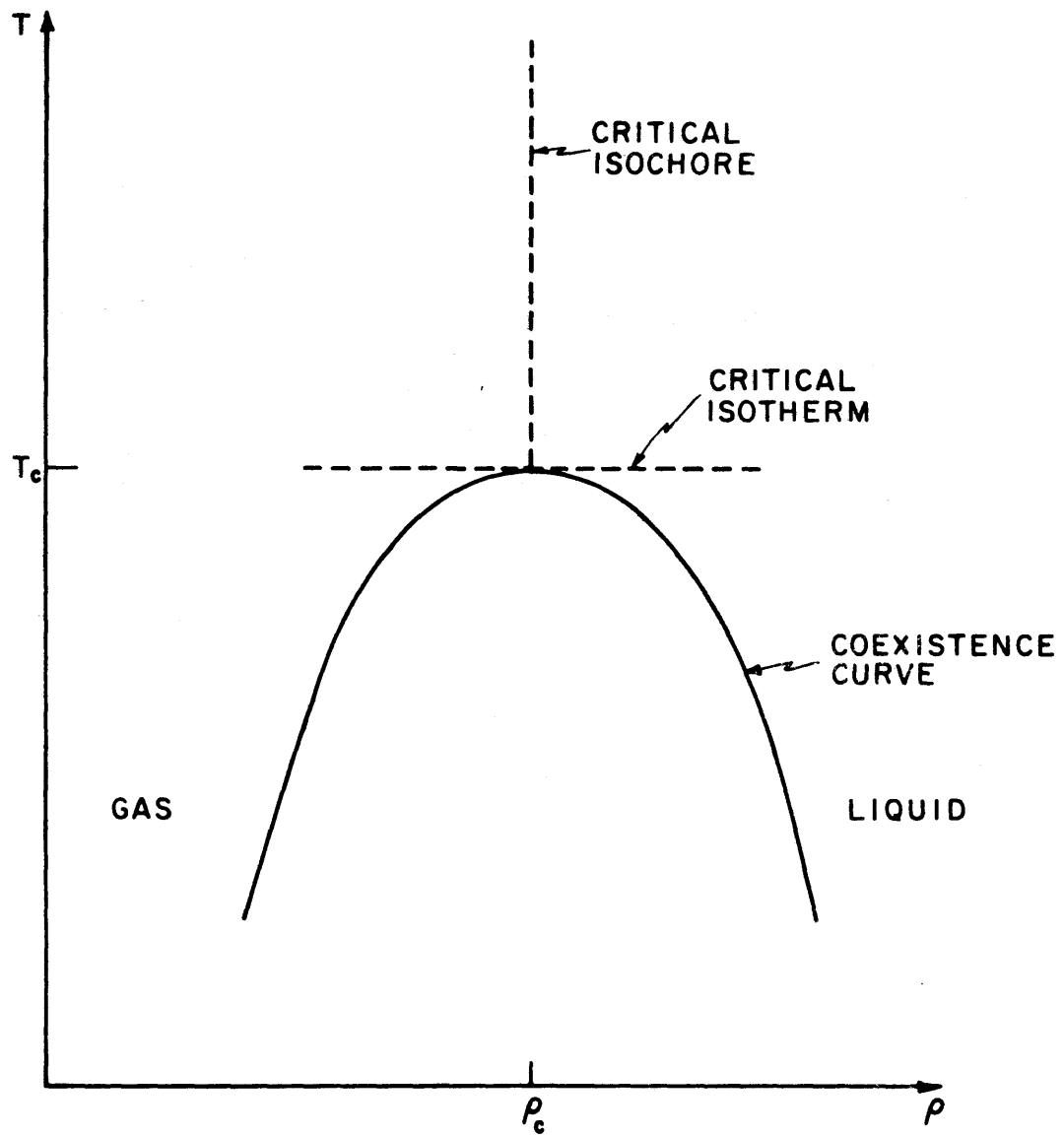
Fig. 2.2 Schematic P- ρ Phase Diagram

a continuous increase in the sample pressure as the sample density continuously increases from gas-like to liquid-like densities.

We next consider what occurs when the same procedure is carried out on a sample held very close to T_C . If the temperature is slightly below T_C phase separation will occur when the gas coexistence curve density is reached. However, the density of the condensed liquid will be nearly equal to the gas density. We see then that as the critical point is approached from below T_C , the difference between the liquid and gas densities approaches zero.

We now consider the case where the sample is held at a temperature slightly above T_C . As gas is added to the chamber the pressure rises as the density increases. As the critical density ρ_C is approached, however, increases in the sample density result in continually smaller increases in the sample pressure. At ρ_C the isotherms for $T > T_C$ but approaching T_C become increasingly "flatter". As seen from Figure 2.2, the critical isotherm exhibits zero slope at critical density. What is implied physically is that changing the sample density produces a negligible change in the sample pressure. Conversely, a small change in the sample pressure produces a very large change in the sample density. The fluid becomes extremely compressible in the critical region and since $(\frac{\partial P}{\partial \rho})$ is zero at the critical point, the isothermal compressibility, $\frac{1}{\rho}(\frac{\partial \rho}{\partial P})_T$, diverges to infinity as the critical point is approached.

In Figure 2.3 we show a schematic ρT phase diagram for the critical region. This diagram may be considered as a map of the principal paths of approach to the critical point. Theories predicting the behavior of the

Fig. 2.3 Schematic p - T Phase Diagram

physical properties of a fluid in the critical region are concerned with the behavior of the property in question as a function of the temperature and density of the fluid as the critical point is approached. The most direct means of checking the validity of the theories is to experimentally measure the property in question as a function of the temperature along the critical isochore, as a function of the temperature along the gas and liquid sides of the coexistence curve, or as a function of the density along the critical isotherm.

Thus far from an examination of phase diagrams we have seen that the two essential features of a fluid near its critical point are (a) that the difference between liquid and gas densities approaches zero as the critical point is approached and (b) that the isothermal compressibility diverges to infinity as the critical point is approached. A phenomenon related to the diverging isothermal compressibility is that near the critical point the random thermal density fluctuations in a fluid become large both in amplitude and in spatial extent.

We can qualitatively understand that the diverging isothermal compressibility is related to large density fluctuations by noting that an infinite value of $(\frac{\partial \rho}{\partial P})_T$ implies that the response of the density to a small pressure fluctuation is infinite. The existence of large density fluctuations is responsible for the phenomenon of critical opalescence.

As the critical point of a fluid is approached along the critical isochore microscopic regions of higher and lower density randomly appear and decay throughout the volume of the fluid. The process may be thought of as the formation and decay of molecular clusters or as the formation and decay of microscopic liquid droplets. As the temperature is continually

lowered toward T_C the density fluctuations become greater in amplitude and in spatial extent. Near T_C the regions of correlated density fluctuations acquire dimensions on the order of the wavelength of light so that a beam of light directed toward the fluid is scattered very strongly resulting in the opacity of the fluid.

We may conclude our brief introduction by remarking that it is the static and dynamic behavior of the density fluctuations in a fluid near its critical point that determine, on the microscopic level, the behavior of the macroscopically measured properties of a fluid near its critical point.

B. Theoretical Predictions for the Behavior of the Static Properties of a Fluid near its Critical Point

1. Relationship between the Magnitude of the Density Fluctuations and the Isothermal Compressibility

We begin our discussion of the theoretical predictions for the behavior of the static properties of a fluid near its critical point by presenting quantitatively the relation between density fluctuations and the isothermal compressibility. From statistical mechanics⁽¹⁾ the probability p of fluctuations in the thermodynamic quantities of a system away from their mean values is proportional to $e^{-W_{\min}/k_B T}$ where W_{\min} is the minimum work required to carry out reversibly the given changes in the fluctuating quantities, k_B is Boltzmann's constant, and T is the

equilibrium temperature. The value of the minimum work is given by the expression

$$W_{\min} = \Delta E - T\Delta S + P\Delta V, \quad (2.1)$$

where ΔE , ΔS and ΔV are the changes in the energy, entropy, and volume and P is the equilibrium pressure. Expanding ΔE in a Taylor series, we obtain to second order that

$$\Delta E = \left(\frac{\partial E}{\partial S}\right)_V \Delta S + \left(\frac{\partial E}{\partial V}\right)_S \Delta V + \frac{1}{2} \left(\frac{\partial^2 E}{\partial S^2}\right) (\Delta S)^2 + 2 \frac{\partial^2 E}{\partial S \partial V} \Delta S \Delta V + \frac{\partial^2 E}{\partial V^2} (\Delta V)^2. \quad (2.2)$$

But $\left(\frac{\partial E}{\partial S}\right)_V = T$ and $\left(\frac{\partial E}{\partial V}\right)_S = -P$ so that

$$\Delta E - T\Delta S + P\Delta V = \frac{1}{2} \left[\frac{\partial^2 E}{\partial S^2} (\Delta S)^2 + 2 \frac{\partial^2 E}{\partial S \partial V} \Delta S \Delta V + \frac{\partial^2 E}{\partial V^2} (\Delta V)^2 \right]. \quad (2.3)$$

It can be shown⁽²⁾ that $\Delta T\Delta S = \left(\frac{\partial^2 E}{\partial S^2}\right)_V (\Delta S)^2 + \left(\frac{\partial^2 E}{\partial S \partial V}\right) \Delta V \Delta S$ and that

$$-\Delta P\Delta V = \frac{\partial^2 E}{\partial V^2} (\Delta V)^2 + \left(\frac{\partial^2 E}{\partial S \partial V}\right) \Delta S \Delta V. \quad \text{So that}$$

$$W_{\min} = \frac{1}{2} (\Delta T\Delta S - \Delta P\Delta V). \quad (2.4)$$

We thus obtain for the probability of fluctuations that

$$p \propto e^{-(\Delta T\Delta S - \Delta P\Delta V)/2k_B T} \quad (2.5)$$

We may now calculate the probability of fluctuations in each of the variables. Taking V and T as the independent variables we have

$$\Delta P = \left(\frac{\partial P}{\partial T}\right)_V \Delta T + \left(\frac{\partial P}{\partial V}\right)_T \Delta V \quad \text{and}$$

$$\Delta S = \left(\frac{\partial S}{\partial T}\right)_V \Delta T + \left(\frac{\partial S}{\partial V}\right)_T \Delta V$$

so that

$$\begin{aligned} \Delta T \Delta S - \Delta P \Delta V &= \left(\frac{\partial S}{\partial T}\right)_V (\Delta T)^2 - \left(\frac{\partial P}{\partial V}\right)_T (\Delta V)^2 \\ &+ \left(\left(\frac{\partial S}{\partial V}\right)_T - \left(\frac{\partial P}{\partial T}\right)_V\right) \Delta V \Delta T \end{aligned} \quad (2.6)$$

But $\left(\frac{\partial S}{\partial V}\right)_T = \left(\frac{\partial P}{\partial T}\right)_V$ so the cross term vanishes. Thus ΔV and ΔT are statistically independent fluctuations. The probability distribution for temperature and volume fluctuations becomes

$$p(\Delta V, \Delta T) \propto e^{-\left[\left(\frac{\partial P}{\partial V}\right)_T (\Delta V)^2 - \left(\frac{\partial S}{\partial T}\right)_V (\Delta T)^2\right] / 2k_B T} \quad (2.7)$$

The distribution is Gaussian so that the mean square fluctuation in the volume becomes:

$$\langle (\Delta V)^2 \rangle = -k_B T \left(\frac{\partial V}{\partial P}\right)_T \quad (2.8)$$

This relation determines the mean square fluctuation in the volume of a part of a system containing a fixed number of particles, N . In order to obtain the mean square fluctuation in the number of particles in a fixed volume within a system we first divide both sides of the equation by N^2 to find the mean square fluctuation in the volume per particle:

$$\langle \left(\Delta \frac{V}{N}\right)^2 \rangle = \frac{-k_B T}{N^2} \left(\frac{\partial V}{\partial P}\right)_T \quad (2.9)$$

We can write $\Delta \frac{V}{N} = V \Delta \frac{1}{N} = -\frac{V}{N^2} \Delta N$. Substituting, we find

$$\langle (\Delta N)^2 \rangle = \frac{-k_B T N^2}{V^2} \left(\frac{\partial V}{\partial P}\right)_T \quad (2.10)$$

We can now explicitly relate the mean square fluctuation in density to the isothermal compressibility, κ_T . Recalling that $\kappa_T = -\frac{1}{V} \left(\frac{\partial V}{\partial P}\right)_T$ and

letting $n = \frac{N}{V}$ we have

$$\langle (\Delta N)^2 \rangle = k_B T n N \kappa_T \quad (2.11)$$

Recalling that the compressibility of an ideal gas, κ_T , is given by

$\kappa_T = \frac{1}{n k_B T}$ we obtain

$$\frac{\kappa_T}{\kappa_I} = \frac{\langle (\Delta N)^2 \rangle}{N} \quad (2.12)$$

or, more explicitly,

$$\frac{\kappa_T}{\kappa_I} = \frac{\langle (N - \langle N \rangle)^2 \rangle}{\langle N \rangle}, \quad (2.13)$$

where $\langle N \rangle$ is the mean value of the number of particles and $N - \langle N \rangle$ is the fluctuation away from the mean value. We see then that the divergence of the isothermal compressibility is directly related to the large amplitude density fluctuations that occur near the critical point of a fluid.

Also we see that while the fluctuations in N are Poissonian far from T_C , they become much larger than Poissonian as $T \rightarrow T_C$.

2. Relationship between the Spatial Range of the Density Fluctuations and the Isothermal Compressibility

We have remarked earlier that the spatial extent of regions of correlated density fluctuations as well as the amplitude of the fluctuations become large near the critical point of a fluid. We will now proceed to relate the spatial range of density fluctuations to the isothermal compressibility of the fluid. We begin by introducing the function ⁽³⁾

$$G(\underline{r}, \underline{r}') \equiv \langle [n(\underline{r}) - \langle n(\underline{r}) \rangle][n(\underline{r}') - \langle n(\underline{r}') \rangle] \rangle \quad (2.14)$$

In this expression $n(\underline{r})$ is the particle density given by

$$n(\underline{r}) \equiv \sum_{i=1}^N \delta(\underline{r} - \underline{r}_i) \quad (2.15)$$

where \underline{r}_i is the spatial coordinate of the i^{th} particle. Also, $\langle n(\underline{r}) \rangle$ is the average particle density given by

$$\langle n(\underline{r}) \rangle = \langle \frac{N}{V} \rangle \equiv n \quad (2.16)$$

We see then that $G(\underline{r}, \underline{r}')$ is a measure of the correlation of fluctuations in the density away from the average value.

We may expand Eq. (2.14) to obtain

$$\begin{aligned} G(\underline{r}, \underline{r}') &= \langle n(\underline{r})n(\underline{r}') \rangle - \langle n(\underline{r}) \rangle \langle n(\underline{r}') \rangle \\ &= \langle \langle n(\underline{r}) \rangle n(\underline{r}') \rangle + \langle \langle n(\underline{r}) \rangle \times n(\underline{r}') \rangle \end{aligned} \quad (2.17)$$

We note, however, that $\langle n(\underline{r}) \rangle = \langle n(\underline{r}') \rangle = n$ so that

$$G(\underline{r}, \underline{r}') = \langle n(\underline{r})n(\underline{r}') \rangle - n^2 \quad (2.18)$$

We may also assume that our system is spatially uniform so that $G(\underline{r}, \underline{r}') = G(\underline{r} - \underline{r}')$. We may rewrite Eq. (2.17) to obtain

$$G(\underline{r} - \underline{r}') = \langle \sum_{i=1}^N \sum_{j=1}^N \delta(\underline{r} - \underline{r}_i) \delta(\underline{r}' - \underline{r}_j) \rangle - n^2 \quad (2.19)$$

We note that terms with $i = j$ are not excluded from the summation so that $G(\underline{r} - \underline{r}')$ includes not only correlation between different particles but also the correlation of a particle with itself. To show this explicitly we may write

$$G(\underline{r} - \underline{r}') \equiv n\delta(\underline{r} - \underline{r}') + n^2\Gamma(\underline{r} - \underline{r}') \quad (2.20)$$

In this expression $\Gamma(\underline{r} - \underline{r}')$ is the dimensionless net pair density-density correlation function. It represents the contribution to $G(\underline{r} - \underline{r}')$ due to the correlation between different particles.

We may now proceed to relate $\Gamma(\underline{r} - \underline{r}')$ to the isothermal compressibility of the fluid. We begin by noting that

$$\langle (N - \langle N \rangle)^2 \rangle = \langle \int d\underline{r} [n(\underline{r}) - \langle n(\underline{r}) \rangle] \int d\underline{r}' [n(\underline{r}') - \langle n(\underline{r}') \rangle] \rangle \quad (2.21)$$

Using Eq. (2.14) we obtain

$$\langle (N - \langle N \rangle)^2 \rangle = \int d\underline{r} \int d\underline{r}' G(\underline{r} - \underline{r}') \quad (2.22)$$

Simplifying,

$$\langle (N - \langle N \rangle)^2 \rangle = V \int d\underline{r} G(\underline{r}) \quad (2.23)$$

Using Eq. (2.13) we obtain

$$\frac{\kappa_T}{\kappa_I} = \frac{1}{n} \int d\underline{r} G(\underline{r}) \quad (2.24)$$

Using Eq. (2.20) we obtain

$$\frac{\kappa_T}{\kappa_I} = \frac{1}{n} \int d\underline{r} [n\delta(\underline{r}) + n^2\Gamma(\underline{r})] \quad (2.25)$$

So that

$$\frac{\kappa_T}{\kappa_I} = 1 + n \int \Gamma(\underline{r}) d\underline{r} \quad (2.26)$$

The deviation of $\Gamma(\underline{r})$ from zero is a direct measure of the influence of one molecule upon another in a fluid. In an ideal gas the molecules do not interact so that $\Gamma(\underline{r}) = 0$ and from Eq. (2.26), $\frac{\kappa_T}{\kappa_I} = 1$ as expected.

For a real fluid the divergence of κ_T at the critical point means that $\int \Gamma(\underline{r}) d\underline{r}$ also diverges. This can occur only if $\Gamma(\underline{r})$ decays to zero more slowly than $1/r^3$.⁽⁴⁾ Near the critical point, then, the net pair density-density correlation function becomes long range.

Summarizing, we see that

$$\frac{\kappa_T}{\kappa_I} = \frac{\langle (N - \langle N \rangle)^2 \rangle}{\langle N \rangle} = 1 + n \int \Gamma(\underline{r}) d\underline{r}, \quad (2.27)$$

so that the divergence of the isothermal compressibility near the critical point of a fluid is related both to the increase in the mean square amplitude of the density fluctuations and to the increase in the spatial range over which fluctuations in the density are correlated.

3. Ornstein-Zernike Relation between the Isothermal Compressibility, κ_T , and the Long Range Correlation Length, ξ

What we have shown thus far is that an understanding of the static properties of a fluid near its critical point requires that we investigate the behavior of the isothermal compressibility as well as the behavior of the range over which fluctuations in the density are correlated.

In order to explicitly relate the divergence of κ_T to the increase in the range of $\Gamma(\underline{r})$ it is desirable to obtain an explicit expression for $\Gamma(\underline{r})$. Such an expression has been obtained by Ornstein and Zernike,⁽⁵⁾ and a review of that original work is presented by Fisher.⁽⁴⁾ Ornstein and Zernike argue that the correlation $\Gamma(\underline{r}_1 - \underline{r}_2)$ between molecules 1 and 2 in a fluid can be regarded as being caused by two means. First,

there is the direct influence of 1 on 2 which is described by a direct correlation function, $C(\underline{r}_1 - \underline{r}_2)$. This function is considered to have a range similar to that of the molecular interaction potential and is thus short-ranged. Second, there is the indirect influence of 1 on 2, which is propagated directly from 1 to a third molecule at \underline{r}_3 which, in turn, influences the molecule at \underline{r}_2 .

Expressing this theory mathematically, one has

$$\Gamma(\underline{r}_1 - \underline{r}_2) = C(\underline{r}_1 - \underline{r}_2) + n \int C(\underline{r}_1 - \underline{r}_3) \Gamma(\underline{r}_3 - \underline{r}_2) d\underline{r}_3 \quad (2.28)$$

Taking the Fourier transform of this expansion, one obtains

$$\Gamma(\underline{q}) = C(\underline{q}) + nC(\underline{q})\Gamma(\underline{q})$$

or,
$$C(\underline{q}) = \frac{\Gamma(\underline{q})}{1 + n\Gamma(\underline{q})} \quad (2.29)$$

where

$$\Gamma(\underline{q}) = \int e^{i\underline{q} \cdot \underline{r}} \Gamma(\underline{r}) d\underline{r}$$

and
$$C(\underline{q}) = \int e^{i\underline{q} \cdot \underline{r}} C(\underline{r}) d\underline{r} \quad (2.30)$$

In these expressions \underline{q} is the wavevector associated with the density fluctuations in the fluid.

Now,

$$\lim_{\underline{q} \rightarrow 0} \Gamma(\underline{q}) = \int \Gamma(\underline{r}) d\underline{r} \quad (2.31)$$

So that from Eq. (2.26) we have

$$\frac{\kappa_{\text{II}}}{\kappa_{\text{I}}} = \lim_{\underline{q} \rightarrow 0} [1 + n\Gamma(\underline{q})] \quad (2.32)$$

In order to relate κ_T to the range of $\Gamma(r)$ we must investigate the expression $1 + n\Gamma(q)$. From Eq. (2.29) we have

$$1 + n\Gamma(q) = \frac{1}{1 - nC(q)} \quad (2.33)$$

Ornstein and Zernike assume that $C(q)$ can be expanded in a Taylor series about $q = 0$. Specifically,

$$C(q) = C(0) + \sum_{\ell=0}^{\infty} C_{\ell}(n)q^{\ell} \quad (2.34)$$

It can be shown⁽³⁾ that the coefficients C_{ℓ} vanish for odd ℓ and that

$$C_{\ell}(n) \propto \int_0^{\infty} r^{\ell+2} C(r) dr \quad (2.35)$$

Therefore,

$$\frac{1}{1 + n\Gamma(q)} = 1 - nC(q) = 1 - n[C(0) + C_2(n)q^2 + O(q^4)] \quad (2.36)$$

This expression may be re-written as

$$\frac{1}{1 + n\Gamma(q)} = C_2(n) \left[\frac{1 - nC(0)}{C_2(n)} - nq^2 + O(q^4) \right] \quad (2.37)$$

or,

$$\frac{1}{1 + n\Gamma(q)} = -nC_2(n) \left[\frac{1 - nC(0)}{-nC_2(n)} + q^2 + O(q^4) \right] \quad (2.38)$$

We now define $R^2 \equiv -nC_2(n)$. We note that $R^2 \propto \int r^2 C(\underline{r}) d\underline{r}$ so that R has become known as the direct correlation range. Therefore,

$$\frac{1}{1 + n\Gamma(q)} = R^2 \left[\frac{1 - nC(0)}{R^2} + q^2 + O(q^4) \right]. \quad (2.39)$$

We next define $\kappa^2 \equiv \frac{1 - nC(0)}{R^2}$ so that

$$\frac{1}{1 + n\Gamma(q)} = R^2[\kappa^2 + q^2 + \alpha(q^4)] . \quad (2.40)$$

If we neglect all terms of order q^4 and higher we obtain

$$1 + n\Gamma(q) = \frac{R^{-2}}{\kappa^2 + q^2} . \quad (2.41)$$

Taking the Fourier transform and using Eq. (2.20) we obtain

$$G(\underline{r}) \propto \frac{n}{R^2} \frac{e^{-\kappa r}}{r} . \quad (2.42)$$

We now define $\xi \equiv 1/\kappa$ so that the pair correlation function has the form

$$G(r) \propto \frac{e^{-r/\xi}}{r} \quad (2.43)$$

The parameter ξ is known as the Ornstein-Zernike long range correlation length. From Eqs. (2.32) and (2.41) we see that

$$\lim_{q \rightarrow 0} 1 + n\Gamma(q) = \lim_{q \rightarrow 0} \frac{R^{-2}}{1/\xi^2 + q^2} = \frac{\kappa_T}{\kappa_I} . \quad (2.44)$$

Therefore

$$\frac{\kappa_T}{\kappa_I} = \frac{\xi^2}{R^2} . \quad (2.45)$$

We have thus obtained an explicit relation between the isothermal compressibility and the correlation range of density fluctuations for a fluid near its critical point. Since κ_T diverges at the critical point, ξ also diverges so that near the critical point $G(r) \rightarrow \frac{1}{r}$ allowing the range of correlation to become large.

4. Explicit Predictions for the Behavior of the Static Properties of a Fluid near its Critical Point

Thus far we have indicated that both κ_T and ξ do, in fact, diverge as the critical point of a fluid is approached. We have not yet, however, indicated the explicit manner in which these quantities are expected to diverge. We shall, then, present a brief review of the theoretical predictions for the explicit behavior of κ_T and ξ as well as the other related static properties of a fluid near its critical point.

We may begin by introducing the idea of critical point exponents. It is a common feature of critical phenomena that when the critical point is approached along the critical isochore, along the coexistence curve, or along the critical isotherm that several properties of the fluid either diverge toward infinity or approach zero in a manner that is characterized by a power law behavior. We have already seen that the difference between liquid and gas densities approaches zero as the critical point is approached from below T_C . Quantitatively, this relation may be expressed as:

$$\frac{\rho_l - \rho_g}{2\rho_C} = B\left(\frac{T_C - T}{T_C}\right)^\beta \quad (2.46)$$

The exponent β thus determines the shape of the coexistence curve in the ρT plane.

For a liquid-vapor critical point the density, or, more precisely, the quantity $|\rho - \rho_C|$ is known as the order parameter. Order parameters for all critical point systems have the common properties that (a) they vanish at temperatures above T_C and (b) they approach zero continuously as $T \rightarrow T_C$ from below. All systems exhibiting critical point phenomena undergo large

thermal fluctuations in the order parameter. Order parameter fluctuations are directly related to the divergences of the susceptibilities for all critical point systems. In general, the susceptibility is the derivative of the thermodynamic variable representing the order parameter with respect to its thermodynamic conjugate field. For a liquid-vapor critical point the thermodynamic conjugate to the density, ρ , is the chemical potential per unit mass, μ .⁽⁶⁾ So the susceptibility is $(\frac{\partial \rho}{\partial \mu})_T$. As the critical point is approached from below T_C along the coexistence curve the divergence of the susceptibility is given by

$$\left(\frac{\partial \rho}{\partial \mu}\right)_T = c' \left(\frac{T_C - T}{T_C}\right)^{-\gamma'} . \quad (2.47)$$

Similarly, as the critical point is approached from above T_C along the critical isochore the divergence is given by

$$\left(\frac{\partial \rho}{\partial \mu}\right)_T = c \left(\frac{T - T_C}{T_C}\right)^{-\gamma} . \quad (2.48)$$

We may easily relate $(\frac{\partial \rho}{\partial \mu})_T$ to a more familiar quantity, the isothermal compressibility, κ_T , by noting that $dP = \rho d\mu$ so that $(\frac{\partial \rho}{\partial \mu})_T = \rho (\frac{\partial \rho}{\partial P})_T$.

Since $\kappa_T = \frac{1}{\rho} (\frac{\partial \rho}{\partial P})_T$ we have $(\frac{\partial \rho}{\partial \mu})_T = \rho^2 \kappa_T$. We see then that the exponents γ and γ' determine the explicit temperature dependence of the divergence of κ_T as the critical point is approached along the critical isochore and along the coexistence curve.

Another quantity of interest is the variation of pressure with density as the critical point is approached along the critical isotherm. In order

to obtain this relation one must begin with a more fundamental relation between the order parameter, ρ , and its conjugate, μ . As the critical point is approached along the critical isotherm one has⁽⁷⁾

$$|\mu - \mu_C| = D \left| \frac{\rho - \rho_C}{\rho_C} \right|^\delta \quad (2.49)$$

The exponent δ thus determines the shape of the critical isotherm in the $\mu\rho$ plane. In order to relate the pressure to the density along T_C we begin by differentiating Eq. (2.49) so that

$$\frac{d\mu}{d\rho} \propto \delta(\rho - \rho_C)^{\delta-1} . \quad (2.50)$$

Since $dP = \rho d\mu$ we have

$$dP \propto \rho \cdot \delta(\rho - \rho_C)^{\delta-1} d\rho . \quad (2.51)$$

We may formally write

$$P - P_C \propto \int \rho \cdot \delta(\rho - \rho_C)^{\delta-1} d\rho . \quad (2.52)$$

Integrating by parts,

$$P - P_C \propto \rho(\rho - \rho_C)^\delta - \int (\rho - \rho_C)^\delta d\rho \quad (2.53)$$

or,

$$P - P_C \propto \rho(\rho - \rho_C)^\delta - \frac{1}{\delta + 1} (\rho - \rho_C)^{\delta+1} .$$

Simplifying,

$$P - P_C \propto (\rho - \rho_C)^\delta [\delta \cdot \rho + \rho_C] . \quad (2.54)$$

The shape of the critical isotherm in the $P\rho$ plane is thus determined by the relation

$$\frac{|P - P_C|}{\delta \cdot \rho + \rho_C} = D_0 \left| \frac{\rho - \rho_C}{\rho_C} \right|^\delta . \quad (2.55)$$

We have seen that the correlation length, ξ , is expected to diverge as the critical point is approached. The divergence of ξ along the critical isochore is given by

$$\xi = \xi_0 \left(\frac{T - T_C}{T_C} \right)^{-\nu} \quad (2.56)$$

and the divergence of ξ along the coexistence curve is given by

$$\xi = \xi'_0 \left(\frac{T_C - T}{T_C} \right)^{-\nu'} . \quad (2.57)$$

The exponents ν and ν' thus determine the explicit temperature dependences of the divergence of ξ as the critical point is approached from above and from below.

The final static property that is expected to diverge with a simple power law behavior as the critical point is approached is the specific heat per unit mass at constant volume, C_V . The divergence of C_V along the critical isochore is given by

$$C_V = A \left(\frac{T - T_C}{T_C} \right)^{-\alpha} \quad (2.58)$$

and the divergence of C_V along the coexistence curve is given by

$$C_V = A' \left(\frac{T_C - T}{T_C} \right)^{-\alpha'} \quad (2.59)$$

We may introduce one final critical point exponent associated with the static properties. Fisher⁽⁴⁾ has analyzed on theoretical grounds

the validity of the Ornstein-Zernike theory for the behavior of the pair correlation function for density fluctuations. He finds that the theory is inadequate very close to the critical point and proposes a modified form for the pair correlation function given by

$$G(r) \propto e^{-r/\xi}/r^{1+\eta_F} . \quad (2.60)$$

We note that when $\eta_F = 0$ the expression for $G(r)$ becomes the Ornstein-Zernike expression given in Eq. (2.43). The magnitude of the critical exponent η_F thus becomes a measure of the departure of the behavior of the pair correlation function from the prediction of the Ornstein-Zernike theory.

We have introduced a number of critical point exponents which characterize the power law behavior of several of the static properties of a fluid near its critical point. We must note, however, that not all of the static properties exhibit power law behavior as the critical point is approached. Both the specific heat per unit mass at constant pressure, C_p , and the adiabatic compressibility, κ_s , diverge toward infinity as the critical point is approached. Neither of these quantities, however, exhibits a power law behavior. From thermodynamics the specific heat at constant pressure is given by

$$C_p = C_v + \frac{T}{\rho} \left(\frac{\partial P}{\partial T} \right)_v^2 \left(\frac{\partial \rho}{\partial \mu} \right)_T \quad (2.61)$$

As the critical point is approached along the critical isochore both C_v and $\left(\frac{\partial \rho}{\partial \mu} \right)_T$ diverge with a power law behavior, while the quantity $\left(\frac{\partial P}{\partial T} \right)_v$ remains nearly constant. Therefore, the divergence of C_p is approximately given by

$$C_P \sim \left(\frac{T - T_C}{T_C}\right)^{-\alpha} + \left(\frac{T - T_C}{T_C}\right)^{-\gamma} \quad (2.62)$$

Since the critical exponents α and γ do not have the same magnitudes, we see that C_P does not diverge with a power law behavior as the critical point is approached along the critical isochore.

As the critical point is approached along the coexistence curve again both C_V and $\left(\frac{\partial \rho}{\partial \mu}\right)_T$ diverge with power law behavior. In this case, however, the density, ρ , varies and the quantity $\left(\frac{\partial P}{\partial T}\right)_V$ is no longer nearly constant. In fact, $\left(\frac{\partial P}{\partial T}\right)_V$ changes markedly as the critical point is approached along the coexistence curve. To explicitly examine the behavior of $\left(\frac{\partial P}{\partial T}\right)_V$ along the coexistence curve we begin by writing in general

$$dP = \left(\frac{\partial P}{\partial T}\right)_V dT + \left(\frac{\partial P}{\partial \rho}\right)_T d\rho \quad (2.63)$$

Indicating a change in temperature along the coexistence curve by $\left(\frac{\partial T}{\partial T}\right)_{\ell V}$, we have

$$\left(\frac{\partial P}{\partial T}\right)_{\ell V} = \left(\frac{\partial P}{\partial T}\right)_V + \left(\frac{\partial P}{\partial \rho}\right)_T \left(\frac{\partial \rho}{\partial T}\right)_{\ell V},$$

so that

$$\left(\frac{\partial P}{\partial T}\right)_V = \left(\frac{\partial P}{\partial T}\right)_{\ell V} - \left(\frac{\partial P}{\partial \rho}\right)_T \left(\frac{\partial \rho}{\partial T}\right)_{\ell V}. \quad (2.64)$$

Using $dP = \rho d\mu$, the explicit expression for C_P along the coexistence curve becomes

$$C_P = C_V + \frac{T}{\rho^2} \left[\left(\frac{\partial P}{\partial T}\right)_{\ell V} - \rho \left(\frac{\partial \mu}{\partial \rho}\right)_T \left(\frac{\partial \rho}{\partial T}\right)_{\ell V} \right]^2 \left(\frac{\partial \rho}{\partial \mu}\right)_T. \quad (2.65)$$

Along the coexistence curve near the critical point $\left(\frac{\partial P}{\partial T}\right)_{\ell V}$, which is the slope of the vapor pressure curve in the PT plane, remains nearly constant.

However, the quantity $\rho \left(\frac{\partial \mu}{\partial \rho} \right)_T \left(\frac{\partial \rho}{\partial T} \right)_{\ell v}$ approaches zero as the critical point is approached so that $\left(\frac{\partial P}{\partial T} \right)_v$ indeed changes markedly along the coexistence curve.

From Eqs. (2.61) and (2.65) it is clear that C_P does not diverge with a power law behavior as the critical point is approached along either the critical isochore or along the coexistence curve.

The final diverging static property we will discuss is the adiabatic compressibility, κ_s . From thermodynamics one obtains the relation

$$\frac{C_P}{C_V} = \frac{\kappa_T}{\kappa_S}. \quad (2.66)$$

Re-writing, we obtain

$$\rho^2 \kappa_S = \left(\frac{\partial \rho}{\partial \mu} \right)_T \frac{C_V}{C_P} \quad (2.67)$$

We see directly, then, that since C_P does not diverge with a power law behavior κ_S also does not.

Thus far, we have indicated that the behavior of several of the static properties of a fluid near its critical point may be characterized by critical point exponents. In order to obtain explicit theoretical predictions for the behavior of the static properties it is necessary to predict values for the various critical exponents. In order to make such predictions it is necessary to begin with an equation of state that is valid for a fluid in the region of its critical point. Equations of state for a fluid near its critical point have been proposed by Van der Waals and by Landau⁽¹⁾ but they are based on assumptions that are known to be invalid. Further, the values of the critical exponents predicted by these theories disagree with

experimental measurements. More recently, Widom⁽⁷⁾ and Kadanoff⁽⁶⁾ have proposed an equation of state that does appear to be valid for a fluid in the neighborhood of its critical point. Their theory has become known as the scaling law equation of state. Although the theory does not predict explicit values for each of the critical exponents, it does predict a set of relations between the exponents. We thus have the following scaling law predictions:

$$\gamma = \gamma' \quad (2.69)$$

$$\alpha = \alpha' \quad (2.70)$$

$$\alpha + 2\beta + \gamma = 2 \quad (2.71)$$

$$\alpha + \beta(\delta + 1) = 2 \quad (2.72)$$

$$\gamma(\delta + 1) = (2 - \alpha)(\delta - 1) \quad (2.73)$$

$$\gamma = \beta(\delta - 1) \quad (2.74)$$

$$\nu = \nu' \quad (2.75)$$

$$3\nu = 2 - \alpha \quad (2.76)$$

$$(2 - \eta_F)\nu = \gamma \quad (2.77)$$

$$1 + \eta_F = \frac{6}{\delta + 1} = \frac{6\beta}{2 - \alpha} = \frac{2\beta}{\nu} \quad (2.78)$$

$$\frac{3\gamma}{2\beta + \gamma} = 2 - \eta_F \quad (2.79)$$

An inspection of these relations reveals that if any two of the critical exponents are known then all the rest may be determined.

A further development of the scaling law theory is given by the parametric linear model equation of state developed by Schofield, Litster and Ho.⁽⁸⁾ In their formulation, if any two of the critical exponents are

known then the entire equation of state is determined. Thus, not only does one obtain a prediction for the temperature dependence of the static properties as the critical point is approached but also a prediction for the magnitude of those properties.

We have seen from Eqs. (2.47) and (2.48) that as the critical point is approached along the critical isochore that $(\frac{\partial P}{\partial \mu})_T = C(\frac{T - T_C}{T_C})^{-\gamma}$, and as the critical point is approached along the coexistence curve that $(\frac{\partial \rho}{\partial \mu})_T = C'(\frac{T_C - T}{T_C})^{-\gamma'}$. The linear model equation of state predicts that

$$\frac{C}{C'} = \frac{\gamma}{\beta} \left[\frac{1 - 2\beta}{2\beta} \frac{\gamma}{\gamma - 1} \right]^{\gamma-1} \quad (2.80)$$

We thus have a prediction for the ratio of the magnitudes of $(\frac{\partial \rho}{\partial \mu})_{T > T_C}$ and $(\frac{\partial \rho}{\partial \mu})_{T < T_C}$.

We may conclude our discussion of the theoretical predictions for the behavior of the static properties of a fluid near its critical point by remarking that a test of the theories requires that the quantities we have discussed be experimentally measured along the appropriate paths approaching the critical point and that their temperature and density dependence be examined. In the next section we show how a measurement of the intensity of light scattered from a fluid near its critical point provides a measurement of both the isothermal compressibility and the long range correlation length.

C. Derivation of the Einstein-Ornstein-Zernike Equation Relating the Intensity of Light Scattered from a Fluid near its Critical Point to κ_T and to ξ

We shall begin our calculation of the intensity of light scattered from a fluid near its critical point by considering the situation shown in

Fig. 2.4a. A plane, monochromatic light wave with electric field given by

$$\underline{E}_i(\underline{r}, t) = \underline{E}_0 e^{i(\underline{k}_0 \cdot \underline{r} - \omega_0 t)} \quad (2.81)$$

is incident upon a volume V of a medium whose polarizability per unit volume is $\underline{\underline{\alpha}}(\underline{r}, t)$. We wish to calculate the electric field which will be observed at a point P in the medium. We will let P be far enough away from the scattering volume, V , so that $|\underline{R} - \underline{r}| \approx |\underline{R}| = R$ for all points in V .

Due to the polarizability of the medium, the incident electric field will induce a polarization in each volume element, d^3r , given by

$$\underline{P}(\underline{r}, t) = \underline{\underline{\alpha}}(\underline{r}, t) \underline{E}_i(\underline{r}, t) d^3r \quad (2.82)$$

In general, $\underline{\underline{\alpha}}(\underline{r}, t)$ is a tensor so that \underline{P} and \underline{E}_i need not be in the same direction. However, for a simple fluid, there is no anisotropy so that $\underline{\underline{\alpha}}(\underline{r}, t)$ may be considered to be a scalar, $\alpha(\underline{r}, t)$. Since the fluid exhibits random thermal fluctuations we may write

$$\alpha(\underline{r}, t) = \langle \alpha \rangle + \delta\alpha(\underline{r}, t) \quad (2.83)$$

where $\langle \alpha \rangle$ is the average polarizability for the entire scattering volume and $\delta\alpha(\underline{r}, t)$ represents the random fluctuations away from the average.

The oscillating polarization given in Eq. (2.82) will radiate in a manner similar to an oscillating dipole. Using the far field approximation for the field produced by an oscillating dipole one obtains⁽²⁾

$$\underline{E}_s(\underline{R}, t) = \int_V \frac{1}{R} \frac{1}{\langle \epsilon \rangle c_m^2} \hat{k}_s \times [\hat{k}_s \times \ddot{\underline{P}}(\underline{r}, t_r)] d^3r \quad (2.84)$$

where $\hat{k}_s = \frac{(\underline{R} - \underline{r})}{|\underline{R} - \underline{r}|}$, a unit vector in the direction of the scattered field,

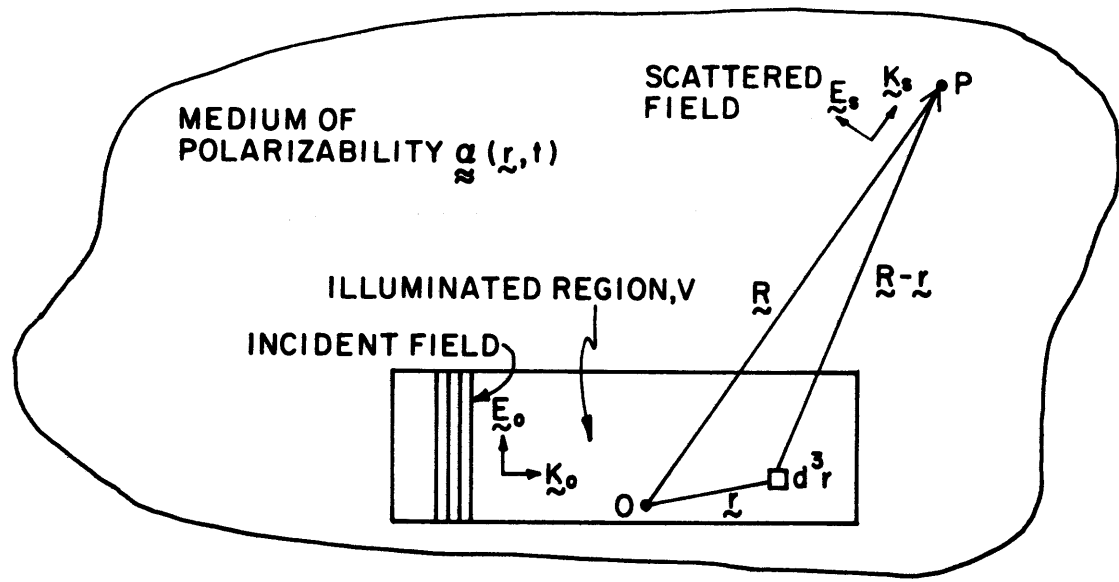


Fig. 2.4a Experimental Situation for Light Scattering

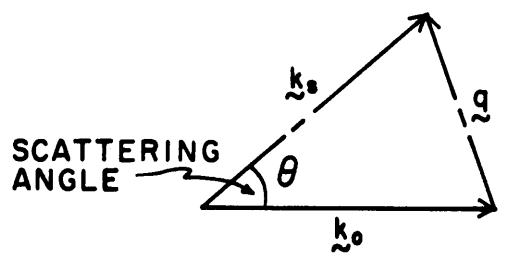


Fig. 2.4b Geometric Representation of the Scattering Process

c_m is the velocity of light in the medium, $t_r = t - \frac{|\underline{R} - \underline{r}|}{c_m}$, the retarded time, $\langle \epsilon \rangle$ is the average dielectric constant of the medium, and $\langle \epsilon \rangle c_m^2 = c^2$.

In order to calculate $\underline{P}(\underline{r}, t_r)$ we note that the time variation of $\alpha(\underline{r}, t)$ is very slow compared with that of $\underline{E}_1(\underline{r}, t)$ so from Eq. (2.82) we obtain

$$\ddot{\underline{P}}(\underline{r}, t_r) = \alpha(\underline{r}, t) \underline{E}_0 (-\omega_0^2) e^{i\mathbf{k}_0 \cdot \underline{r} - i\omega_0 t + i\omega_0 (|\underline{R} - \underline{r}|/c_m)} \quad (2.85)$$

Now, since $R \gg r$ we may write

$$|\underline{R} - \underline{r}| \approx R - \hat{\mathbf{k}}_s \cdot \underline{r} \quad (2.86)$$

We may also define $\underline{k}_s \equiv \frac{\omega_0}{c_m} \hat{\mathbf{k}}_s \equiv k_0 \hat{\mathbf{k}}_s$, which is a wave vector of the same length as the incident wave vector but pointing in the direction of observation. Equation (2.85) thus becomes

$$\ddot{\underline{P}}(\underline{r}, t_r) = \alpha(\underline{r}, t) \underline{E}_0 (-\omega_0^2) e^{i\mathbf{k}_s \cdot \underline{R} - i\omega_0 t} \cdot e^{i\mathbf{k}_0 \cdot \underline{r} - i\mathbf{k}_s \cdot \underline{r}} \quad (2.87)$$

Using this result in Eq. (2.84) along with Eq. (2.83) we obtain the following expression for the scattered field:

$$\underline{E}_s(\underline{R}, t) = \frac{1}{\langle \epsilon \rangle} \underline{k}_s \times (\underline{k}_s \times \underline{E}_0) \frac{1}{R} e^{i(\mathbf{k}_s \cdot \underline{R} - \omega_0 t)} \cdot \int_V [\langle \alpha \rangle + \delta\alpha(\underline{r}, t)] e^{i(\mathbf{k}_0 - \mathbf{k}_s) \cdot \underline{r}} d^3r \quad (2.88)$$

We see that Eq. (2.88) contains two terms: one with $\langle \alpha \rangle$ and one with $\delta\alpha(\underline{r}, t)$. Upon carrying out the integration over V on the first of these terms we obtain

$$\int_V \langle \alpha \rangle e^{i(\underline{k}_0 - \underline{k}_s) \cdot \underline{r}} d^3r = (2\pi)^3 \langle \alpha \rangle \delta^3(\underline{k}_0 - \underline{k}_s) \quad (2.89)$$

so that this term corresponds solely to radiation in which the direction of scattering, \hat{k}_s , is equal to the direction of the incident radiation, \hat{k}_0 . The physical interpretation is that in a perfectly uniform, non-fluctuating medium, incident light will not be scattered but will continue in the direction of its initial propagation. Thus scattering is produced entirely by the fluctuating term. Therefore, we shall consider only the term with $\delta\alpha(\underline{r}, t)$.

Equation (2.88) can be placed in a much more revealing form if we decompose the fluctuations in the polarizability into their Fourier components. We may write

$$\delta\alpha(\underline{r}, t) = \frac{1}{(2\pi)^{3/2}} \int_{-\infty}^{\infty} \delta\alpha(\underline{q}, t) e^{i\underline{q} \cdot \underline{r}} d^3q \quad (2.90)$$

Here, \underline{q} is the wavevector associated with the fluctuations. Recalling that α is related to the dielectric constant through $\epsilon = 1 + 4\pi\alpha$, we have $\delta\alpha(\underline{r}, t) = \frac{1}{4\pi} \delta\epsilon(\underline{r}, t)$. Using these relations, Eq. (2.88) becomes

$$\begin{aligned} \underline{E}_s(\underline{R}, t) = & \frac{1}{\langle \epsilon \rangle (2\pi)^{3/2}} \underline{k}_s \times (\underline{k}_s \times \underline{E}_0) \frac{1}{4\pi R} e^{i(\underline{k}_s \cdot \underline{R} - \omega_0 t)} \\ & \cdot \int_{-\infty}^{\infty} \delta\epsilon(\underline{q}, t) \left[\int_V e^{i(\underline{k}_0 - \underline{k}_s + \underline{q}) \cdot \underline{r}} d^3r \right] d^3q \end{aligned} \quad (2.91)$$

The term in square brackets in Eq. (2.91) is just the three dimensional delta function; that is,

$$\int_V e^{i(\underline{k}_0 - \underline{k}_s + \underline{q}) \cdot \underline{r}} d^3r = (2\pi)^3 \delta^3(\underline{k}_0 - \underline{k}_s + \underline{q}) \quad (2.92)$$

Thus we can express the scattered field as

$$\underline{E}_s(\underline{R}, t) = \frac{(2\pi)^{3/2}}{\langle \epsilon \rangle} \underline{k}_s \times (\underline{k}_s \times \underline{E}_0) \frac{1}{4\pi R} e^{i(\underline{k}_s \cdot \underline{R} - \omega_0 t)} \delta \epsilon(\underline{q}, t) \quad (2.93)$$

where $\underline{q} \equiv \underline{k}_s - \underline{k}_0$. The scattered field is thus a function only of the Fourier component of the fluctuations with wavevector \underline{q} . The wavevector \underline{q} is thus known as the scattering vector. In Fig. 2.4b we see a geometrical representation of the scattering process which is valid for non-propagating fluctuations. Since $|\underline{k}_s| = |\underline{k}_0|$ we have

$$q = 2k_0 \sin\left(\frac{\theta}{2}\right) \quad (2.94)$$

or, since $k_0 = \frac{2\pi}{\lambda_m}$, where λ_m is the wavelength of light in the medium, we have

$$q = \frac{4\pi n}{\lambda_0} \sin\left(\frac{\theta}{2}\right), \quad (2.95)$$

where λ_0 is the vacuum wavelength of light and n is the refractive index of the medium. We see that we may observe scattering from fluctuations with varying q simply by varying the scattering angle θ .

Finally, by using $\underline{k}_s \equiv \frac{\omega}{c_m} \hat{k}_s$ we have, for the electric field scattered a distance R away from the scattering volume in a simple fluid,

$$\underline{E}_s(\underline{q}, t) = -E_0 \left(\frac{\omega_0}{c}\right)^2 \frac{e^{i(\underline{k}_s \cdot \underline{R} - \omega_0 t)}}{4\pi R} \sin \phi (2\pi)^{3/2} \delta \epsilon(\underline{q}, t) \quad (2.96)$$

where ϕ is the angle between the direction of polarization of the incident light and the direction of \underline{k}_s .

Now, the power or intensity of light scattered into a solid angle Ω and observed a distance R away from the scattering volume is given by⁽²⁾

$$P_s = \frac{c}{8\pi} \langle |E_s(\mathbf{q}, t)|^2 \rangle_t R^2 \Omega ; \quad (2.97)$$

that is, the intensity is proportional to the time average of the square of the scattered field. We obtain directly from Eq. (2.96) that

$$P_s = \left(\frac{c}{8\pi} E_0^2\right) \left(\frac{\omega_0}{c}\right)^4 \frac{\sin^2 \phi}{(4\pi)^2} (2\pi)^3 \langle |\delta \epsilon(\mathbf{q}, t)|^2 \rangle_t \Omega \quad (2.98)$$

Using $c = \frac{\omega_0 \lambda_0}{2\pi}$, assuming $\phi = 90^\circ$ which is the usual experimental situation, and noting that $\frac{c}{8\pi} E_0^2$ is the power/unit area, $\frac{P_I}{A}$, of the light incident on the scattering volume, we obtain

$$\frac{P_s}{P_I} = \frac{\pi^2 \Omega}{4 \lambda_0^4 A} (2\pi)^3 \langle |\delta \epsilon(\mathbf{q}, t)|^2 \rangle_t \quad (2.99)$$

Next, we may express the fluctuations in the dielectric constant of the medium in terms of the fluctuations in the thermodynamic variables of the medium. Choosing the temperature and the density as the independent variables we may write

$$\delta \epsilon(\mathbf{r}, t) = \left(\frac{\partial \epsilon}{\partial \rho}\right)_T \delta \rho(\mathbf{r}, t) + \left(\frac{\partial \epsilon}{\partial T}\right)_\rho \delta T(\mathbf{r}, t) \quad (2.100)$$

In terms of the Fourier transforms of these quantities we may also write

$$\delta \epsilon(\mathbf{q}, t) = \left(\frac{\partial \epsilon}{\partial \rho}\right)_T \delta \rho(\mathbf{q}, t) + \left(\frac{\partial \epsilon}{\partial T}\right)_\rho \delta T(\mathbf{q}, t) \quad (2.101)$$

where

$$\delta \rho(\mathbf{q}, t) = \frac{1}{(2\pi)^{3/2}} \int d\mathbf{r} e^{-i\mathbf{q}\cdot\mathbf{r}} \delta \rho(\mathbf{r}, t)$$

and

$$\delta T(\mathbf{q}, t) = \frac{1}{(2\pi)^{3/2}} \int d\mathbf{r} e^{-i\mathbf{q}\cdot\mathbf{r}} \delta T(\mathbf{r}, t) \quad (2.102)$$

Now, using Eq. (2.101) and the ergodic theorem of statistical mechanics which states the equivalence between the time average and the ensemble average of fluctuating thermodynamics quantities, we may write Eq. (2.99) as

$$\frac{P_S}{P_I} = \frac{\pi^2 \Omega}{\lambda_0^3 A} (2\pi)^3 \left[\left(\frac{\partial \epsilon}{\partial \rho} \right)_T^2 \langle |\delta \rho(\mathbf{q}, t)|^2 \rangle + \left(\frac{\partial \epsilon}{\partial T} \right)_\rho^2 \langle |\delta T(\mathbf{q}, t)|^2 \rangle + 2 \left(\frac{\partial \epsilon}{\partial \rho} \right)_T \left(\frac{\partial \epsilon}{\partial T} \right)_\rho \langle \delta \rho(\mathbf{q}, t) \delta T(\mathbf{q}, t) \rangle \right] \quad (2.103)$$

We recall from Eq. (2.6) that fluctuations in the volume (or density) and fluctuations in the temperature are statistically independent. Therefore, $\langle \delta \rho(\mathbf{q}, t) \delta T(\mathbf{q}, t) \rangle = 0$. We recall from Eq. (2.7) that the probability distribution for temperature and volume fluctuations is given by:

$$p(\Delta V, \Delta T) \propto e^{-\left[C_V \frac{(\Delta T)^2}{T} + \frac{1}{V \kappa_T} (\Delta V)^2 \right]} \quad 2k_B T \quad (2.104)$$

We may write the probability distribution for temperature and density fluctuations by noting that $\left(\frac{\Delta V}{V} \right)^2 = \left(\frac{\Delta \rho}{\rho} \right)^2$. We thus have

$$p(\Delta \rho, \Delta T) \propto e^{-\int d\mathbf{r} \left[\frac{C_V (\Delta T(\mathbf{r}))^2}{2k_B T^2} + \frac{(\Delta \rho(\mathbf{r}))^2}{2k_B T \rho^2 \kappa_T} \right]} \quad (2.105)$$

$$\text{Now, } \delta \rho(\mathbf{r}) = \frac{1}{(2\pi)^{3/2}} \int d\mathbf{q} e^{i\mathbf{q} \cdot \mathbf{r}} \delta \rho(\mathbf{q}) \quad (2.106)$$

Also,

$$|\delta \rho(\mathbf{r})|^2 d\mathbf{r} = \frac{1}{(2\pi)^3} \iint d\mathbf{q} d\mathbf{q}' \delta \rho(\mathbf{q}) \delta \rho(\mathbf{q}') \int e^{i(\mathbf{q}-\mathbf{q}') \cdot \mathbf{r}} d\mathbf{r} \quad (2.107)$$

The last integral is just $(2\pi)^3 \delta(\mathbf{q}-\mathbf{q}')$ so that

$$\int |\delta\rho(\mathbf{r})|^2 d\mathbf{r} = \int \langle |\delta\rho(\mathbf{q})|^2 \rangle d\mathbf{q} . \quad (2.108)$$

We may express the last integral as a sum of the $\delta\rho(\mathbf{q})$ over the volumes of unit cells in \mathbf{q} -space. These volumes have a size given by $|d\mathbf{q}| = \frac{(2\pi)^3}{V}$.

We thus have:

$$\int \langle |\delta\rho(\mathbf{q})|^2 \rangle d\mathbf{q} = \sum_{\mathbf{q}} |\delta\rho(\mathbf{q})|^2 \frac{(2\pi)^3}{V} . \quad (2.109)$$

Therefore,

$$\int |\delta\rho(\mathbf{r})|^2 d\mathbf{r} = \sum_{\mathbf{q}} |\delta\rho(\mathbf{q})|^2 \frac{(2\pi)^3}{V} . \quad (2.110)$$

Similarly,

$$\int |\delta T(\mathbf{r})|^2 d\mathbf{r} = \sum_{\mathbf{q}} |\delta T(\mathbf{q})|^2 \frac{(2\pi)^3}{V} . \quad (2.111)$$

Our expression for the probability of temperature and density fluctuations thus becomes

$$p(\Delta\rho, \Delta T) \propto e^{-\sum_{\mathbf{q}} \frac{(2\pi)^3}{V} \left(\frac{C_V}{2k_B T^2} |\delta T(\mathbf{q})|^2 + \frac{|\delta\rho(\mathbf{q})|^2}{2k_B T \rho^2 \kappa_T} \right)} \quad (2.112)$$

We see that we have a Gaussian distribution for each value of \mathbf{q} so that for the mean square fluctuations we obtain

$$\langle |\delta\rho(\mathbf{q})|^2 \rangle = k_B T \rho^2 \kappa_T \cdot \frac{V}{(2\pi)^3} \quad (2.113)$$

and

$$\langle |\delta T(\mathbf{q})|^2 \rangle = \frac{k_B T^2}{C_V} \cdot \frac{V}{(2\pi)^3}$$

Now, for a simple fluid near its critical point

$$\left(\frac{\partial \epsilon}{\partial \rho}\right)_T^2 \langle |\delta \rho(\mathbf{q})|^2 \rangle \gg \left(\frac{\partial \epsilon}{\partial T}\right)_\rho^2 \langle |\delta T(\mathbf{q})|^2 \rangle \quad (2.114)$$

so we shall write $\delta \epsilon(\mathbf{q}) = \left(\frac{\partial \epsilon}{\partial \rho}\right)_T \delta \rho(\mathbf{q})$. Using Eq. (2.113) in our expression for the intensity of scattered light given in Eq. (2.103) we have

$$\frac{P_S}{P_I} = \frac{\pi^2 L \Omega}{4 \lambda_0} k_B T \left(\frac{\partial \epsilon}{\partial \rho}\right)_T^2 \rho^2 k_T \quad (2.115)$$

where L is the length of the illuminated region in the medium.

We may observe that according to Eq. (2.115) the intensity of scattered light is independent of the scattering angle. We may also observe that in the derivation of Eq. (2.115) we assumed that the fluctuations in the density were uncorrelated. We have already seen, however, that perhaps the most fundamental phenomenon which occurs near the critical point of a fluid is that the spatial range over which density fluctuations are correlated becomes very large. When the spatial extent of the regions of correlated density fluctuations are no longer negligibly small compared to the wavelength of light what results is an angular anisotropy in the intensity of the scattered light. Therefore, in order to adequately calculate the intensity of light scattered from a fluid near its critical point we must account for the correlation of density fluctuations.

We may begin with a general result of scattering theory which relates the molecular structure factor of a medium to the Fourier transform of the net pair density-density correlation function. ^(3,4)

We may write

$$\frac{(P_S/P_I)}{(P_S/P_I)_0} = 1 + n\Gamma(\mathbf{q}) \quad (2.116)$$

where $\Gamma(\mathbf{q})$ is the Fourier transform of $\Gamma(\mathbf{r})$ introduced in Eq. (2.29). In this expression $(P_S/P_I)_0$ is the intensity of scattered light predicted if the density fluctuations were uncorrelated. The proper expression for the intensity of scattered light is then given by (P_S/P_I) . We observe that Eq. (2.115) does yield the proper expression for the intensity of scattered light when density fluctuations are uncorrelated. From Eq. (2.26), however, we see that when density fluctuations are uncorrelated we have an ideal gas so that $\kappa_T = \kappa_I$. We thus have the result that

$$\left(\frac{P_S}{P_I}\right)_0 = \frac{\pi^2 L \Omega}{\lambda_0^4} k_B T \left(\frac{\partial \epsilon}{\partial \rho}\right)_T^2 \rho^2 \kappa_I \quad (2.117)$$

Therefore

$$\frac{P_S}{P_I} = \frac{\pi^2 L \Omega}{\lambda_0^4} k_B T \left(\frac{\partial \epsilon}{\partial \rho}\right)_T^2 \rho^2 \kappa_I [1 + n\Gamma(\mathbf{q})] \quad (2.118)$$

We may use the Ornstein-Zernike result for $[1 + n\Gamma(\mathbf{q})]$ given in Eq. (2.41) so that

$$\frac{P_S}{P_I} = \frac{\pi^2 L \Omega}{\lambda_0^4} k_B T \left(\frac{\partial \epsilon}{\partial \rho}\right)_T^2 \rho^2 \kappa_I \frac{\xi^2/R^2}{1 + q^2 \xi^2} \quad (2.119)$$

From Eq. (2.45), however, we have that $\xi^2/R^2 = \kappa_T/\kappa_I$ so that our final expression for the intensity of light scattered from a fluid near its critical point becomes

$$\frac{P_S}{P_I} = \frac{\pi^2 L \Omega}{\lambda_0^4} k_B T \left(\frac{\partial \epsilon}{\partial \rho}\right)_T^2 \rho^2 \kappa_T \frac{1}{(1 + q^2 \xi^2)} \quad (2.120)$$

We may observe that for $q^2 \xi^2 \ll 1$, Eq. (2.120) becomes equivalent to Eq. (2.115). We see then that the effects of correlated fluctuations upon the intensity of scattered light become important when q becomes large; that is, at large scattering angles, or when ξ becomes large; that is, when the fluid is very close to its critical point.

We see then that measurements of the angular dependence of the intensity of light scattered from a fluid along paths approaching the critical point are able to provide measurements of the magnitude and the temperature dependence of the isothermal compressibility, κ_T , and the long range correlation length, ξ .

Thus far in our discussion of critical point phenomena we have considered only the behavior of time-independent, static properties. In the next section we turn our attention to the behavior of the dynamic properties of a fluid near its critical point.

D. Relationship between the Time Dependence of the Light Scattered from a Fluid near its Critical Point and the Time Dependence of the Isobaric Entropy Fluctuations in the Fluid

We shall begin our discussion of the behavior of the dynamic properties of a fluid near its critical point by relating the time dependence of the light scattered from the fluid to the dynamic properties we wish to consider.

From Eq. (2.96) which is our expression for the electric field scattered from a fluid we see that the time dependence of the scattered light exactly mirrors the time dependence of the fluctuations in the dielectric

constant of the fluid. We have seen that the fluctuations in the dielectric constant are due to the random thermal fluctuations in the thermodynamic variables of the medium. We may choose the entropy and the pressure as the independent variables and write

$$\delta\epsilon(\mathbf{q},t) = \left(\frac{\partial\epsilon}{\partial S}\right)_P \delta S(\mathbf{q},t) + \left(\frac{\partial\epsilon}{\partial P}\right)_S \delta P(\mathbf{q},t) . \quad (2.121)$$

We see then that the time dependence of the scattered light depends separately upon the time dependences of the isobaric entropy fluctuations and the adiabatic pressure fluctuations. The relation between the time dependence of the scattered light and the time dependence of the adiabatic pressure fluctuations was first studied by Brillouin.⁽⁹⁾ In our discussion we will not be concerned with the scattering of light from the fluctuations in pressure. Instead, we will be concerned solely with the relation between the time dependence of the scattered light and the time dependence of the isobaric entropy fluctuations. This relation was first studied by Landau and Placzek.⁽¹⁰⁾

In order to study the time dependence of the fluctuations in entropy we first note that the fluctuations are random variables. The most convenient way to consider the time dependence of a random variable is to consider the amount of correlation such a variable has over a given period of time. We may define the time correlation function of a random variable x by writing

$$R_x(\tau) = \lim_{T \rightarrow \infty} \frac{1}{2T} \int_{-T}^T x(t + \tau)x(t)dt \quad . \quad (2.122)$$

We may use the ergodic theorem stating the equivalence of the time average and the ensemble average of fluctuating quantities so that we may equivalently define the time correlation function of a random variable x by writing

$$R_x(\tau) \equiv \langle x(t + \tau)x(t) \rangle \quad . \quad (2.123)$$

Therefore in order to study the time dependence of the entropy fluctuations in a fluid we must determine the correlation function for those fluctuations. We begin by noting that fluctuations in entropy are proportional to fluctuations in temperature; that is,

$$T\delta S(\mathbf{q}, t) = C_P \delta T(\mathbf{q}, t) \quad (2.124)$$

or
$$T\delta S(\mathbf{r}, t) = C_P \delta T(\mathbf{r}, t) \quad .$$

Next, we use the Onsager regression hypothesis⁽¹¹⁾ which states that the random, spontaneous thermal fluctuations in a fluid regress in time, on the average, in the same manner as would a macroscopically induced fluctuation. Thus we may argue that the time dependence of temperature fluctuations is governed by the Fourier heat diffusion equation; that is,

$$\frac{d}{dt} \delta T(\mathbf{r}, t) = \frac{\Lambda}{\rho C_P} \nabla^2 \delta T(\mathbf{r}, t) \quad . \quad (2.125)$$

The quantity $\frac{\Lambda}{\rho C_P}$ is the thermal diffusivity and Λ is the thermal conductivity. Taking the Fourier transform,

$$\frac{d}{dt} \delta T(\mathbf{q}, t) = - \frac{\Lambda}{\rho C_p} q^2 \delta T(\mathbf{q}, t) \quad . \quad (2.126)$$

Solving,

$$\delta T(\mathbf{q}, t) = \delta T(\mathbf{q}, 0) e^{-\Gamma t} \quad (2.127)$$

where

$$\Gamma \equiv \frac{\Lambda}{\rho C_p} q^2 \quad . \quad (2.128)$$

Explicitly for entropy fluctuations we have

$$\delta S(\mathbf{q}, t) = \delta S(\mathbf{q}, 0) e^{-\Gamma t} \quad . \quad (2.129)$$

We see then that entropy fluctuations decay in time exponentially. The correlation function for entropy fluctuations is given by

$$R_S(\tau) = \langle \delta S(\mathbf{q}, t + \tau) \delta S(\mathbf{q}, t) \rangle \quad . \quad (2.130)$$

We may assume that the fluctuations are a stationary random process so that the correlation function depends only on the time difference, τ . We thus have

$$R_S(\tau) = \langle |\delta S(\mathbf{q}, 0)|^2 \rangle e^{-\Gamma \tau} \quad . \quad (2.131)$$

We see that the time correlation function for entropy fluctuations decays exponentially.

Next, we shall relate the correlation function for entropy fluctuations to the correlation function of the scattered electric field. From Eq. 2.96 we have for the field scattered due to entropy fluctuations that

$$E(\mathbf{q}, t) = J e^{-i\omega_0 t} \delta S(\mathbf{q}, t) \quad (2.132)$$

where

$$J = -E_0 \left(\frac{\omega_0}{C}\right)^2 \frac{1}{4\pi R} e^{i\mathbf{k}_s \cdot \mathbf{R}} \sin \phi (2\pi)^{3/2} \left(\frac{\partial \epsilon}{\partial S}\right)_P \quad . \quad (2.133)$$

So the correlation function for the scattered field is

$$R_E(\tau) = J^2 \langle \delta S(q, \tau) \delta S(q, 0) \rangle e^{-i\omega_0 \tau} . \quad (2.134)$$

Using Eq. (2.131) we thus have

$$R_E(\tau) = J^2 \langle |\delta S(q, 0)|^2 \rangle e^{-\Gamma \tau} e^{-i\omega_0 \tau} . \quad (2.135)$$

We see then that we may obtain a measurement of the decay rate, Γ , of entropy fluctuations by measuring the correlation function of the scattered electric field. Such a measurement will thus provide a measurement of the thermal diffusivity of the fluid.

The question arises as to how one obtains the correlation function of the scattered electric field. According to the Wiener-Khinchine theorem⁽¹²⁾ the time Fourier transform of the correlation function of the scattered field is the spectral power density of the scattered field; that is,

$$S_E(\omega) = \int_{-\infty}^{\infty} R_E(\tau) e^{i\omega \tau} d\tau . \quad (2.136)$$

Thus, we may obtain a measurement of Γ by measuring the spectrum of the scattered field. We can easily show that the spectrum is a Lorentzian.

We have

$$S_E(\omega) = J^2 \langle |\delta S(q, 0)|^2 \rangle \int_{-\infty}^{\infty} e^{-\Gamma \tau} e^{i(\omega - \omega_0) \tau} d\tau . \quad (2.137)$$

Now, since the correlation function has the property that $R_E(\tau) = R_E(-\tau)$ we essentially are taking the real part of the Fourier transform of the correlation function. Therefore

$$S_E(\omega) = J^2 \langle |\delta S(q,0)|^2 \rangle \int_{-\infty}^{\infty} e^{-\Gamma\tau} \cos(\omega - \omega_0)\tau d\tau \quad (2.138)$$

or,

$$S_E(\omega) = 2J^2 \langle |\delta S(q,0)|^2 \rangle \int_0^{\infty} e^{-\Gamma\tau} \cos(\omega - \omega_0)\tau d\tau \quad (2.139)$$

The integral is of the form $\int_0^{\infty} e^{-ax} \cos bxdx$. Its value is $\frac{a}{a^2 + b^2}$.

Therefore

$$S_E(\omega) = J^2 \langle |\delta S(q,0)|^2 \rangle \frac{2\Gamma}{\Gamma^2 + (\omega - \omega_0)^2} \quad (2.140)$$

We see then that the spectrum of light which is scattered due to entropy fluctuations is a Lorentzian centered at the frequency of the incident light. The half-width at half-maximum of this spectrum in Hz. is $\frac{\Gamma}{2\pi}$.

The experimental problem arises that since the spectrum is centered about the incident light frequency, ω_0 , it is difficult to resolve by conventional spectroscopic methods. We will show that the method of self-beating spectroscopy solves the problem by translating the spectrum down in frequency so that it is centered about zero frequency rather than the incident light frequency. We will also show that, most importantly, information on the decay rate, Γ , is retained in this process.

If the scattered light is allowed to fall on the surface of a photomultiplier tube then what is observed at the output of the tube is not the fluctuations in the scattered field which exactly mirror the entropy fluctuations, but rather the fluctuations in the photocurrent which are proportional to the intensity; that is, the square of the field. Specifically, the photocurrent averaged over times short compared to the decay time of fluctuations in the square of the field, yet long compared to the reciprocal

of the incident light frequency, is given by:⁽¹³⁾

$$i(t) = \frac{Ge\eta}{h\nu} \int_A \frac{c}{8\pi} |E(r,t)|^2 dA . \quad (2.141)$$

We see that the photocurrent is proportional to the integral of the power per unit area of the scattered field over the illuminated area in the scattering medium which is projected onto the phototube surface. In our expression G is the gain of the photomultiplier, e is the charge on the electron, η is the quantum efficiency and $h\nu$ is the energy of the light quantum. The photocurrent varies in time due to the fluctuations in the scattered field which may be considered continuous. However, the photocurrent actually consists of a succession of pulses so in examining its time dependence we must account for the effects of shot noise.

We may re-write Eq. (2.141) by arguing⁽¹³⁾ that the spatial integral may be expressed as a sum of the contributions from each of the separate coherence areas in the scattering medium which are projected onto the phototube surface. If the phototube accepts scattered light from N coherence areas, each of size ΔA , we may write

$$i(t) = \sum_{j=1}^N \langle i_j(t) \rangle + \delta i_j(t) \quad (2.142)$$

where

$$\langle i_j(t) \rangle = \frac{Ge\eta c}{8\pi h\nu} \Delta A \langle |E(t)|^2 \rangle$$

and

$$(2.143)$$

$$\delta i_j(t) = \frac{Ge\eta c}{8\pi h\nu} \Delta A (\langle |E(t)|^2 \rangle - |E(r_j, t)|^2) .$$

The correlation function for the photocurrent is given by

$$R_i(\tau) = \langle i(t)i(t + \tau) \rangle \quad (2.144)$$

so that

$$\begin{aligned} R_i(\tau) = \langle \sum_{j=1}^N \sum_{k=1}^N (\langle i_j(t) \rangle + \delta i_j(t)) (\langle i_k(t) \rangle + \delta i_k(t + \tau)) \rangle \\ + Ge \sum_{j=1}^N \langle i_j(t) \rangle \delta(\tau) \quad . \end{aligned} \quad (2.145)$$

The last term represents the shot noise contribution to the photocurrent correlation function and is expressed as a delta function. We may simplify Eq. (2.145) by noting that fluctuations in the photocurrent arising from the field scattered from two different coherence areas are uncorrelated; that is,

$$\langle \delta i_j(t) \delta i_j(t') \rangle = 0 \quad \text{for } j \neq k \quad . \quad (2.146)$$

We may also define the time average photocurrent, i_0 , as

$$i_0 \equiv \sum_j \langle i_j(t) \rangle \quad . \quad (2.147)$$

With these simplifications the photocurrent correlation function becomes

$$R_i(\tau) = i_0^2 \left(1 + \frac{1}{N} \frac{\langle \delta i_j(t) \delta i_j(t + \tau) \rangle}{\langle i_j(t) \rangle^2} \right) + Ge i_0 \delta(\tau) \quad . \quad (2.148)$$

Using Eq. (2.143) we may write

$$\frac{\langle \delta i_j(t) \delta i_j(t + \tau) \rangle}{\langle i_j(t) \rangle^2} = \frac{\langle |E(t)|^2 |E(t + \tau)|^2 \rangle - \langle |E(t)|^2 \rangle^2}{\langle |E(t)|^2 \rangle^2} \quad (2.149)$$

Thus far we have related the correlation function for the photocurrent to the correlation function for the square of the field. But the information we desire is contained in the correlation function for the field rather than in the correlation function for the square of the field. We may relate the two, however, by assuming that the amplitudes of the fluctuations in the electric field are distributed in a Gaussian manner about an average of zero; that is, we assume that $E(t)$ is a Gaussian random variable. We make use of the following theorem:⁽¹⁴⁾ If x_1, x_2, x_3 and x_4 are real random variables with a Gaussian joint probability density function and if all have zero mean, then the ensemble average may be factored according to the rule:

$$\begin{aligned} \langle x_1 x_2 x_3 x_4 \rangle = & \langle x_1 x_2 \rangle \langle x_3 x_4 \rangle + \langle x_1 x_3 \rangle \langle x_2 x_4 \rangle \\ & + \langle x_1 x_4 \rangle \langle x_2 x_3 \rangle . \end{aligned} \quad (2.150)$$

We thus have:

$$\begin{aligned} \langle |E(t)|^2 |E(t + \tau)|^2 \rangle = \\ \langle |E(t)|^2 \rangle^2 + \langle |E(t)E(t + \tau)| \rangle^2 . \end{aligned} \quad (2.151)$$

Using this result along with Eq. (2.149) our expression for the photocurrent correlation function becomes

$$R_i(\tau) = i_0^2 \left(1 + \frac{1}{N} \frac{\langle |E(t)E(t + \tau)| \rangle^2}{\langle |E(t)|^2 \rangle^2} \right) + G e i_0 \delta(\tau) . \quad (2.152)$$

Now, using Eq. (2.135) which is our expression for the correlation function for the scattered field we obtain

$$R_i(\tau) = i_0^2 + \frac{i_0^2 J^4 \langle |\delta S(q,0)|^2 \rangle^2 e^{-2\Gamma\tau}}{N \langle |E(q,0)|^2 \rangle^2} + Gei_0 \delta(\tau) \quad (2.153)$$

or

$$R_i(\tau) = i_0^2 + J_0 e^{-2\Gamma\tau} + Gei_0 \delta(\tau) \quad (2.154)$$

where

$$J_0 = \frac{i_0^2 J^4 \langle |\delta S(q,0)|^2 \rangle^2}{N \langle |E(q,0)|^2 \rangle^2} \quad (2.155)$$

From Eq. (2.154) we see that the correlation function for the photocurrent contains three terms: a constant baseline, a delta function at the origin, and a decaying exponential with decay rate 2Γ . A direct measurement of the photocurrent correlation function thus yields a measurement of Γ and hence a measurement of the thermal diffusivity.

We may also consider the photocurrent spectrum, $S_i(\omega)$. Using the Wiener-Khintchine theorem, we have

$$S_i(\omega) = \int_{-\infty}^{\infty} R_i(\tau) e^{i\omega\tau} d\tau \quad (2.156)$$

Therefore, taking the real part of the Fourier transform of $R_i(\tau)$ we have

$$S_i(\omega) = 2\pi i_0^2 \delta(\omega) + J_0 \int_{-\infty}^{\infty} e^{-2\Gamma\tau} \cos \omega\tau d\tau + Gei_0. \quad (2.157)$$

In analogy with Eq. (2.140) we obtain

$$S_i(\omega) = 2\pi i_0^2 \delta(\omega) + J_0 \left[\frac{4\Gamma}{(2\Gamma)^2 + \omega^2} \right] + Gei_0. \quad (2.158)$$

We see then that the spectrum of the photocurrent also contains three terms: a baseline due to the shot noise, a delta function at the origin due to the

average photocurrent, and a Lorentzian centered at zero frequency. The half-width at half maximum of the Lorentzian in Hz is $\frac{2\Gamma}{2\pi}$.

Thus far we have shown that by using the method of self-beating spectroscopy we may measure the spectrum or, equivalently, the correlation function of light scattered from the random thermal isobaric entropy fluctuations in a fluid near its critical point. We have shown that such measurements are able to provide us with the magnitude and temperature dependence of the thermal diffusivity, $\frac{\Lambda}{\rho C_p}$, of a fluid near its critical point. In the next section we will discuss the theoretical predictions for the behavior of the thermal diffusivity of a fluid near its critical point.

E. Theoretical Predictions for the Behavior of the Dynamic Properties of a Fluid near its Critical Point by Application of the Physical Ideas Embodied in the Mode-Mode Coupling Theory

In this section we shall present a review of the most recent theoretical predictions for the behavior of the dynamic properties of a fluid near its liquid-vapor critical point. In particular, we shall discuss the predictions for the behavior of the thermal conductivity, the shear viscosity, and the thermal diffusivity. Precise predictions for the behavior of these quantities have been made by the application of the physical ideas embodied in what has become known as the mode-mode coupling theory.

1. The Basic Physical Idea of Fixman

The basic physical idea of the mode-mode coupling approach was first set forth by Fixman⁽¹⁵⁾ who presented a theory which qualitatively

explained the anomalous increase in the macroscopically measured shear viscosity of a binary liquid mixture near the critical mixing point. Fixman notes that near the critical mixing point a binary mixture is highly susceptible to concentration fluctuations that are large in amplitude and in spatial extent. When an attempt is made to measure the shear viscosity of the mixture by conventional methods viscous shear forces arising from the application of a viscosimeter are exerted at the fluid boundary. These forces produce a velocity gradient within the mixture which in turn induces large inhomogeneities in concentration. These concentration fluctuations decay away through diffusion. The return to uniform composition through diffusion dissipates energy, however, and the energy loss is interpreted as being due to an excess shear viscosity. We see then that an anomalous increase in the macroscopically measured shear viscosity may be understood, on the microscopic level, as being caused by a coupling between two modes of energy dissipation; namely, a coupling between viscous and diffusive energy dissipation.

2. The First Quantitative Expression of the Mode-Mode Coupling Theory due to Kawasaki

The next advance in the development of the mode-mode coupling approach was due to Kawasaki⁽¹⁶⁾ who, retaining Fixman's fundamental idea, attempted to develop a general and systematic way to determine the anomalies in the transport coefficients of systems near a critical point.

Kawasaki begins by noting that transport coefficients such as the shear and bulk viscosities and the thermal conductivity may be expressed as the time integral of a time correlation function. In general we may write:

$$\theta = \frac{w}{V} \int_0^{\infty} \langle J(t)J(0) \rangle dt . \quad (2.159)$$

In this expression J is the flux corresponding to the transport coefficient θ . For example, if the transport coefficient, θ , is the thermal conductivity then the flux, J , is the heat flux. Also, w is some known function of the temperature and V is the total volume of the system. The brackets denote an equilibrium ensemble average.

Kawasaki next seeks to express the flux in terms of an expansion in powers of the macroscopic variables of the system. In particular, he seeks to express the flux in terms of the spatial Fourier components of the macroscopic variables. If we define A_k^α as the k^{th} Fourier component of the α^{th} macroscopic variable then we may write:

$$J = \sum_{\alpha\beta} \sum_k S_{\alpha\beta}^k A_k^\alpha A_{-k}^\beta + \dots \quad (2.160)$$

where the S 's are coefficients. In this treatment Kawasaki considers only the terms written explicitly in the expansion, ignoring the terms with higher powers of A . He also proves that terms linear in A are absent from the expansion. Kawasaki makes a further very important assumption; that is, he assumes that the part of the flux, J , which does not contain Fourier components of the macroscopic variables, A 's, does not give rise to anomalies in the transport coefficients since it does not involve the critical fluctuations in the macroscopic variables. The underlying assumption is that the cause of the anomalies in transport coefficients is the anomalous increase in the long-wavelength Fourier components of the fluctuations. The upshot of these assumptions is that the magnitude of the transport coefficient

that is eventually determined is the magnitude of only the "critical part" of the transport coefficient; that is, the part due to the fluctuations.

Kawasaki notes that expansions analogous to that given in Eq. (2.160) are often used in plasma physics where the right-hand side of Eq. (2.160) represents what is known as "mode-mode coupling". Thus it is through an analogy with phenomena in plasma physics that the theory which predicts the behavior of the dynamic properties of a fluid near its critical point derives its name.

Substituting Eq. (2.160) into Eq. (2.159) we obtain a general expression for the anomalous part of the transport coefficient, $\Delta\theta$:

$$\Delta\theta = \frac{w}{V} \sum_{\alpha\beta} \sum_k S_{\alpha\beta}^k \int_0^{\infty} \langle A_k^\alpha(t) A_{-k}^\beta(t) J(0) \rangle dt . \quad (2.161)$$

Kawasaki evaluates Eq. (2.161) by making use of the fact that the A's are macroscopic variables and so their time development may be assumed to be governed by macroscopic equations of motion such as the hydrodynamic equations. In general, the hydrodynamic equations are of the form:

$$\frac{d}{dt} A_k^\alpha(t) = - \sum_{\beta} M_k^{\alpha\beta} A_k^\beta(t) \quad (2.162)$$

where the M_k contains the specific form of the equation. In matrix notation we may write this relation as:

$$\frac{d}{dt} \underline{A}_k(t) = - \underline{M}_k \cdot \underline{A}_k(t) . \quad (2.163)$$

In order to evaluate the general expression for $\Delta\theta$, however, we need the equations of motion for the bilinear terms $A_k^\alpha A_{-k}^\beta$. Using the form of Eq. (2.162) the equations of motion are:

$$\frac{d}{dt} A_k^\alpha(t) A_{-k}^\beta(t) = - \sum_{\gamma} \{ M_k^{\alpha\gamma} A_k^\gamma(t) A_{-k}^\beta(t) + M_{-k}^{\beta\gamma} A_k^\alpha(t) A_{-k}^\gamma(t) \} \quad (2.164)$$

Again, in matrix notation we may re-write this relation as:

$$\frac{d}{dt} \underline{Q}_k(t) = -\underline{m}_k \cdot \underline{Q}_k(t) \quad (2.165)$$

where the matrix $\underline{Q}_k(t)$ has the following $\alpha\beta$ element:

$$Q_k^{\alpha\beta}(t) = A_k^\alpha(t) A_{-k}^\beta(t) \quad (2.166)$$

With this notation the integral in the general expression for $\Delta\theta$, (Eq. (2.164)), is written as: $\int_0^\infty \langle Q_k^{\alpha\beta}(t) J(0) \rangle dt$. Now, if we formally solve Eq. (2.165) we obtain

$$\underline{Q}_k(t) = [\underline{m}_k^{-1}] \cdot \frac{d}{dt} \underline{Q}_k(t) \quad (2.167)$$

Using this formal solution allows us to express the integral as $\sum_{\gamma\delta} [\underline{m}_k^{-1}]_{\alpha\beta:\gamma\delta} \langle Q_k^{\gamma\delta} J \rangle$. Therefore, the anomalous part of the transport coefficient becomes:

$$\Delta\theta = \frac{w}{V} \sum_{\alpha\beta} \sum_{\gamma\delta} \sum_k S_{\alpha\beta}^k [\underline{m}_k^{-1}]_{\alpha\beta:\gamma\delta} \langle A_k^\gamma A_{-k}^\delta J \rangle \quad (2.168)$$

After accounting for the coefficients, $S_{\alpha\beta}^k$, Kawasaki shows that

$$\begin{aligned} \Delta\theta &= \frac{w}{2V} \sum_{\alpha\beta} \sum_{\gamma\delta} \sum_k [\underline{m}_k^{-1}]_{\alpha\beta:\gamma\delta} \langle J A_k^{\alpha*} A_{-k}^{\beta*} \rangle \\ &\cdot \langle J A_k^{\gamma\delta} \rangle < |A_k^\alpha|^2 >^{-1} < |A_{-k}^\beta|^2 >^{-1} \quad (2.169) \end{aligned}$$

Thus, in order to calculate $\Delta\theta$, one must evaluate quantities of the form $\langle J A_k^{\alpha\beta} \rangle$. Kawasaki notes that, unfortunately, there is no general way

to evaluate these quantities. He points out, however, that when $\Delta\theta$ is the anomalous shear viscosity of a binary liquid mixture, $\Delta\eta$, then the quantities $\langle JA_{k-k}^{\alpha,\beta} \rangle$ may be evaluated. Using local concentration and local temperature as the fluctuating macroscopic variables, and using the continuity equations for mass and concentration, the Navier-Stokes equation, and the energy transport equation as the macroscopic equations of motion, Kawasaki applies his formalism to the calculation of $\Delta\eta$. He finds that $\Delta\eta$ is proportional to ξ , the Ornstein-Zernike long range correlation length for concentration fluctuations. Thus, Kawasaki predicts that near the critical mixing point the shear viscosity of a binary liquid mixture, a dynamic property, diverges with the same temperature dependence as the long range correlation length, a static property.

In Kawasaki's formalism the divergence of the viscosity can be attributed to two effects: (1) the increase of the long-wavelength Fourier components of the fluctuations in concentration and temperature which enter the expression for the flux and (2) the increase in the lifetimes of these components of the fluctuations, a result obtained from the macroscopic equations of motion.

3. The Specific Predictions of Kadanoff and Swift for the Temperature Dependences of Transport Coefficients of a Fluid near its Critical Point

The next advance in the development of the mode-mode coupling approach was due to Kadanoff and Swift⁽¹⁷⁾ who constructed a perturbation

theory for the determination of transport coefficients near the critical point which, they show, is equivalent to the expansion procedure of Kawasaki. However, whereas Kawasaki was unable to evaluate his expressions for transport coefficients, Kadanoff and Swift were able to obtain specific predictions for the temperature dependences of transport coefficients near the liquid-vapor critical point.

Kadanoff and Swift begin by noting that, in general, any time dependent problem in classical statistical mechanics may be formulated in terms of the Liouville equation. In state vector notation the Liouville equation is

$$\left(\frac{\partial}{\partial t} + L\right) |t\rangle = 0 \quad (2.170)$$

where the state vector $|t\rangle$ describes the state of the system at time t . The state vector is defined so that its components are the probabilities for finding N particles in the system with one particle having position r_1 and momentum p_1 , another with position r_2 and momentum p_2 and so forth. Formally, one writes:

$$\langle p_1, p_2, \dots, p_N, r_1, r_2, \dots, r_N | t \rangle = \langle p, r, t | t \rangle = f_N(p, r, t) . \quad (2.171)$$

The Liouville operator has the matrix element:

$$\begin{aligned} \langle p', r', N' | L | p, r, N \rangle &= \sum_{\alpha=1}^N \left[\frac{\partial \mathcal{H}}{\partial p_{\alpha}} \frac{\partial \mathcal{H}}{\partial r_{\alpha}} - \frac{\partial \mathcal{H}}{\partial r_{\alpha}} \frac{\partial \mathcal{H}}{\partial p_{\alpha}} \right] \\ &\cdot \langle p', r', N' | p, r, N \rangle \end{aligned} \quad (2.172)$$

where \mathcal{H} is the Hamiltonian for the system. In the Kadanoff and Swift formalism the equilibrium state vector is denoted as $|1\rangle$ and its components,

as one expects, are given by the grand canonical ensemble equilibrium distribution with chemical potential μ and temperature T ; that is,

$$\langle p, r, N | \rangle = \exp\left\{-\frac{1}{k_B T} [H(p, r) - \mu N]\right\} / [h^{3N} N! Z(T, \mu)] \quad (2.173)$$

We note that $L|\rangle = 0$ as expected since the equilibrium state does not evolve in time. Also, we may express the average of any physical quantity X in the state $|\rangle$ as:

$$\langle X \rangle_t = \langle |X_{Op}| \rangle_t, \quad (2.174)$$

while the average of X in the grand canonical ensemble is expressed as:

$$\langle X \rangle = \langle |X_{Op}| \rangle. \quad (2.175)$$

In the last two expressions X_{Op} is a diagonal matrix in the p 's and r 's.

Kadanoff and Swift indicate that the important physical quantities or operators are the densities and the currents of conserved quantities. They write the number density operator as $n_{Op}(\underline{r})$, the momentum density operator as $\underline{g}_{Op}(\underline{r})$ and the energy density operator as $\epsilon_{Op}(\underline{r})$. The currents corresponding to these densities are $\underline{j}(\underline{r})$, the number current; $\tau_{ij}(\underline{r})$, the stress tensor; and $\underline{j}^\epsilon(\underline{r})$, the energy current. These currents are defined by the following relations:

$$-\nabla \cdot \underline{j}_{Op}(\underline{r}) = [L, n_{Op}(\underline{r})] \quad (2.176)$$

$$-\nabla \cdot \tau(\underline{r}) = [L, \underline{g}(\underline{r})] \quad (2.177)$$

$$-\nabla \cdot \underline{j}_{Op}^\epsilon(\underline{r}) = [L, \epsilon_{Op}(\underline{r})] \quad (2.178)$$

where we have used standard Poisson bracket notation. Kadanoff and Swift also define an entropy density operator:

$$s_{Op}(\underline{r}) = \frac{1}{T} \left[\epsilon_{Op}(\underline{r}) - \frac{\langle \epsilon + p \rangle}{\langle n \rangle} n_{Op}(\underline{r}) \right], \quad (2.179)$$

and an entropy current operator:

$$j_{Op}^S(\underline{r}) = \frac{1}{T} \left[j_{Op}^\epsilon(\underline{r}) - \frac{\langle \epsilon \rangle + \langle p \rangle}{\langle n \rangle} j_{Op}(\underline{r}) \right]. \quad (2.180)$$

In these expressions the brackets denote a grand canonical ensemble average and p is the pressure.

Having defined the important operators, Kadanoff and Swift point out that the states important for transport phenomena are those which describe situations in which the equilibrium parameters, such as temperature or velocity, vary slowly from point to point. They form these "local equilibrium" states by using linear combinations of the densities of the conserved quantities. Five combinations are defined: $a_i(\underline{r})$ with $i = 1 \dots 5$. These combinations are used in the form of Fourier transforms:

$$a_i(\underline{q}) = \int d^3r e^{-i\mathbf{q}\cdot\mathbf{r}} a_i(\underline{r}). \quad (2.181)$$

The expressions for the five states are:

$$a_1(\underline{q}) = \frac{s_{Op}(\underline{q})}{[k_B \rho c_p(\underline{q})]^{1/2}} \quad (2.182)$$

$$a_2(\underline{q}) = \frac{(\rho/k_B T)^{1/2}}{\langle n \rangle} c(\underline{q}) n_{Op}(\underline{q}) + \left(\frac{1}{k_B \rho} \left[\frac{1}{c_V(\underline{q})} - \frac{1}{c_p(\underline{q})} \right] \right)^{1/2} s_{Op}(\underline{q}) \quad (2.183)$$

$$a_3(\underline{q}) = \epsilon_x(\underline{q}) \left(\frac{1}{k_B T \rho} \right)^{1/2} \quad (2.184)$$

$$a_4(q) = g_y(q) \left(\frac{1}{k_B T \rho} \right)^{1/2} \quad (2.185)$$

$$a_5(q) = g_z(q) \left(\frac{1}{k_B T \rho} \right)^{1/2} \quad (2.186)$$

In these expressions the q -dependent thermodynamic quantities reduce to their static values at $q = 0$. Thus, $C_p(q)$, $C_v(q)$, and $c(q)$ reduce to the specific heat at constant pressure, the specific heat at constant volume, and the adiabatic sound velocity at $q = 0$.

In state vector notation we may write:

$$a_i(q) | > = |i, q >$$

and
$$\langle | a_i(-q) = \langle i, q | . \quad (2.187)$$

Having defined the important operators and states, Kadanoff and Swift next consider transport processes. They point out that the transport modes of a system appear as slowly decaying solutions to the Liouville equation (Eq. (2.170)). An eigenstate of L with eigenvalue s will decay in time as e^{-st} . Therefore, for the slowly decaying modes, the eigenvalue s has a small real part.

Classifying the eigenvalues of L according to wavenumber q , one may write:

$$s_\nu | \nu, q > = L | \nu, q > , \quad (2.188)$$

which is the equation for the ν^{th} eigenstate corresponding to the eigenvalue s_ν . Now, if the eigenstate $| \nu, q >$ is important for transport phenomena then it is mostly composed of the local equilibrium states $| i, q >$. We may apply $\langle i, q |$ to Eq. (2.188) to obtain:

$$\begin{aligned}
s_v \langle i, \mathbf{q} | v, \mathbf{q} \rangle &= \langle i, \mathbf{q} | L | v, \mathbf{q} \rangle \\
&= \sum_{j=1}^5 \langle i, \mathbf{q} | L | j, \mathbf{q} \rangle \langle j, \mathbf{q} | v, \mathbf{q} \rangle + \langle i, \mathbf{q} | LP | v, \mathbf{q} \rangle
\end{aligned} \tag{2.189}$$

where P is a projection operator which rejects the states $|i, \mathbf{q}\rangle$; that is,

$$P = 1 - \sum_{j=1}^5 |j, \mathbf{q}\rangle \langle j, \mathbf{q}| . \tag{2.190}$$

Kadanoff and Swift show that

$$P | v, \mathbf{q} \rangle = \frac{1}{s_v - PLP} \sum_{j=1}^5 PL | j, \mathbf{q} \rangle \langle j, \mathbf{q} | v, \mathbf{q} \rangle \tag{2.191}$$

so that Eq. (2.189) may be written as:

$$\sum_{j=1}^5 [s_v \delta_{ij} - L_{ij}(\mathbf{q}) - U_{ij}(\mathbf{q}, s_v)] \langle j, \mathbf{q} | v, \mathbf{q} \rangle = 0 \tag{2.192}$$

$$\text{where} \quad L_{ij}(\mathbf{q}) = \langle i, \mathbf{q} | L | j, \mathbf{q} \rangle \tag{2.193}$$

$$\text{and} \quad U_{ij}(\mathbf{q}, s) = \langle i, \mathbf{q} | LP \frac{1}{s - PLP} PL | j, \mathbf{q} \rangle . \tag{2.194}$$

We see then that the eigenvalues of the Liouville operator are determined by the condition that the matrix $(s\delta_{ij} - L_{ij} - U_{ij})$ has zero determinant. The next task is to find the significant terms in this 5×5 matrix.

Kadanoff and Swift show that the only nonvanishing elements of L_{ij} are L_{23} and L_{32} . They show that

$$L_{23} = L_{32} = iq_x c(\mathbf{q}) \tag{2.195}$$

where they assume \underline{q} is in the x-direction. We see that if all the elements of U_{ij} were equal to zero then we would have only two non-zero eigenvalues:

$$s_{\pm} = \pm i c q_x \quad . \quad (2.196)$$

Since the eigenstates have a time dependence given by e^{-st} , we see that the purely imaginary eigenvalues, s_{\pm} , describe the oscillatory behavior of undamped sound waves. Therefore, all dissipative processes must be described by the elements of U_{ij} . And so, all the transport coefficients arise from the elements of U_{ij} . In Table 2.1 we show the Kadanoff and Swift result for the significant terms in the matrix $(\delta_{ij}s - L_{ij} - U_{ij})$. In the matrix λ is the thermal conductivity, η is the shear viscosity and ζ is the bulk viscosity. We see that the first row describes dissipation by heat flow; the second and third rows describe dissipation by sound waves; and the fourth and fifth rows describe dissipation by viscous flow.

The eigenvalues determined from the matrix are the decay rates for heat flow, sound waves, and viscous flow. Thus, the heat flow mode has a decay rate given by:

$$s_T(\underline{q}) = \frac{\lambda(\underline{q}, s) q^2}{\rho c_P(\underline{q})} \quad . \quad (2.197)$$

For sound waves one obtains:

$$s_{\pm}(\underline{q}) = \pm i q_x c(\underline{q}) + \frac{1}{2} q^2 D_s(\underline{q}, s) \quad (2.198)$$

where $D_s(\underline{q}, s)$ is the damping term given by:

$$D_s(\underline{q}, s) = \frac{4/3 \eta(\underline{q}, s) + \zeta(\underline{q}, s)}{\rho} + \frac{\lambda(\underline{q}, s)}{\rho} \left(\frac{1}{c_V(\underline{q})} - \frac{1}{c_P(\underline{q})} \right) \quad . \quad (2.199)$$

Table 2.1 The Matrix ($s\delta_{ij} - L_{ij} - U_{ij}$)

	Heat flow	Sound waves	Viscous flow
Heat flow	$s - \frac{\lambda q^2}{\rho c_P}$	$-\frac{\lambda q^2}{\rho} \left(\frac{1}{c_V c_P} - \frac{1}{c_P^2} \right)^{1/2}$	0
Sound waves	$-\frac{\lambda q^2}{\rho} \left(\frac{1}{c_V c_P} - \frac{1}{c_P^2} \right)^{1/2}$	$s - \frac{\lambda q^2}{\rho} \left(\frac{1}{c_V} - \frac{1}{c_P} \right)$	$-icq_x$
	0	$-icq_x$	$s - \frac{(\zeta + 4/3\eta)q^2}{\rho}$
Viscous flow	0	0	$s - \frac{\eta q^2}{\rho}$
	0	0	$s - \frac{\eta q^2}{\rho}$

Finally, the viscous flow mode has a decay rate given by:

$$s_{\eta}(\mathbf{q}) = \frac{\eta(\mathbf{q}, s) \mathbf{q}^2}{\rho} \quad (2.200)$$

Having obtained expressions for the decay rates for the three types of transport processes in a fluid system Kadanoff and Swift proceed to calculate these decay rates, thereby obtaining expressions for the transport coefficients.

They begin by noting that in the general expression for the transport coefficients given in Eq. (2.194), there appear structures of the form $X = \frac{1}{PLP - s}$. In particular, the expression for the thermal conductivity is:

$$-q^2 \lambda(\mathbf{q}, s) = \langle |S_{OP}(-\mathbf{q})LPXPLS_{OP}(\mathbf{q})| \rangle / k_B T \quad (2.201)$$

and the expression for the shear viscosity is:

$$-q^2 \eta(\mathbf{q}, s) = \langle |g_y(-\mathbf{q})LPXPLg_y(\mathbf{q})| \rangle / k_B T \quad (2.202)$$

To gain a convenient representation for X , Kadanoff and Swift note that since the projection operator P in X rejects the local equilibrium states, it almost entirely removes the lowest eigenstates of the Liouville operator L (which are the transport states) and leaves the remaining states almost untouched. Thus, they show that

$$X(\mathbf{q}) = \frac{1}{PLP - s} = \sum_{v'=6}^{\infty} \frac{|v', \mathbf{q}\rangle \langle v', \mathbf{q}|}{s_{v'}(\mathbf{q}) - s} \quad (2.203)$$

where the transport states, $v' = 1 \dots 5$, have been omitted.

Now what is of interest is the calculation of divergences of the transport coefficients near the critical point. We have seen that, near the critical

point, a fluid is characterized by the presence of long wavelength fluctuations which decay away very slowly. Kadanoff and Swift thus argue that divergences in the transport coefficients can be expected to arise from states ν' which decay away very slowly. These slowly decaying states will give small values of $s_{\nu'}(\mathbf{q})$. Now, the smallest values of $s_{\nu'}(\mathbf{q})$ are those associated with the transport states. However, if one wishes to calculate the thermal conductivity or the shear viscosity using Eq. (2.201) or Eq. (2.202), we see that according to Eq. (2.203) the transport states are excluded. Kadanoff and Swift thus seek the next set of available states which will still yield small values of $s_{\nu'}(\mathbf{q})$. These are the so-called intermediate states which involve multiple transport processes. As an example we can consider a state which involves two independent transport processes with wave vectors \mathbf{q}' and $\mathbf{q} - \mathbf{q}'$. Kadanoff and Swift show that this state can be written as:

$$\sum_{\nu'} | \nu', \mathbf{q} \rangle \langle \nu', \mathbf{q} | = \frac{1}{2} \sum_{\nu_1=1}^5 \sum_{\nu_2=1}^5 \int \frac{d^3 \mathbf{q}'}{(2\pi)^3} \cdot a_{\nu_1}(\mathbf{q}') a_{\nu_2}(\mathbf{q} - \mathbf{q}') | \rangle \langle | a_{\nu_1}(-\mathbf{q}') a_{\nu_2}(\mathbf{q}' - \mathbf{q}) \quad (2.204)$$

where the a_{ν} terms are linear combinations of the a_j terms which are associated with the simple transport processes. The eigenvalue for this state is given by

$$s_{\nu'}(\mathbf{q}) = s_{\nu_1}(\mathbf{q}') + s_{\nu_2}(\mathbf{q}' - \mathbf{q}) \quad (2.205)$$

We see that the decay rate for the multiple process is given by the sum of the decay rates for the simple processes.

At this point we may note the analogy between Eq. (2.204) and Kawasaki's expression (Eq. (2.161)) for the divergent part of a transport coefficient. We see that both expressions involve bilinear combinations of terms representing simple processes. Such expressions are, as we have seen, indicative of what is meant by "mode-mode coupling". We see that the modes that are coupled in the Kadanoff and Swift formulation are the transport modes. The state represented by Eq. (2.204) decays away through some combination of heat flow, sound waves, and viscous flow with a decay rate given by the sum of the decay rates for each of the constituent processes.

A given intermediate state might, however, involve more than just two processes. With this in mind Kadanoff and Swift present a general perturbation expression for the quantity X which may be used in Eqs. (2.201) and (2.202) to calculate the divergent parts of the thermal conductivity and the shear viscosity. They write:

$$\begin{aligned}
X(q) = & \frac{1}{2!} \sum_{\nu, \nu'=1}^5 \int \frac{d^3 q'}{(2\pi)^3} \frac{a_{\nu}(q') a_{\nu'}(q - q') | \rangle \langle | a_{\nu}(-q') a_{\nu'}(q' - q)}{s_{\nu}(q') + s_{\nu'}(q - q') - s} \\
& + \frac{1}{3!} \sum_{\nu, \nu', \nu''=1}^5 \int \frac{d^3 q'}{(2\pi)^3} \frac{d^3 q''}{(2\pi)^3} \\
& \cdot \frac{a_{\nu}(q') a_{\nu''}(q'') a_{\nu'}(q - q' - q'') | \rangle \langle | a_{\nu}(-q') a_{\nu''}(-q'') a_{\nu'}(q' + q'' - q)}{s_{\nu}(q - q' - q'') + s_{\nu'}(q') + s_{\nu''}(q'')} - \\
& + \frac{1}{4!} [\quad \quad \quad] + \dots \quad . \quad (2.206)
\end{aligned}$$

Having obtained general expressions for the divergent parts of transport coefficients, Kadanoff and Swift proceed with explicit calculations of these

quantities. They begin by considering the general expression for the shear viscosity given in Eq. (2.202). They wish to calculate the contribution to the divergent part of the shear viscosity from the multiple process which involves two heat-flow modes. Using the expression for $X(q)$, as it relates to two heat-flow modes, in Eq. (2.202), and noting from Eq. (2.190) that the projection operators P may be replaced by unity, Kadanoff and Swift obtain:

$$-q^2 \Delta \eta_{TT}(q, s) = \frac{1}{2k_B T} \int \frac{d^3 q'}{(2\pi)^3} \frac{\langle |g_y(-q) L a_1(q') a_1(q - q')| \rangle}{s_T(a') + s_T(q - q') - s} \cdot \langle |a_1(q' - q) a_1(-q') L g_y(q)| \rangle . \quad (2.207)$$

In this expression the quantity $\Delta \eta_{TT}(q, s)$ is the divergent part of the shear viscosity due to decay by two heat flow modes. They re-write this result as

$$q^2 \Delta \eta_{TT}(q, s) = \frac{1}{2k_B T} \int \frac{d^3 q'}{(2\pi)^3} \cdot \frac{|M_{q, q'}|^2}{[\rho C_P(q') \rho C_P(q - q')] [s_T(q') + s_T(q - q') - s]} \quad (2.208)$$

where the matrix element is given by:

$$M_{q, q'} = \langle |g_y(-q) L S_{OP}(q') S_{OP}(q - q')| \rangle . \quad (2.209)$$

Kadanoff and Swift evaluate this matrix element and obtain:

$$M_{q, q'} = \rho k_B^2 T [i q'_y C_p(q - q') + i(q'_y - q_y) C_p(q')] . \quad (2.210)$$

Substituting into Eq. (2.208) we find:

$$q^2 \Delta \eta_{TT}(q, s) = \frac{1}{2k_B T} \int \frac{d^3 q'}{(2\pi)^3} (q'_y)^2 \frac{[C_P(-q + q') - C_P(q')]}{C_P(-q' + q) C_P(q')}^2 \cdot \frac{1}{s_T(q') + s_T(q - q') - s} \quad (2.211)$$

Now, in the static, long-wavelength limit $q \rightarrow 0$ and $s \rightarrow 0$, Kadanoff and Swift show that:

$$\Delta \eta_{TT}(0, 0) = \frac{1}{4} \int \frac{d^3 q'}{(2\pi)^3} (q'_y)^2 \frac{[\frac{\partial}{\partial q'_x} C_P(q')]^2}{s_T(q') [C_P(q')]^2} \quad (2.212)$$

Now, the decay rate for heat-flow, $s_T(q')$, becomes small for long wavelengths. Therefore, the integral in Eq. (2.212) may be expected to contain large contributions from small values of q' . Kadanoff and Swift hypothesize that the main contributions to the integral arise from $q' \leq 1/\xi$, where ξ is the Ornstein-Zernike long range correlation length. They also make the approximation that:

$$\frac{\partial}{\partial q'_x} C_P(q') \cong \frac{q'_x}{(q')^2} C_P(q') \quad (2.213)$$

They also define the quantity:

$$s_T^* \equiv s_T(q') \Big|_{q'=1/\xi} \equiv \left(\frac{\lambda^*}{\rho C_P} \right) \frac{1}{\xi} \quad (2.214)$$

Thus, s_T^* is the heat-flow decay rate at $q' = 1/\xi$ and λ^* is the thermal conductivity at this decay rate and at $q' = 1/\xi$. Using Eqs. (2.213) and (2.214) in Eq. (2.212), the expression for the divergent part of the shear viscosity due to two heat modes, for $q \leq 1/\xi$ and $s \leq s_T^*$, becomes:

$$\Delta\eta_{TT}(q, s) \sim \frac{k_B T \rho C_P}{\lambda^*} \frac{1}{\xi} \quad . \quad (2.215)$$

We note that if the restrictions on q and s are not satisfied then the contributions to $\Delta\eta_{TT}$ are considerably reduced.

Examination of Eq. (2.215) reveals that the product of the transport coefficients $\Delta\eta_{TT}(0,0)$ and λ^* must indeed diverge as the critical point is approached. Recalling Eq. (2.57) for the divergence of ξ and Eq. (2.62) for the approximate divergence of C_P , we obtain the result:

$$\Delta\eta_{TT}(0,0)\lambda^* \sim \left(\frac{T - T_C}{T_C}\right)^{-\gamma+\nu} \quad . \quad (2.216)$$

Since $\gamma > \nu$, we have the prediction that either $\Delta\eta_{TT}(0,0)$ or λ^* , or both, diverge as the critical point is approached.

Kadanoff and Swift go on to show that the contribution to the divergent part of the shear viscosity from a multiple process which involves three or more heat flow modes is of the same order of magnitude as the contribution from the two heat flow mode process. Thus the prediction of Eq. (2.216) remains intact.

Having considered the contributions to the divergent part of the shear viscosity from heat flow modes, Kadanoff and Swift next consider the contributions to the divergent part of the thermal conductivity from the multiple process which involves decay by one heat flow mode and one viscous flow mode. They begin by considering the general expression for the thermal conductivity given in Eq. (2.201). Using the expression for $X(q)$ (given in Eq. (2.206)), as it relates to one heat flow mode and one viscous flow mode, in Eq. (2.201), they obtain:

$$q^2 \Delta \lambda_{\eta T}(q, s) = \frac{1}{k_B^3} \int \frac{d^3 q'}{(2\pi)^3} \frac{|N_{q, q'}|^2}{\rho^2 C_P(q') [s_T(q') + s_\eta(q - q') - s]} \quad (2.217)$$

where the matrix element is given by:

$$N_{q, q'} = \langle |S_{OP}(-q) L P \hat{n} \cdot q(q - q') S_{OP}(q')| \rangle, \quad (2.218)$$

where the unit vector \hat{n} is in the direction of the momentum. Noting that the projection operator may be replaced by unity, Kadanoff and Swift evaluate this matrix element and obtain:

$$N_{q, q'} = i q \cdot \hat{n} k_B^2 \rho C_P(q'). \quad (2.219)$$

Substituting into Eq. (2.217) they find:

$$\Delta \lambda_{\eta T}(q, s) = \frac{k_B^T}{3} \int \frac{d^3 q'}{(2\pi)^3} \frac{C_P(q')}{s_T(q') + s_\eta(q - q') - s}. \quad (2.220)$$

Again, they assume that the main contributions to the integral arise from $q' \leq 1/\xi$. They also note that, since the heat flow decay rate is very slow near the critical point, the viscous flow decay rate, $s_\eta(q')$, dominates the heat flow decay rate, $s_T(q')$, in the denominator. They also define the quantity:

$$s_\eta^* \equiv \eta(q') \Big|_{q'=1/\xi} \equiv \left(\frac{\eta}{\rho}\right) \frac{1}{\xi^2}. \quad (2.221)$$

Thus, s_η^* is the viscous flow decay rate at $q' = 1/\xi$ and η^* is the shear viscosity at this decay rate and at $q' = 1/\xi$. Using Eq. (2.221) together with the two preceding assumptions in Eq. (2.220), the expression for the divergent part of the thermal conductivity due to a heat flow mode and a viscous flow mode, for $q \leq 1/\xi$ and $s \leq s_\eta^*$, becomes:

$$\Delta\lambda_{\eta T}(q,s) \sim \frac{k_B T \rho C_P}{\eta^* \xi} . \quad (2.222)$$

We note that if the restrictions on q and s are not satisfied then the denominator in Eq. (2.220) becomes large enough to considerably reduce the contributions to $\Delta\lambda_{\eta T}$.

Kadanoff and Swift also argue that contributions to the divergent part of the thermal conductivity from a multiple process which involves two or more heat flow modes together with a viscous flow mode is of the same order of magnitude as the contribution from the process involving one heat flow mode and one viscous flow mode. Thus, the expression, Eq. (2.222), remains intact.

Assuming for the moment that there are no contributions to $\Delta\eta$ or $\Delta\lambda$ from processes other than those considered thus far, Kadanoff and Swift are now able to use Eqs. (2.215) and (2.222) to obtain specific predictions for the temperature dependence of both $\Delta\eta$ and $\Delta\lambda$ near the critical point. They first note that from Eqs. (2.214) and (2.221) one observes that $s_T^* \ll s_\eta^*$ due to the presence of the large factor C_P in the denominator of s_T^* . Therefore, η^* is the shear viscosity evaluated at frequencies much higher than s_T^* . However, there are no contributions to $\Delta\eta$ from frequencies higher than s_T^* . Therefore, η^* cannot have a divergent part near the critical point and must remain finite. With η^* shown to be finite, Eq. (2.222) provides an explicit prediction for the temperature dependence of the divergent part of the thermal conductivity of a fluid near the liquid vapor critical point. Using Eq. (2.57) for the divergence of ξ and Eq. (2.62) for the approximate divergence of C_P , we obtain the result:

$$\Delta\lambda(0,0) \sim \left(\frac{T - T_C}{T_C}\right)^{-\gamma+\nu} . \quad (2.223)$$

This prediction remains valid for frequencies up to s_η^* . Therefore, the prediction of Eq. (2.223) may be used in Eq. (2.216) to evaluate λ^* . We see that we obtain the prediction:

$$\Delta\eta(0,0) \sim \left(\frac{T - T_C}{T_C}\right)^0 ; \quad (2.224)$$

that is, the shear viscosity does not diverge as a power of $(T - T_C)/T_C$. Kadanoff and Swift point out, however, that their prediction does not preclude a logarithmic divergence or a cusp in the low frequency shear viscosity of a fluid near the critical point.

The predictions for the temperature dependences of the divergent parts of the thermal conductivity, Eq. (2.223), and the shear viscosity, Eq. (2.224), are valid only if there are no contributions to these quantities from processes which have not been considered. Thus far processes which involve the production of sound waves have not been considered. Since the characteristic frequency for sound waves is c/ξ , which is much higher than s_T^* or s_η^* , contributions to $\Delta\lambda$ or $\Delta\eta$ from processes involving sound waves must be considered. Kadanoff and Swift do consider the contributions to $\Delta\lambda$ from multiple processes which involve the production of sound waves. They find that the process which involves decay by two sound waves does not produce an appreciable contribution to $\Delta\lambda(\mathbf{q},s)$. However, they find that the process which involves decay by three sound waves does produce a contribution. They find that for $q \leq 1/\xi$ and $s \leq c/\xi$:

$$\Delta\lambda_{\text{ppp}}(\mathbf{q},s) \sim \frac{k_B T_C}{c\xi^2} . \quad (2.225)$$

Using Eq. (2.57) for the divergence of ξ , Eq. (2.62) for the approximate divergence of C_p , noting that the low frequency adiabatic sound velocity, c , is proportional to $(\kappa_s)^{-1/2}$, and using Eq. (2.67) to relate the approximate divergence of κ_s to the divergence of C_V , we obtain the result:

$$\Delta\lambda_{\text{ppp}}(0,0) \sim \left(\frac{T - T_C}{T_C}\right)^{-\gamma+2\nu-\alpha/2} . \quad (2.226)$$

From Eq. (2.77) we see that $\gamma - 2\nu \approx 0$; so that the contribution to the divergent part of the thermal conductivity from processes involving sound waves is, at most, weakly divergent.

Kadanoff and Swift also consider the contributions to the divergent part of the shear viscosity, $\Delta\eta$, from processes involving sound waves. For the process which involves decay by three sound waves they find that for $q \leq 1/\xi$ and $s \leq c/\xi$:

$$\Delta\eta_{\text{ppp}}(\mathbf{q}, s) \sim \frac{k_B T_C P}{c \xi^2 C_V} . \quad (2.227)$$

By comparing this expression with Eq. (2.225) and using Eq. (2.58) for the divergence of C_V we obtain the result:

$$\Delta\eta_{\text{ppp}}(0,0) \sim \left(\frac{T - T_C}{T_C}\right)^{-\gamma+2\nu+\alpha/2} . \quad (2.228)$$

We see however, from Eq. (2.77), that since $2\nu \geq \gamma$, that $\Delta\eta_{\text{ppp}}(0,0)$ does not diverge. In other words, there is no contribution to the divergent part of the shear viscosity from processes involving sound waves. We have shown, therefore, that, indeed, η^* does not have a divergent part. The prediction for the temperature dependence of the contribution to the divergent part of the thermal conductivity from the process involving heat flow and viscous flow given in Eqs. (2.222) and (2.223) thus remains intact. Furthermore, by comparing Eqs. (2.223) and (2.226) we see that the temperature dependence of the divergent part of the thermal conductivity is essentially that given by Eq. (2.223).

We may now summarize the predictions of Kadanoff and Swift for the divergent parts of the thermal conductivity and the shear viscosity.

Their predictions apply to three different frequency regions: Low Fre-

quency: $s \leq s_T^* = \frac{\lambda^*}{\rho C_P} \frac{1}{\xi^2}$; Intermediate Frequency: $s_T^* < s \leq s_\eta^* = \frac{\eta^*}{\rho} \frac{1}{\xi^2}$;

High Frequency: $s_\eta^* < s \leq \frac{c}{\xi}$. In the low and intermediate frequency regions, $\Delta\lambda \sim \frac{k_B T \rho C_P}{\eta^* \xi} + \frac{k_B T C_P}{c \xi^2}$. In the high frequency region, $\Delta\lambda \sim \frac{k_B T C_P}{c \xi^2}$.

In the low frequency region, $\Delta\eta \sim \frac{k_B T \rho C_P}{\lambda^* \xi} + \frac{k_B T C_P}{c \xi^2 C_V}$. In the intermediate

and high frequency regions, $\Delta\eta \sim \frac{k_B T C_P}{c \xi^2}$. We see then that at low fre-

quencies the thermal conductivity of a fluid near the critical point contains a divergent part which has a temperature dependence which is essentially governed by the expression $\Delta\lambda \sim \frac{k_B T \rho C_P}{\eta^* \xi}$ where both C_P and ξ are

divergent quantities and ρ , T , and η^* are slowly varying quantities. We

see that Kadanoff and Swift predict that $\frac{\Delta\lambda}{\rho C_P} \sim \frac{k_B T}{\eta^* \xi}$. So we have the pre-

diction that the temperature dependence of the "critical part" of the thermal diffusivity, D_C , is given by:

$$D_C \sim \frac{1}{\xi} \sim \left(\frac{T - T_C}{T_C} \right)^\nu. \quad (2.229)$$

4. Explicit Predictions for the Magnitude and Temperature Dependence of the Critical Part of the Thermal Diffusivity of a Fluid near its Critical Point

The next advance in the development of the mode-mode coupling approach was again due to Kawasaki^{(18), (19)} who, using microscopic kinetic

equations, explicitly calculated the time correlation function for entropy fluctuations and obtained an explicit expression for the decay rate of the entropy fluctuations and hence an explicit expression for the "critical part" of the thermal diffusivity of a pure fluid near the critical point.

Kawasaki points out that his theory is a two-step theory where rapid random motions irrelevant to critical phenomena are incorporated into coefficients in the kinetic equations so that only the dynamical problem which is associated exclusively with the critical fluctuations is left in solving the kinetic equations. It is for this reason that the theory predicts only the "critical part" of any calculated quantity.

Kawasaki begins by introducing the generalized Langevin equation for Brownian motion. For a set of dynamical variables \underline{A}_j the equation is:

$$\frac{d}{dt} \underline{A}(t) = i\Omega \cdot \underline{A}(t) - \int_0^t \phi(s) \cdot \underline{A}(t-s) ds + \underline{F}(t) \quad (2.230)$$

where \underline{A} is a column matrix. In this expression Ω is a matrix having real eigenvalues which give frequencies of collective oscillations such as adiabatic sound waves. The quantity $\underline{F}(t)$ represents the random force acting upon the collective motions. The matrix $\phi(s)$ represents a memory function which contains dissipation. Equation (2.230) was originally derived primarily for the purpose of a statistical-mechanical study of ordinary transport phenomena where the set \underline{A} corresponds to a complete set of ordinary macroscopic variables such as mass density, local velocity, and local temperature, and where $\phi(s)$ has a very short memory. Kawasaki adapts Eq. (2.230) to the study of critical point dynamics. He begins by considering a set of Fourier transformed macroscopic variables, \underline{a}_q^α ,

where q denotes the wavenumber and α denotes a particular variable. Included in a_q^α are all the slowly varying variables including those which exhibit critical point fluctuations. Citing his own previous work⁽¹⁶⁾ and the work of Kadanoff and Swift,⁽¹⁷⁾ Kawasaki points out that in any sensible theory of critical dynamics one must consider products of the a_q^α as well as individual a_q^α since the modes represented by these variables are strongly coupled near the critical point. Thus, in adapting Eq. (2.230) to critical dynamics, the column matrix \underline{A} becomes:

$$\underline{A} = \begin{pmatrix} a_q \\ A_{q'} \end{pmatrix}, \quad (2.231)$$

where $\underline{A}_{q'}$ consists of products of at least two a_q . With this new set of variables Kawasaki shows that Eq. (2.230) becomes:

$$\frac{d}{dt} \underline{a}_q(t) = (i\omega_q - \gamma_q) \cdot \underline{a}_q(t) + (i\Omega_{q'} - \Gamma_{q'}) \cdot \underline{A}_{q'}(t) + \underline{f}_q(t) \quad (2.232)$$

where

$$\gamma_q \equiv \int_0^\infty \phi_q(t) dt \quad (2.233)$$

and

$$\Gamma_{q'} \equiv \int_0^\infty \phi_{q'}(t) dt \quad (2.234)$$

Equation (2.232) is a closed set of kinetic equations governing the slow time evaluation of critical fluctuations $a_q^\alpha(t)$. The rapid random motions have been separated into the damping matrices γ_q and $\Gamma_{q'}$. In order to render the equation useful for applications Kawasaki introduces simplifying assumptions. Noting that the elements of $\Gamma_{q'}$ represent nonlinear transport

coefficients that arise from the rapid random molecular motions of \underline{f}_q , Kawasaki assumes that Γ'_q can be ignored in Eq. (2.232) since such transport coefficients are not expected to be important near the critical point.

Therefore we obtain:

$$\frac{d}{dt} a_q(t) = (i\omega_q - \gamma_q) a_q(t) + i\Omega'_q \cdot A'_q(t) \quad (2.235)$$

as the final general kinetic equation for critical fluctuations which may be applied to specific cases.

We are interested in the dynamics of entropy fluctuations near the liquid-vapor critical point. Applying his general kinetic equation to the case of entropy fluctuations Kawasaki obtains:

$$\frac{d}{dt} S_q(t) = -\frac{q^2 \lambda_0}{C_{Pq}} \delta S_q(t) - \sum_{\sigma} i q^{\sigma} V^{-1/2} \sum_{\mathbf{k}} \delta S_q(t) v_{q-\mathbf{k}}^{\sigma}(t) + f_q^S \quad (2.236)$$

for the kinetic equation for entropy fluctuations, δS_q .

In this expression λ_0 is the non-anomalous part of the thermal conductivity, C_{Pq} is the q -dependent heat capacity per unit volume at constant pressure, V is the volume of the system, f_q^S is the random force acting upon S_q , and $v_q^{\sigma}(t)$ are the transverse components of the local velocity, where $\sigma = x, y, z$. The kinetic equation for $v_q^{\sigma}(t)$ is:

$$\begin{aligned} \frac{d}{dt} v_q^{\sigma}(t) = & -\frac{\eta_0}{\rho} q^2 v_q^{\sigma}(t) - \frac{T}{2\rho V^{1/2}} \sum_{\mathbf{k}} i(k^{\sigma} - \frac{\mathbf{q} \cdot \mathbf{k}}{q}) q^{\sigma} \\ & \cdot \left(\frac{1}{C_{Pk}} - \frac{1}{C_{Pq-k}} \right) \delta S_{\mathbf{k}}(t) \delta S_{q-\mathbf{k}}(t) + f_q^V. \end{aligned} \quad (2.237)$$

In this expression, η_0 is the non-anomalous part of the shear viscosity, ρ is the mass density, and f_q^v is the random force acting upon v_q^σ .

Having obtained the relevant kinetic equations for entropy fluctuations, Kawasaki next seeks to obtain the time correlation function for entropy fluctuations. He finds that

$$\frac{\langle \delta S_q(t) \delta S_q(0) \rangle}{\langle |\delta S_q|^2 \rangle} = e^{-\Gamma_q t} \quad (2.238)$$

where

$$\Gamma_q = \frac{k_B T}{\eta^*} \frac{1}{(2\pi)^3} \int d\mathbf{k} \left[\left(\frac{q}{k}\right)^2 - \left(\frac{q \cdot k}{k^2}\right)^2 \right] \frac{C_P(q-k)}{C_P q} \quad (2.239)$$

so that entropy fluctuations of wavevector q decay exponentially in time with a decay rate given by Γ_q . In the expression for Γ_q the quantity η^* has the same significance as in the Kadanoff and Swift theory, (Eq. (2.221)). Kawasaki evaluates the integral in the expression for Γ_q by assuming an Ornstein-Zernike form for the k -dependent heat capacity. Specifically, he assumes:

$$C_P(q-k) \propto \left[\frac{1}{\xi^2} + (q-k)^2 \right]^{-1} \quad (2.240)$$

where ξ is the Ornstein-Zernike long range correlation length. After performing the integration Kawasaki finds that

$$\Gamma_q = A \xi^{-3} K(q \xi) \quad (2.241)$$

where

$$A = k_B T / 6\pi \eta^* \quad (2.242)$$

and

$$K(q\xi) = \frac{3}{4} \left[1 + q^2 \xi^2 + (q^3 \xi^3 - \frac{1}{q\xi}) \tan^{-1}(q\xi) \right]. \quad (2.243)$$

Kawasaki thus presents us with an explicit expression for the wavevector dependence of the decay rate of thermally excited entropy fluctuations in a pure fluid near its liquid vapor critical point. The expression contains all slowly varying quantities, save one, the long range correlation length, ξ . We see then that the behavior of the decay rate of entropy fluctuations is governed by the behavior of ξ .

We may examine the expression for Γ_q for large and small values of $q\xi$. For $q\xi \gg 1$ the function $K(q\xi)$ becomes

$$K(q\xi) = \frac{3\pi}{8} q^3 \xi^3 + \dots, \quad (2.244)$$

so that for $q\xi \gg 1$,

$$\Gamma_q = \frac{k_B T q^3}{16\pi\eta}. \quad (2.245)$$

This expression is expected to hold very close to the critical point where ξ becomes very large. Now, for $q\xi \ll 1$, the function $K(q\xi)$ becomes:

$$K(q\xi) = q^2 \xi^2 + \frac{3}{5} q^4 \xi^4 + \dots \quad (2.246)$$

so that for $q\xi \ll 1$,

$$\Gamma_q = \frac{k_B T}{6\pi\eta \xi^3} \left[q^2 \xi^2 (1 + \frac{3}{5} q^2 \xi^2) \right]. \quad (2.247)$$

This expression is a prediction for the decay rate of critical entropy fluctuations in the hydrodynamic region; that is, for $q\xi \ll 1$. Previously,

(Eq. (2.128)) we have shown that in the hydrodynamic region the thermal diffusivity, $\frac{\Lambda}{\rho C_P}$, is given by $\frac{\Gamma}{q}$. Therefore, Eq. (2.247) provides us with a prediction for the critical part of the thermal diffusivity, $D_C \equiv \left(\frac{\Lambda}{\rho C_P}\right)_C$. From Eq. (2.247) we obtain

$$\frac{\Gamma}{q} \equiv D_C = \frac{k_B T}{6\pi\eta^* \xi} \left(1 + \frac{3}{5} q^2 \xi^2\right). \quad (2.248)$$

Since $q \xi \ll 1$, we can further simplify the expression so that:

$$D_C = \left(\frac{\Lambda}{\rho C_P}\right)_C = \frac{k_B T}{6\pi\eta^* \xi}. \quad (2.249)$$

We see that this prediction is in agreement with the predictions of Kadanoff and Swift, Eqs. (2.222) and (2.229). We thus have a prediction for the magnitude and temperature dependence of the critical part of the thermal diffusivity of a fluid near its critical point. The validity of this prediction may be checked by using the method of self-beating spectroscopy to measure the correlation function of light scattered from the random thermal isobaric entropy fluctuations in a fluid near its critical point. Equation (2.249) has an appealing physical interpretation. The quantity D_C is the diffusion coefficient for the transfer of heat from one region of space to another. If one regards the flow of heat as taking place by the diffusion of spheres of radius ξ , then, from the Stokes-Einstein relation, we know that the diffusion coefficient of spheres of radius ξ is given by $D = \frac{k_B T}{6\pi\eta \xi}$. We may thus regard the diffusion of heat as occurring by means of the spatial diffusion of regions of radius ξ .

We may remark that Swift⁽²⁰⁾ has shown that the calculation of the

decay rate of entropy fluctuations in a pure fluid near its liquid-vapor critical point is analogous to the calculation of the decay rate of concentration fluctuations in a binary liquid mixture near its critical mixing point. Therefore, in analogy with Eq. (2.249), we may write:

$$(D_m)_C = \frac{k_B T}{6\pi\eta^* \xi} \quad (2.250)$$

where D_m is the solute particle diffusion coefficient in the binary mixture. Kawasaki thus predicts that particle diffusion in a binary mixture occurs by means of the diffusion of regions of spatial extent ξ . Ferrell,⁽²¹⁾ using the general expression given in Eq. (2.159) for transport coefficients as his starting point, has also calculated the solute particle diffusion coefficient in a binary liquid mixture near its critical mixing point. He obtains a result identical to that given in Eq. (2.250).

Most recently, the mode-mode coupling approach has been further refined by Kawasaki and Lo.⁽²²⁾ With this refinement, the decay rate for critical entropy fluctuations in a pure fluid near its liquid-vapor critical point is:

$$\Gamma_q = A' \xi^{-3} K(q\xi) C(q\xi) \quad (2.251)$$

where

$$A' = \frac{k_B T}{6\pi\eta(T)} \quad (2.252)$$

and $K(q\xi)$ is given in Eq. (2.243). Comparing Eqs. (2.251) and (2.252) with Eqs. (2.241) and (2.242), we see that

$$C(q, \xi) = \frac{\eta(T)}{\eta^*} \quad . \quad (2.253)$$

In these expressions $\eta(T)$ is the temperature dependent, macroscopically measured, hydrodynamic shear viscosity. Kawasaki and Lo show that, in the hydrodynamic region, $\frac{\eta(T)}{\eta^*} = 1.055$. With this refinement, the mode-mode coupling prediction for the magnitude and temperature dependence of the critical part of the thermal diffusivity in the hydrodynamic region for a pure fluid near its critical point becomes:

$$D_C = \left(\frac{\Lambda}{\rho C_P}\right)_C = \frac{k_B T}{6\pi \left(\frac{\eta(T)}{1.055}\right) \xi} \quad . \quad (2.254)$$

Each of the quantities appearing in Eq. (2.254) may be determined from experimental measurements. Once they have been determined one is able to check the validity of this essential prediction of the mode-mode coupling approach for the behavior of the dynamic properties of a fluid near its liquid-vapor critical point.

References For Chapter II

1. L. D. Landau and E. M. Lifshitz, Statistical Physics, (Addison-Wesley, Reading, Mass., 1958).
2. G. B. Benedek, in Statistical Physics, Phase Transitions and Superfluidity, edited by M. Chretien et al. (Gordon and Breach, New York, 1968). Vol. 2, p. 1.
3. H. E. Stanley, Introduction to Phase Transitions and Critical Phenomena, (Oxford University Press, New York, 1971).
4. M. E. Fisher, J. Math. Phys. 5, 944 (1964).
5. L. S. Ornstein and F. Zernike, Proc. Acad. Sci. Amsterdam 17, 793 (1914); Physik Z. 19, 134 (1918).
6. L. P. Kadanoff et al., Rev. Mod. Phys. 39, 395 (1967).
7. B. Widom, J. Chem. Phys. 43, 3898 (1965).
8. P. Schofield, J. D. Litster and J. T. Ho, Phys. Rev. Letters 23, 1098 (1969).
9. L. Brillouin, Ann. de Physique 17, 88 (1922).
10. L. Landau and G. Placzek, Physik Z. Sowjetunion 5, 173 (1934).
11. L. Onsager, Phys. Rev. 38, 2265 (1931).
12. F. Reif, Fundamentals of Statistical and Thermal Physics, (McGraw-Hill, New York, 1965).
13. G. B. Benedek, in Matiere et Rayonnement, Livre de Jubile l'honneur du Professeur A. Kastler, edited by the French Physical Society (Presses Universitaires de France, Paris, France, 1969), pp. 49-84.
14. J. B. Lastovka, Ph. D. Thesis, Department of Physics, M. I. T., 1967, (unpublished).
15. M. Fixman, J. Chem. Phys. 36, 310 (1962).
16. K. Kawasaki, Phys. Rev. 150, 291 (1966).
17. L. P. Kadanoff and J. Swift, Phys. Rev. 166, 89 (1968).

18. K. Kawasaki, Ann. Phys. 61, 1 (1970).
19. K. Kawasaki, Phys. Rev. A 1, 1750 (1970).
20. J. Swift, Phys. Rev. 173, 257 (1968).
21. R. Ferrell, Phys. Rev. Letters 24, 1169 (1970).
22. K. Kawasaki and S. Lo, Phys. Rev. Letters 29, 48 (1972).

Chapter III

EXPERIMENTAL APPARATUS AND METHODS

A. Introduction

In this chapter we shall discuss the apparatus and methods used to obtain measurements of quantities which were relevant to the particular experimental study of liquid-vapor critical point phenomena described in this thesis. In particular we shall discuss the apparatus and methods used to obtain measurements of the following quantities:

- (1) the sample temperature (T).
- (2) the sample pressure (P).
- (3) the sample density (ρ).
- (4) the scattering vector (q).
- (5) the ratio of scattered power to incident power, P_S/P_I .
- (6) the frequency spectrum and the time correlation function of the light scattered quasielastically from the thermally excited entropy fluctuations in the sample.

B. The Sample

We shall begin our discussion by focussing on the sample itself. All measurements described in this thesis were carried out on a single sample of sulfur hexafluoride, SF_6 , contained in a sealed chamber. The sample was obtained from a cylinder of Air Products and Chemicals instrument-grade SF_6 with an estimated impurity content of less than 20ppm. SF_6 was used in this study of liquid-vapor critical point phenomena for two reasons: (1) SF_6 molecules are non-polar and spherically symmetric,

thus satisfying the criterion that the study involve a simple, inert sample and (2) SF_6 has convenient critical properties: $T_C = 45.557^\circ\text{C}$, $P_C = 37.11 \text{ atm.}$; $\rho_C = 0.732 \text{ gm/cm}^3$; thus easing the experimental difficulties involved in leak prevention and temperature control.

C. The Sample Chamber

In Fig. 3.1 is shown a schematic, cross-sectional top view of the sample chamber. In Fig. 3.2 is shown a view of the sample chamber that is observed when one looks head-on through the entrance window.

The main body of the sample chamber as well as the two end flanges were constructed from beryllium copper which was chosen because of its strength and high thermal conductivity. The main body of the sample chamber was drilled out to a diameter of 1.0". A cylindrical spacer, 2" in length, also constructed of beryllium copper, fills the hole. A cross-sectional view of this spacer is shown in Fig. 3.2. The height of the oblong-shaped open region in the spacer is 0.233", while the width of this region is 0.750". The main function of the spacer in the sample chamber is to decrease the volume of SF_6 needed to fill the chamber and especially to decrease the height of the column of SF_6 that is observed during experimentation. It is advantageous to decrease the height so that the gravitationally induced density gradient in the sample becomes less severe near the critical point.

The hole, containing the spacer, through the main body of the sample chamber is terminated at each end by a highly polished optical quartz window (Schott BK7). The absolute refractive index of the windows at

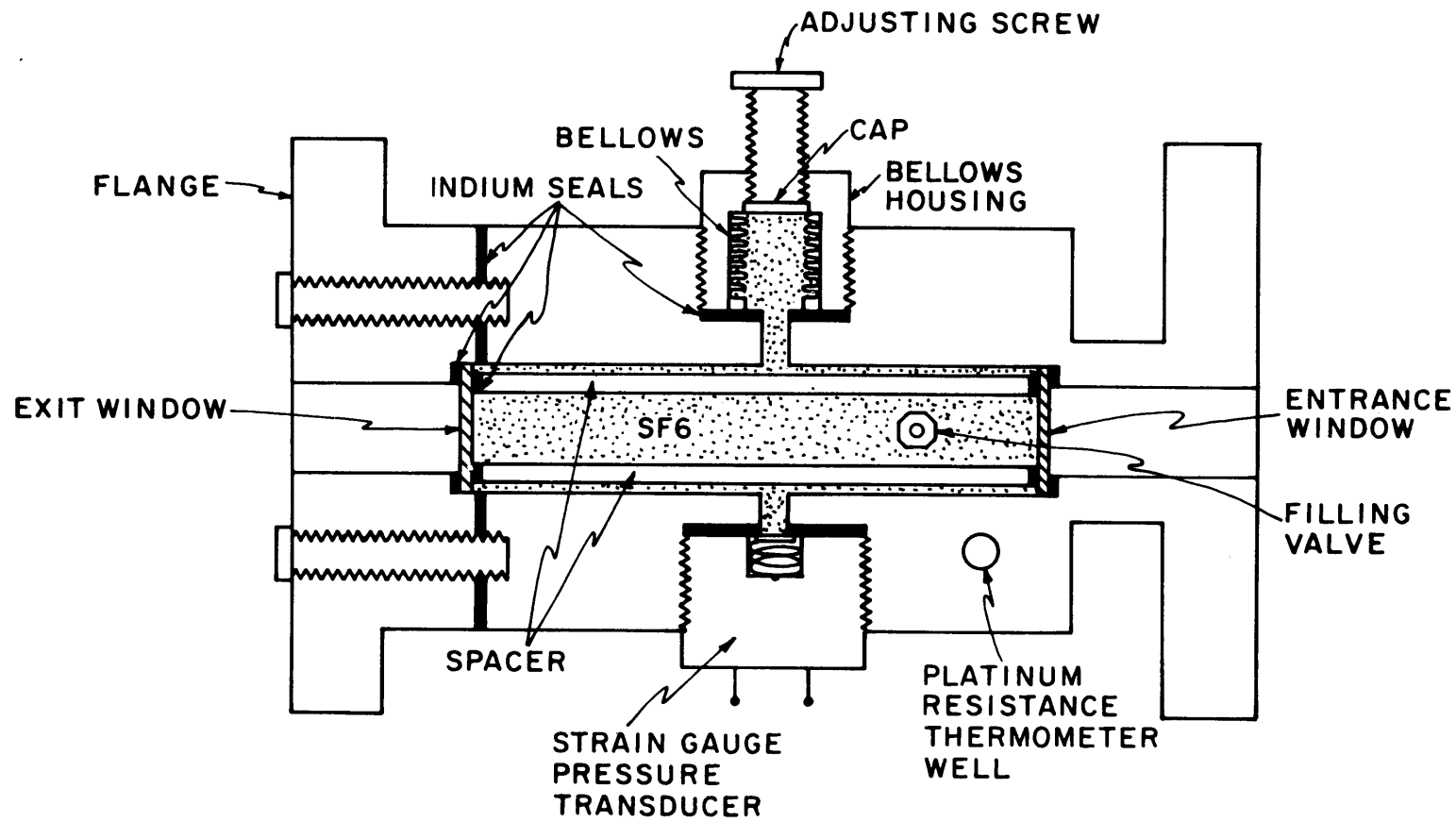


Fig. 3.1 Schematic Top View of the Sample Chamber

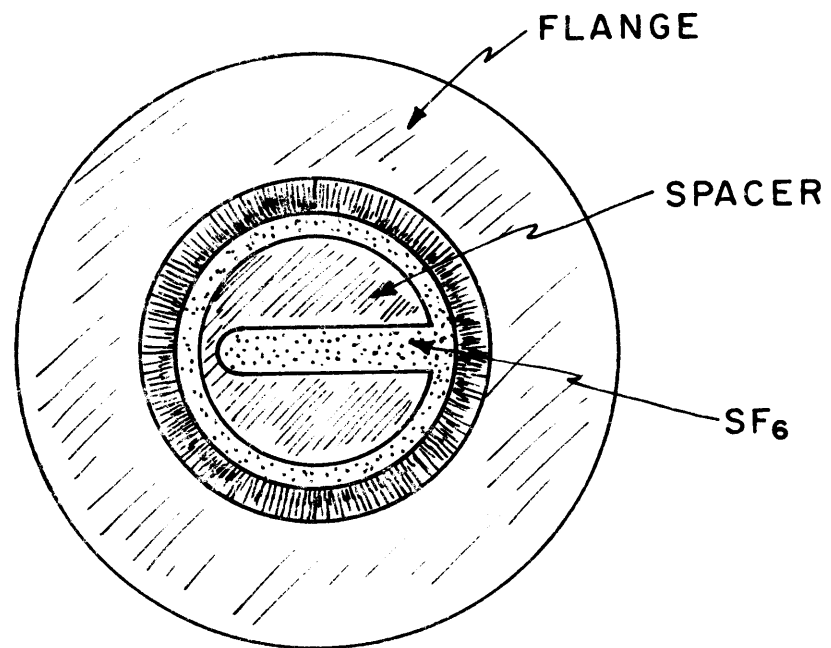


Fig. 3.2 Schematic End View of the Sample Chamber

45°C and at a wavelength of 6328Å is 1.5155. The windows were sealed to the chamber using pure indium as a packing material. The design was such that the pressure exerted by the SF₆ sealed the windows securely against the chamber. Indium was also used to seal all the other joints between the main body of the chamber and its appendages.

Another hole, 1.75" deep and 0.25" in diameter, was drilled into the body of the sample chamber from the top. This hole was used as a well to accommodate the platinum resistance thermometer used to measure the sample chamber temperature.

SF₆ was admitted into the sample chamber through a Whitey valve which was tapped into the top of the chamber. The valve was constructed of stainless steel and contained teflon packing which was in contact with the SF₆ while the chamber was being filled but which was isolated from the SF₆ when the valve was closed.

One side of the sample chamber was machined out to accommodate a Baldwin-Lima-Hamilton strain-gauge pressure transducer. The voltage across the output terminals of this device is related to the strain impressed on its sensing element which arises from the pressure exerted by the SF₆ sample.

The other side of the sample chamber was machined out to accommodate a bellows assembly. The bellows itself was constructed of stainless steel and was purchased from the Robertshaw Bellows Company. The bellows has a mean radius of 0.375" and a mean length of 0.875". A stainless steel end cap of diameter 0.75" was silver soldered to the bellows. The bellows is able to be compressed by means of a .75" diameter screw with 40 turns/inch. The assembly is surrounded by a beryllium copper housing.

The bellows was used to adjust the sample density by adjusting the total volume available for a given mass of SF_6 . From the mean length and mean radius of the bellows we obtain that the volume available for the SF_6 in the bellows is 0.39 in^3 . From the dimensions of the open region of the spacer; i.e., $2.0" \times 0.75" \times 0.233"$, we obtain that the volume available for the SF_6 in the main body of the sample chamber is $.35 \text{ in}^3$. Since the remainder of the volume available for the SF_6 in the sample chamber is very small, we see that the total volume of SF_6 is approximately 0.75 in^3 .

From the dimensions of the bellows and the pitch of the adjusting screw we see that one turn of the screw changes the volume by 0.011 in^3 . Therefore one turn of the bellows adjusting screw changes the density of the SF_6 by approximately 1.5%.

D. Control and Measurement of the Sample Temperature

Having described the sample and the sample chamber, we shall next discuss the control and measurement of the sample temperature.

1. Temperature Control

In Fig. 3.3 is shown a schematic diagram of the temperature control system. The sample chamber was mounted inside a rectangular copper box. Plexiglass was used between the flanges of the sample chamber and the box in order to thermally isolate the chamber from the box. The box was mounted on top of a multi-layered plexiglass base plate in order to thermally isolate the box from its surroundings. The box was fitted with a plexiglass top.

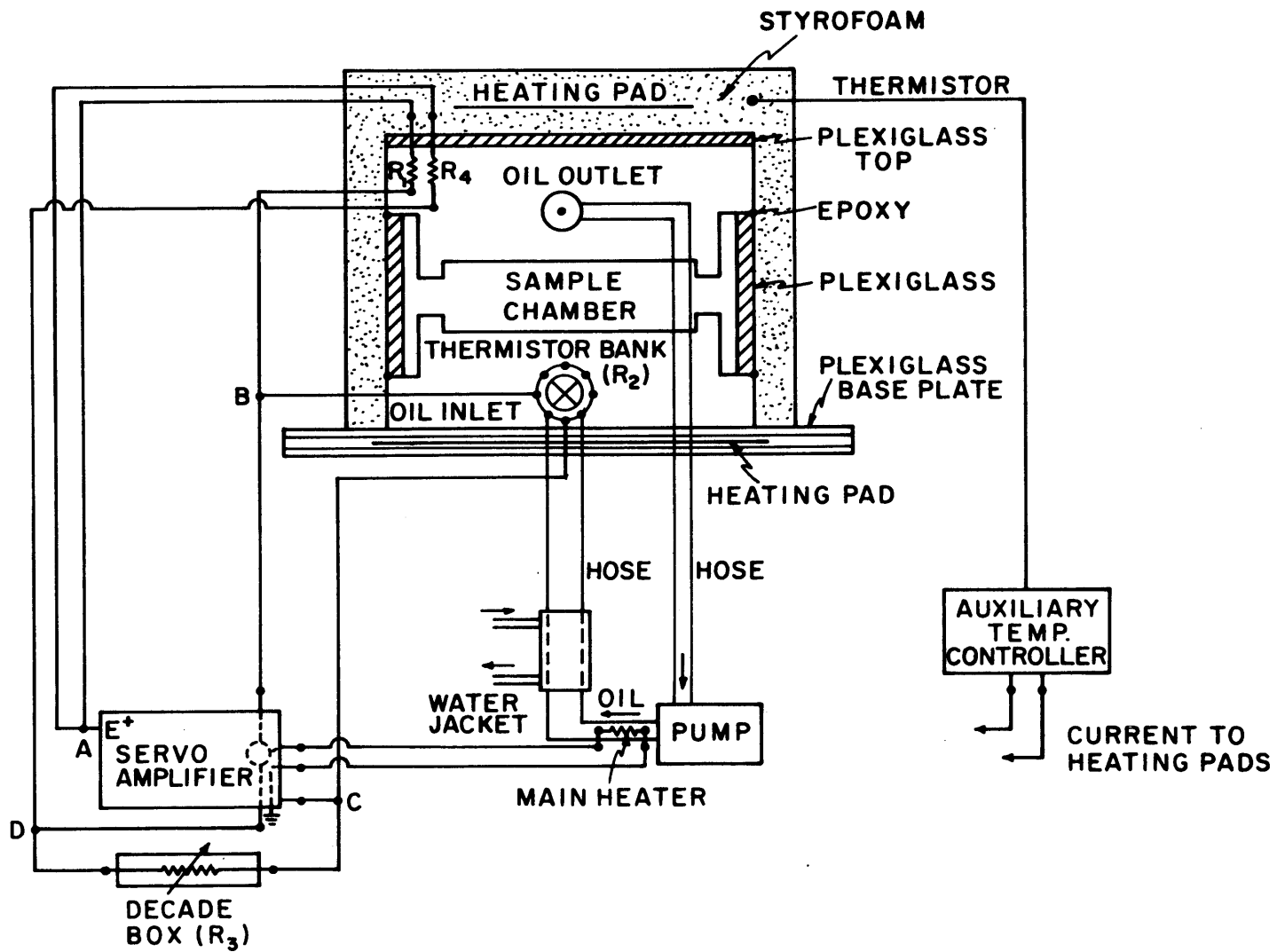


Fig. 3.3 Schematic Diagram of the Temperature Control System

Silicone oil was pumped into the box through the inlet port shown in the figure, and returned to the pump through the outlet port. A series of baffles was placed in the box to insure effective circulation of the oil around the sample chamber. The silicone oil was prevented from seeping into the ports leading to the entrance and exit windows of the sample chamber by means of epoxy seals at the joints between the flange, the plexiglass, and the box.

The primary control of the sample temperature was accomplished by controlling the temperature of the circulating silicone oil. A bank of thermistors, connected in parallel, was mounted at the inlet port of the box. In general, the resistance of a thermistor decreases as its temperature increases. Specifically, the resistance-temperature relation for a thermistor is given by:

$$\frac{R(T)}{R(T_0)} = e^{\beta(T)\left(\frac{1}{T} - \frac{1}{T_0}\right)} \quad (3.1)$$

For the thermistor bank the quantity $\beta(T)$ was a slowly varying function of temperature increasing in value from 3910°K at 317.7°K , about 1°K below the critical temperature, T_C , to 3918°K at 321.1°K , about 2.4°K above T_C , which was the temperature range covered in the experiments. A typical resistance value for the thermistor bank is $R(310.5^\circ\text{K}) = 618.2\Omega$.

The thermistor bank formed one arm of a simple four-arm resistance bridge. In Fig. 3.4 is shown a block diagram of this feedback circuit. The thermistor bank is labelled R_2 in Figs. 3.3 and 3.4. The other arms of the bridge were formed by two fixed value resistors, labelled R_1 and R_4 in Figs. 3.3 and 3.4 and by a General Radio decade resistance box,

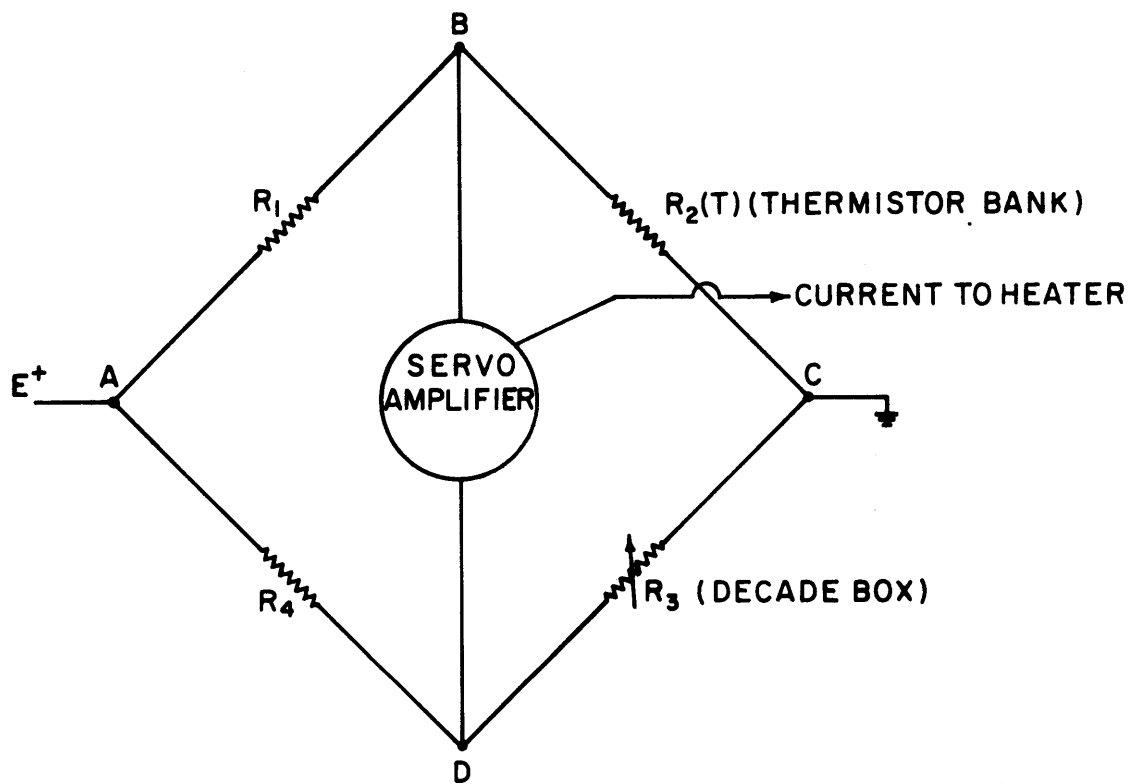


Fig. 3.4 Temperature Control Feedback Circuit

labelled R_3 in Figs. 3.3 and 3.4. The resistance box could be pre-set to a 0.01Ω precision. The fixed resistors as well as most of the resistance of the decade box were immersed in the box housing the circulating oil to eliminate changes in their resistances due to fluctuations in room temperature.

Temperature control of the circulating oil was achieved in the following way. From Fig. 3.4 we see that if the resistances $(R_1 + R_2)$ and $(R_3 + R_4)$ are not equal, then a current will flow between points B and D through the servo amplifier. This current is amplified and delivered to the main heater which is located inside the tubing leading from the pump. The heated oil is cooled somewhat by coming in contact with a water jacket through which tap water is circulated. The thermistor bank resistance responds to the new oil temperature. At a given setting of the decade box a steady state condition is reached $(R_1 + R_2) > (R_3 + R_4)$ so that just enough heat is continuously supplied to the oil to maintain it at the desired temperature. Fluctuations in the oil temperature are sensed by the thermistor bank. The fluctuations are compensated for by an appropriate increase or decrease of heat supplied to the oil.

The temperature of the oil was changed by merely setting a new value on the decade box. The decade box settings ranged from 410Ω at 2.4°K above T_c to 468Ω at 1°K below T_c . In this temperature range the variation of decade box resistance with sample temperature was approximately $17\Omega/^\circ\text{K}$. With this sensitivity and with the 0.01Ω precision of the decade box we see that the sample temperature could easily be pre-set to $\pm 0.001^\circ\text{K}$.

In order to decrease heat loss to the surroundings, the box housing the circulating oil was covered on all four sides and on top with thick styrofoam insulation. Slots were cut in the styrofoam to allow the passage of light into and out of the sample chamber. To further decrease heat loss to the surroundings, heating pads were inserted into the styrofoam at the top and at the bellows side of the sample chamber. An additional heating pad was sandwiched between two layers of the plexiglass base plate. It was desired that the temperature in the vicinity of the heating pads be brought close to the temperature of the circulating oil. This was accomplished to an accuracy of $\pm 1^{\circ}\text{K}$ by means of an auxiliary temperature controller which used a thermistor as its sensing element.

In the course of the experiments it was found that not only could the sample temperature be preset to $\pm 0.001^{\circ}\text{K}$, but also the sample temperature could be maintained for several days to $\pm 0.001^{\circ}\text{K}$. Also, visual observation of the sample very close to the critical point yielded no evidence that temperature gradients might be present. If temperature gradients were present then convective motion possibly accompanied by boiling in the liquid phase or condensation of droplets in the vapor phase would have been observed.

2. Temperature Measurement

The temperature of the sample chamber was measured using a Leeds and Northrup platinum resistance thermometer which was inserted into the well shown in Fig. 3.1. The thermometer was calibrated by the Leeds and Northrup Standardizing Laboratory against secondary standards furnished

by the National Bureau of Standards in accordance with the 1948 International Practical Temperature Scale. The resistance-temperature relation for a platinum resistance thermometer is given by the Callender-van Dusen equation:

$$\frac{R(T)}{R(0)} = 1 + At + Bt^2 \quad (3.2)$$

In this relation, t is the temperature in $^{\circ}\text{C}$, $R(0)$ is the resistance of the thermometer at 0°C and $R(T)$ is the resistance at $T^{\circ}\text{C}$. For the thermometer used in the experiments, $A = 3.985017 \times 10^{-3}$ and $B = -5.856693 \times 10^{-7}$.

The quantity $R(0)$ was determined and periodically checked by inserting the thermometer into a standard triple point of water cell, $T = 0.01^{\circ}\text{C}$. $R(0)$ was found to be 25.545Ω .

The thermometer was equipped with four leads; two of the leads allowed current to pass through the thermometer, and the other two allowed measurement of the voltage across the thermometer. The resistance of the thermometer was determined by comparing its resistance to that of a standard resistor. The value of the standard resistor at $T = 25^{\circ}\text{C}$ was 9.99994Ω . The comparison was achieved by connecting the thermometer and the standard resistor in series, thus insuring that the same current, 2 ma, was passing through each. The voltage appearing across the thermometer was then compared to that appearing across the standard resistor using a Leeds and Northrup model K-5 potentiometer. The variation of resistance with temperature for the standard resistor was also determined and, during each measurement of the sample chamber temperature, the temperature of the standard resistor was also measured and the appropriate standard resistance was used.

With the K-5 potentiometer voltages could be measured with a precision of $\pm 0.1 \mu\text{V}$. In the temperature range covered in the experiments, the voltage across the thermometer changed with temperature by $0.2 \mu\text{V}/0.001^\circ\text{K}$. Thus the temperature of the sample chamber could be easily measured with an absolute accuracy of $\pm 0.001^\circ\text{K}$.

E. Measurement of the Sample Pressure

The pressure exerted by the SF_6 sample was measured by means of the Baldwin-Lima-Hamilton strain-gauge pressure transducer shown in Fig. 3.1. The voltage appearing across the output terminals of this device is related to the pressure exerted on its sensing element by:

$$\frac{V}{V_0} = A\left(\frac{P}{P_{\max}}\right) + B\left(\frac{P}{P_{\max}}\right)^2 \quad (3.3)$$

The values of the coefficients were $A = 2.968 \times 10^{-3}$ and $B = 3 \times 10^{-5}$.

The voltage reference value was $V_0 = 0.9\text{V}$ and the maximum pressure tolerated by the device was $P_{\max} = 750 \text{ psi}$.

The sample pressure was determined by comparing the voltage appearing across the pressure transducer to the reference voltage using a Leeds and Northrup model K-5 potentiometer. In the pressure range covered in the experiments, the voltage across the transducer changed with pressure by about $4 \mu\text{V}/\text{psi}$. Since voltages could be measured with the K-5 potentiometer with a precision of $\pm 0.1 \mu\text{V}$, the sample pressure could be determined with a precision of $\pm 0.025 \text{ psi}$.

Although a given measurement of the sample pressure could be performed with a high degree of precision it was observed that measurements

of the sample pressure were not reproducible over times as short as one day. Instead, when the sample pressure was held constant by maintaining a constant sample temperature and density, the measured sample pressure was observed to rise linearly with time. Hence, at any time, the measured sample pressure was always greater than the actual sample pressure. It was assumed that the time drift was attributable to mechanical hysteresis in the strain gauge.

Because of the pressure transducer time drift no attempt was made in the course of the experiments to perform absolute measurements of the sample pressure. Indeed, at the conclusion of the experiments it was estimated that the measured sample pressure was 24.3 psi greater than the actual sample pressure.

Instead, as will be shown, what was determined were the relative changes in the sample pressure as the temperature and density of the sample were changed. These relative pressure measurements were accurately obtained by determining and then applying appropriate corrections for the time drift of the pressure transducer. Specifically, during measurements along the critical isochore of SF_6 , it was found that the drift was 0.074 psi/day. During measurements along the coexistence curve of SF_6 , it was found that the drift was 0.046 psi/day. With the application of these corrections relative pressure measurements were made with an accuracy of $\pm 1.5\%$.

F. Measurement of the Sample Density

Having described the apparatus and methods used to obtain measurements of the sample temperature and pressure, we shall next discuss the techniques used to obtain measurements of the sample density.

1. Optical Measurement of the Absolute Density

We shall begin by describing a technique which may be used to obtain absolute measurements of the sample density. In general, for a dielectric medium, the refractive index, n , and the density, ρ , are related by the Lorentz-Lorenz equation:⁽¹⁾

$$\frac{n^2 - 1}{n^2 + 2} \frac{1}{\rho} = L, \quad (3.4)$$

where L is approximately constant for all densities ranging from dilute gas densities to saturated liquid densities. The Lorentz-Lorenz constant, L , was obtained for SF_6 using the refractive index data of Francis⁽²⁾ and the density data of Otto and Thomas.⁽³⁾ At 20°C the density of saturated liquid SF_6 is 1.39 gm/cm^3 while the refractive index is 1.170. Using these values we obtain $L = 0.0788 \text{ cm}^3/\text{gm}$. We see then that a measurement of the refractive index of the sample allows us to determine the sample density.

In Fig. 3.5 is shown a schematic representation of the technique used to measure the refractive index of the SF_6 sample. The incident beam of intensity P_0 strikes the entrance window of the sample chamber with an angle of incidence θ_1 . At the air-glass interface the beam undergoes a reflection at an angle θ_1 as well as a refraction in the glass medium at an angle θ_2 . The incident beam is polarized perpendicular to the plane of incidence so that according to the Fresnel reflection formula⁽⁴⁾ the intensity of the beam reflected from the air-glass interface is

$$P_1 = R_{12}P_0 \quad (3.5)$$

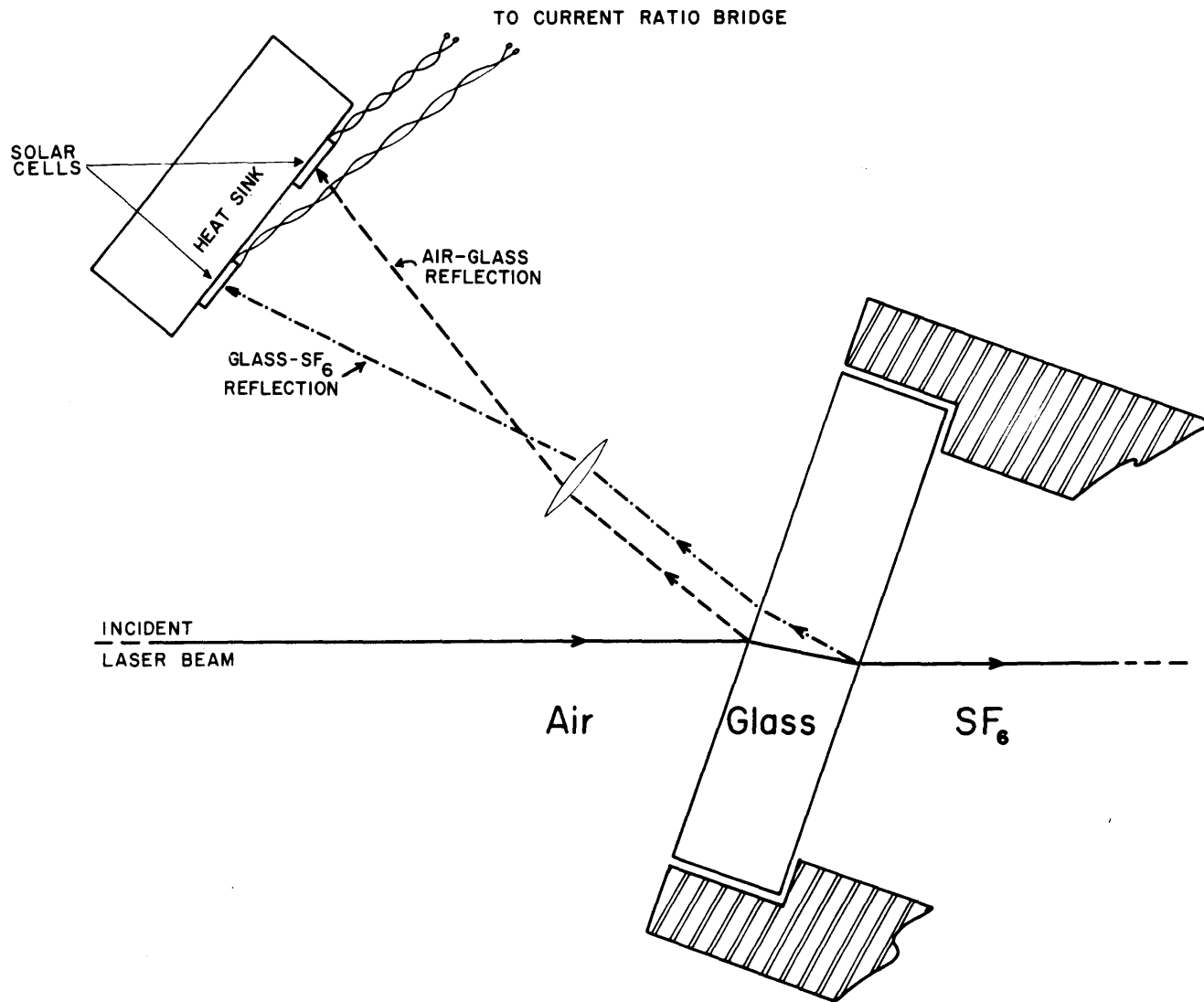


Fig. 3.5 Optical Measurement of the SF₆ Refractive Index

where

$$R_{12} = \frac{\sin^2(\theta_1 - \theta_2)}{\sin^2(\theta_1 + \theta_2)} . \quad (3.6)$$

Now, the intensity of the beam travelling through the glass at angle θ_2 is $(1 - R_{12})P_0$. This beam strikes the glass-SF₆ interface and undergoes a reflection at angle θ_2 as well as a refraction at an angle θ_3 in the SF₆ medium. Again applying the Fresnel reflection formula we see that the intensity of the beam reflected from the glass-SF₆ interface is

$$P' = R_{23}(1 - R_{12})P_0 \quad (3.7)$$

where

$$R_{23} = \frac{\sin^2(\theta_2 - \theta_3)}{\sin^2(\theta_2 + \theta_3)} . \quad (3.8)$$

This reflected beam strikes the air-glass interface and undergoes another reflection back into the glass at angle θ_2 as well as a refraction at angle θ_1 back out into the air. The intensity of the beam reflected back into the glass is $R_{12}P'$ so that the intensity of the refracted beam finally emerging into the air is

$$P_2 = (1 - R_{12})P' = R_{23}(1 - R_{12})^2P_0 \quad (3.9)$$

From Eqs. (3.5) and (3.9) we see that the ratio of the intensities of the two beams reflected from the front and back faces of the entrance window is

$$\frac{P_2}{P_1} = R_{23} \frac{(1 - R_{12})^2}{R_{12}} . \quad (3.10)$$

We may relate R_{12} and R_{23} to the refractive indices of the air, glass, and SF_6 media by applying Snell's law. We have:

$$\theta_2 = \sin^{-1}\left(\frac{n_1}{n_2} \sin \theta_1\right) \quad (3.11)$$

and

$$\theta_3 = \sin^{-1}\left(\frac{n_2}{n_3} \sin \theta_2\right) \quad , \quad (3.12)$$

where n_1 = refractive index of air, n_2 = refractive index of glass, and n_3 = refractive index of SF_6 . Now, since θ_1 may be measured and n_1 and n_2 are known, we are able to calculate R_{12} . Further, using Eqs. (3.8), (3.10) and (3.12) we may relate n_3 to P_2/P_1 . Thus, a measurement of the ratio P_2/P_1 allows us to obtain the refractive index, n_3 , of the SF_6 sample. The refractive index may then be used in Eq. (3.4) to obtain the density of the sample.

In order to measure the ratio P_2/P_1 the reflected beams are focussed by a lens onto two solar cells as shown in Fig. 3.5. Each solar cell emits a current which is directly proportional to the intensity of light incident on its surface. In Fig. 3.6 is shown a schematic diagram of the current ratio bridge circuit used to measure the ratio P_2/P_1 . A Keithley microvoltmeter was used to measure the voltage across a General Radio decade resistance box. The current $i_2 = AP_2$ passes through the entire resistance, while the current $i_1 = AP_1$ passes through some fraction, β , of the entire resistance. The fraction, β , is adjusted until one measures zero voltage. Under the zero voltage condition,

$$i_2(1 - \beta)R + (i_2 - i_1)\beta R = 0 \quad (3.13)$$

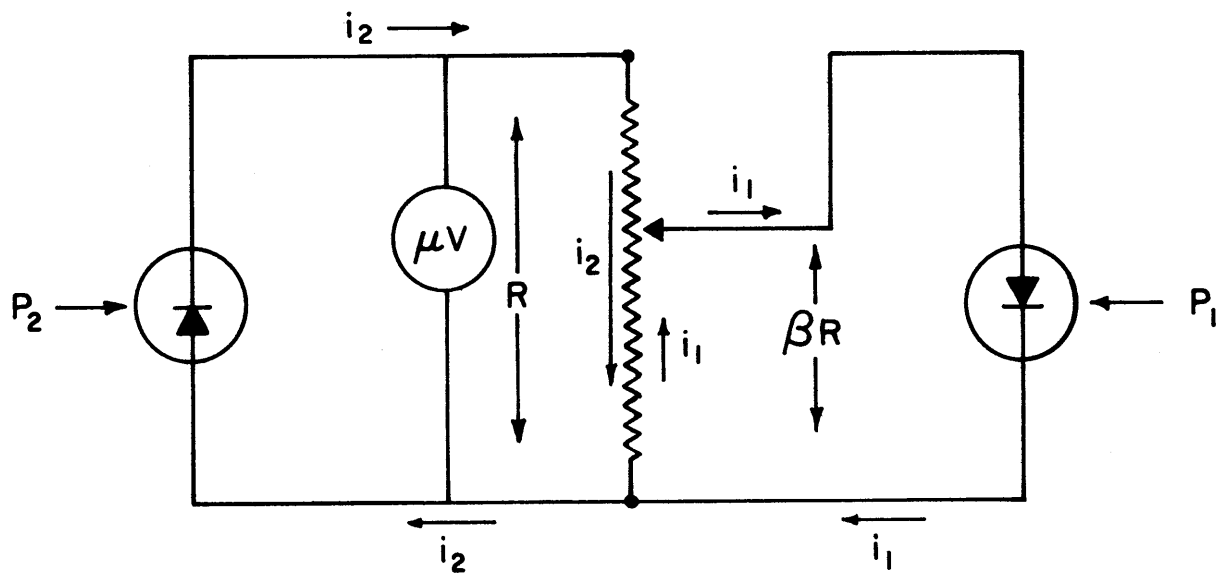


Fig. 3.6 Current Ratio Bridge Circuit

so that

$$\beta = \frac{i_2}{i_1} = \frac{P_2}{P_1} \quad . \quad (3.14)$$

We see then that a measurement of the fraction β allows us to obtain the ratio P_2/P_1 which ultimately allows us to obtain the density of the SF_6 sample.

2. Measurement of the Density Relative to ρ_C by Meniscus Height

Observations

Having described the technique which may be used in general to obtain absolute measurements of the sample density, we shall next describe a more precise technique which was used in the course of the experiments to determine the density of the sample relative to the critical density, ρ_C . This technique involves the observation of the height of the liquid level (the meniscus) in the SF_6 sample as a function of temperature below the critical temperature, T_C .

In order to predict the variation of meniscus height with temperature we may begin by considering that our sample is enclosed in a chamber of total height, H , and cross-sectional area, A . We will assume that both the liquid and gas phases are present. The liquid fills the chamber to a height h . The gas fills the remainder of the chamber. Therefore, we may write:

$$\rho_\ell hA + \rho_g(H - h)A = \rho HA \quad , \quad (3.15)$$

where ρ_ℓ is the liquid density, ρ_g is the gas density, and ρ is the average sample density. We may introduce the critical density, ρ_C , into the expression by writing:

$$(\rho_l - \rho_C)h + (\rho_g - \rho_C)(H - h) = (\rho - \rho_C)H . \quad (3.16)$$

Now, in Eq. (2.46) it was shown that the temperature-density relation for the coexisting phases near the critical point is:

$$\frac{\rho_l - \rho_g}{2\rho_C} = \frac{B}{2} \left(\frac{T_C - T}{T_C} \right)^\beta . \quad (3.17)$$

Further, because the coexistence curve is not symmetric about ρ_C , but is instead symmetric about the line of rectilinear diameters, one has the relation

$$\frac{\rho_l + \rho_g}{2\rho_C} = 1 + D \left(\frac{T_C - T}{T_C} \right) . \quad (3.18)$$

The coefficients B and D and the critical exponent β have been measured for SF_6 by Saxman⁽⁵⁾ who found:

$$\frac{\rho_l - \rho_g}{2\rho_C} = 1.81 \epsilon^{0.333} \quad (3.19)$$

and

$$\frac{\rho_l + \rho_g}{2\rho_C} = 1 + 0.60 \epsilon \quad (3.20)$$

where

$$\epsilon \equiv \left(\frac{T_C - T}{T_C} \right) .$$

To explicitly relate meniscus height to temperature we begin by noting that from Eq. (3.17) we have

$$\rho_l = \rho_C B \epsilon^\beta + \rho_g . \quad (3.21)$$

Inserting this result in Eq. (3.20) yields

$$\rho_g = \rho_C [1 + .6\epsilon - \frac{1}{2} B\epsilon^\beta] \quad . \quad (3.22)$$

Similarly, from Eq. (3.17) we have

$$\rho_g = \rho_\ell - \rho_C B\epsilon^\beta \quad . \quad (3.23)$$

Inserting this result in Eq. (3.20) yields

$$\rho_\ell = \rho_C [1 + .6\epsilon + \frac{1}{2} B\epsilon^\beta] \quad . \quad (3.24)$$

Inserting Eqs. (3.22) and (3.24) into Eq. (3.15) yields:

$$\begin{aligned} \rho_C [1 + .6\epsilon + \frac{1}{2} B\epsilon^\beta] h + \rho_C [1 + .6\epsilon - \frac{1}{2} B\epsilon^\beta] H \\ - \rho_C [1 + .6\epsilon - \frac{1}{2} B\epsilon^\beta] h = \rho H \quad . \end{aligned} \quad (3.25)$$

Subtracting the quantity $\rho_C H$ from each side yields

$$\begin{aligned} \rho_C [1 + .6\epsilon + \frac{1}{2} B\epsilon^\beta - 1] h + \rho_C [1 + .6\epsilon - \frac{1}{2} B\epsilon^\beta - 1] H \\ - \rho_C [1 + .6\epsilon - \frac{1}{2} B\epsilon^\beta - 1] h = (\rho - \rho_C) H \quad . \end{aligned} \quad (3.26)$$

Simplifying, we obtain

$$\frac{(\rho - \rho_C)}{\rho_C} H = B\epsilon^\beta h + .6\epsilon H - \frac{1}{2} B\epsilon^\beta H \quad . \quad (3.27)$$

Simplifying further we obtain

$$\frac{h}{H} = \frac{(\rho - \rho_C)}{\rho_C} \frac{\epsilon^{-\beta}}{B} + \frac{1}{2} - \frac{.6\epsilon^{1-\beta}}{B} \quad . \quad (3.28)$$

From Eq. (3.28) we see that the relative height of the meniscus depends upon the average density of the sample relative to ρ_C and the temperature of the sample relative to T_C . If we consider the change in height, Δh , with a change in temperature we may write

$$\frac{\Delta h}{H} = \left(\frac{\rho - \rho_C}{\rho_C} \right) \frac{\Delta(\epsilon^{-\beta})}{B} - \frac{.6}{B} \Delta(\epsilon^{1-\beta}) \quad (3.29)$$

We may re-write Eq. (3.29) as

$$\frac{\Delta h}{\Delta(\epsilon^{-\beta})} = \frac{H}{B} \left(\frac{\rho - \rho_C}{\rho_C} \right) - \frac{.6H}{B} \Delta\epsilon \quad , \quad (3.30)$$

or,

$$\frac{\rho - \rho_C}{\rho_C} = \frac{\Delta h}{\Delta(\epsilon^{-\beta})} \frac{B}{H} + .6(\Delta\epsilon) \quad . \quad (3.31)$$

From Eq. (3.31) we see that the quantity $\left(\frac{\rho - \rho_C}{\rho_C} \right)$ may be determined by measuring the meniscus height at a number of temperatures and computing the slope, $\Delta h / \Delta(\epsilon^{-\beta})$.

Measurements of the meniscus position in the SF_6 sample were made using a 30X telescope in a cathetometer. The relative position, h , was determined with an accuracy of ± 0.001 ". Using $B = 3.62$ and the measured height of the sample chamber, $H = 0.233$ ", in Eq. (3.31), we may estimate that the quantity $\frac{\rho - \rho_C}{\rho_C}$ can be determined to $\pm 0.1\%$.

In the course of the experiments the density of the SF_6 sample was brought to within 0.1% of ρ_C by adjusting the bellows and measuring the result using the technique of meniscus height observation.

3. The Question of Density Gradients

Having discussed the techniques used to obtain measurements of the sample density, we shall next briefly discuss the problem of density gradients. We have seen that, near its critical point, the isothermal compressibility, κ_T , of a simple fluid becomes very large. We may easily show that, when κ_T is very large, a very large density gradient

is produced in the fluid. We begin by assuming that the sample is contained in a chamber of height H . The pressure at the bottom of the chamber is greater than the pressure at the top of the chamber by the amount $\Delta P = \bar{\rho}gH$, where $\bar{\rho}$ is the average density of the sample and g is the acceleration due to gravity. Therefore, throughout the sample, the pressure varies with height; that is, $P = P(h)$. Now, since $\kappa_T = \frac{1}{\rho} \left(\frac{\partial \rho}{\partial P} \right)_T$, we see that a small change in pressure leads to a very large change in density when κ_T is large. Therefore, $\rho = \rho(h)$.

We next show how it is possible to predict the variation of density with height, $\rho(h)$, in a sample. For simplicity, we may assume that the average density of the sample is the critical density, ρ_C . Now, as the critical point is approached along the critical isochore, the compressibility increases so that the density gradient increases. If the height of the sample chamber is H , then the fluid is at critical density only at the mid-height, $H/2$. Above the mid-height the density is less than ρ_C , while below the mid-height the density is greater than ρ_C . The quantity $\rho(h)$ may be obtained at each temperature by calculating the quantity $\rho(\mu(h), T)$, where $\mu(h)$ is the chemical potential per unit mass as a function of height. Now, when a fluid is in equilibrium in an external field, μ is a constant throughout its volume. In a gravitational field the total chemical potential, M , is given by⁽⁶⁾

$$M(h) = M_0 + U(h) \quad . \quad (3.32)$$

In this expression, M_0 is the chemical potential in the absence of the field and $U(h)$ is the gravitational potential energy, $U(h) = mgh$, of the molecules in the field. Dividing by the mass we may write

$$\mu(h) = \mu_0 + gh \quad . \quad (3.33)$$

Now, the chemical potential, M_0 , or chemical potential per unit mass, μ_0 , exists only at the mid-height of the sample. Therefore, $\mu(h)$ varies linearly with h above and below the mid-height. Further, $|\mu_0 - \mu(h)|$ varies symmetrically above and below the mid-height. We might point out that while $\mu(h)$ varies linearly and symmetrically about the mid-height that the pressure, $P(h)$, does not.

The quantity $\mu_0(\rho_C, T)$ may be calculated by means of the parametric representation of the equation of state.⁽⁷⁾ The quantity $\mu(h)$ may then be calculated using Eq. (3.33). Finally, the quantity $\rho(h) = \rho(\mu(h), T)$ may be calculated by again using the parametric equation of state.

This technique was used to theoretically predict the variation of density with height for SF_6 at a number of temperatures above T_C along the critical isochore.⁽⁸⁾ In Fig. 3.7 is shown this variation of the relative density, ρ/ρ_C , with height for SF_6 at four of these temperatures. The density versus height profiles are plotted for a sample chamber of total height $H = 6$ mm. which is the approximate effective height of the chamber used in the course of the experiments. Curve A represents the variation of density with height for SF_6 at the critical point. We see that ρ/ρ_C varies by 15.2% over the entire height of the chamber and that ρ/ρ_C varies by 6.4% over a total height of just 0.1 mm. about the mid-height of the cell. Curves B, C, and D show that the severity of the density gradient decreases rapidly as the relative temperature, $\Delta T = T - T_C$, increases.

Having discussed the presence of density gradients in the SF_6 sample very near the critical point, we may next inquire into the effect of the gradients upon the measurements carried out on the sample. From Fig. 3.7

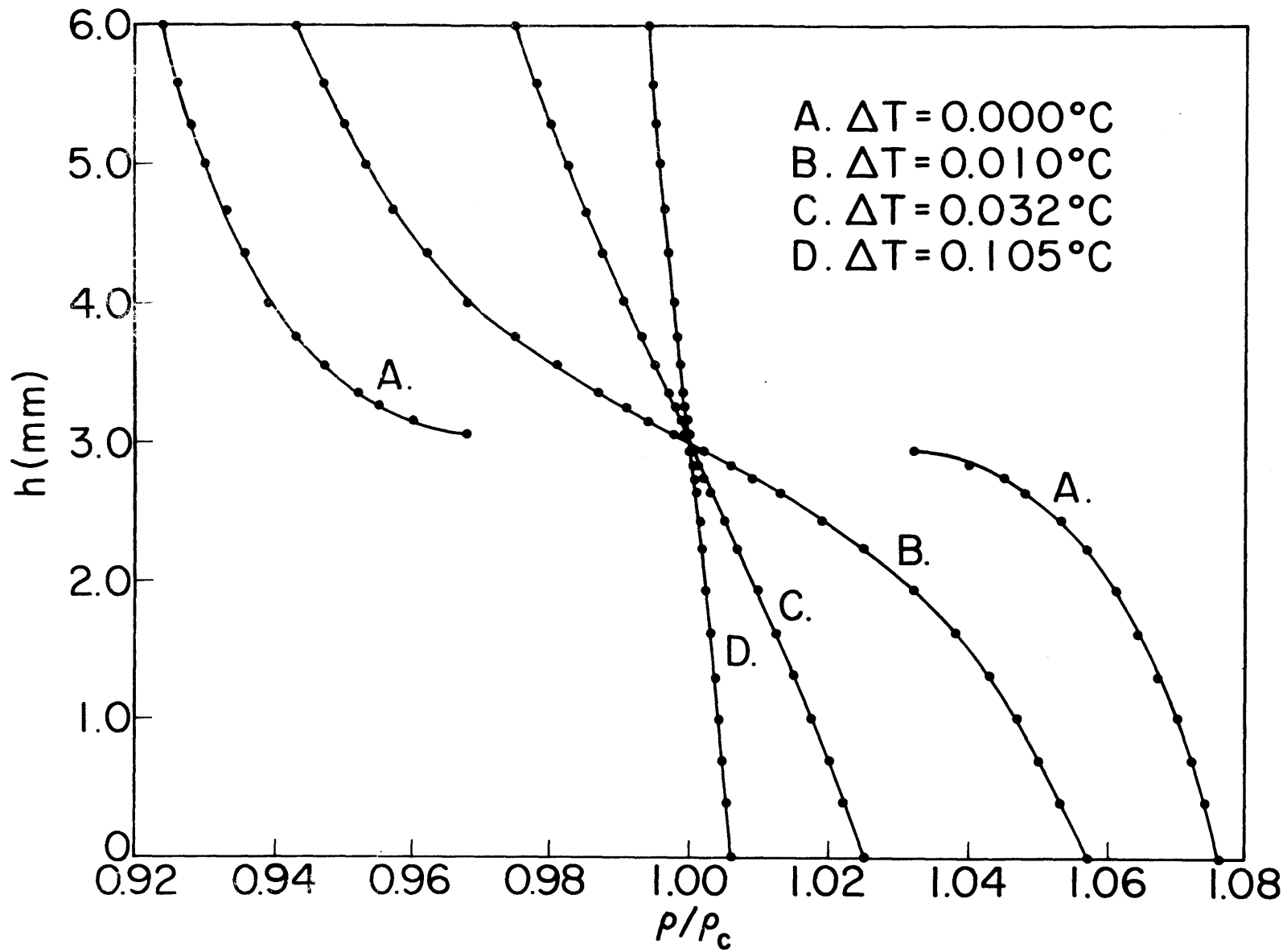


Fig. 3.7 SF₆ Density-Height Profile: $\rho = \rho_c, T \geq T_c$

it is clear that in order to study the light scattered from the sample at $\rho = \rho_0$ and $T > T_C$ it was necessary that the incident beam be focussed at the mid-height of the cell. The diameter of the focussed beam was approximately 0.3 mm so that for $\Delta T = 0.032^\circ\text{C}$ the beam sampled the relative density range $\rho/\rho_C = \pm 0.1\%$ when it was focussed at the mid-height. Since the sample was brought to ρ_C with a precision of 0.1% it was estimated that measurements for $\Delta T > 0.032^\circ\text{C}$ could indeed be considered as measurements along the critical isochore.

Density gradients affect measurements taken at temperatures below T_C to a much lesser degree. At a fixed temperature difference, $T_C - T_0$, the density varies only slightly with height within each of the coexisting phases, since the isothermal compressibility has a significantly smaller value than at an equal temperature difference, $T_0 - T_C$, above T_C along the critical isochore. Therefore, if the incident beam is focussed either slightly below the meniscus in the liquid phase, or slightly above the meniscus in the vapor phase, then one can be assured that the densities which the beam is sampling are very nearly equal to the coexistence curve densities. In the experiments the incident beam was focussed, in both the liquid and vapor phases, to within 1 mm of the meniscus.

We next consider an unavoidable effect of density gradients upon light scattering measurements. From the Lorentz-Lorenz equation, Eq. (3.4), we see that a density gradient will produce a refractive index gradient in the sample. When a beam enters a medium in which there exists a refractive index gradient then the beam will curve in the direction of the gradient. We may consider our sample to be made up of layers of

increasing refractive index. Directly from Snell's law we may write

$$n_0 \cos j_0 = (n_0 + dn) \cos j , \quad (3.34)$$

where n_0 is the refractive index of the sample layer where the beam enters and $(n_0 + dn)$ is the refractive index of the layer immediately below. The quantity j_0 is just $(90^\circ - \theta_i)$, where θ_i is the angle of incidence at the entering layer. Similarly, j is just $(90^\circ - \theta_r)$, where θ_r is the angle of refraction in the lower layer. If the refractive index gradient is given by $\frac{dn}{dz}$, where z increases in the downward direction, then we may write

$$n_0 \cos j_0 \cong n_0 \cos j + \frac{dn}{dz} z , \quad (3.35)$$

since j is a small angle. Now, expanding the cosine terms in a Taylor series we obtain

$$n_0 \left(1 - \frac{j_0^2}{2}\right) = n_0 \left(1 - \frac{j^2}{2}\right) + \frac{dn}{dz} z . \quad (3.36)$$

Simplifying, we have

$$j^2 = j_0^2 + 2 \frac{dn}{dz} \frac{z}{n_0} . \quad (3.37)$$

We thus see explicitly that the beam will indeed curve in the direction of the refractive index gradient and, further, that the curvature increases with increasing gradient and with increasing path length.

Since the beam entering the sample curves, the scattering angle, which is the angle between the direction of the incident beam and the direction of the scattered light that is accepted by the collection optics, differs from the scattering angle one has if the beam did not curve. For the optical arrangement used in the experiments (which is

discussed in detail in Section III.G.2.) the change in the square of the scattering vector, q^2 , due to the curvature of the beam at temperatures close to T_C along the critical isochore has been estimated. (9) It was found that for $T - T_C > 0.080^\circ\text{K}$ corrections to q^2 were negligible. However, the correction to q^2 increased from 1% to 4% as $T - T_C$ decreased from 0.080°K to 0.046°K . The latter represents the lowest temperature to which the sample was brought in the experiments as the critical point was approached along the critical isochore. For the measurements taken at temperatures below T_C it was not necessary to apply corrections to q^2 since the density gradient and hence the curvature of the beam in each of coexisting phases was small.

G. The Optical System

Having described the apparatus and methods used to control and measure the temperature, pressure, and density of the SF_6 sample, we shall next discuss the optical system used to study the spectrum and the intensity of light scattered from the sample.

1. Description of the Components

We shall begin with a description of the components of the optical system. In Fig. 3.8 is shown a schematic representation of the arrangement of the optical system. The light source is a Spectra-Physics model 131 helium-neon laser with an output power of 1 mW. The wavelength is 6328\AA . The spatial filter immediately in front of the laser serves to block out any stray light emitted by the laser and to form a beam with well defined diameter. The beam passes through a lens and, after

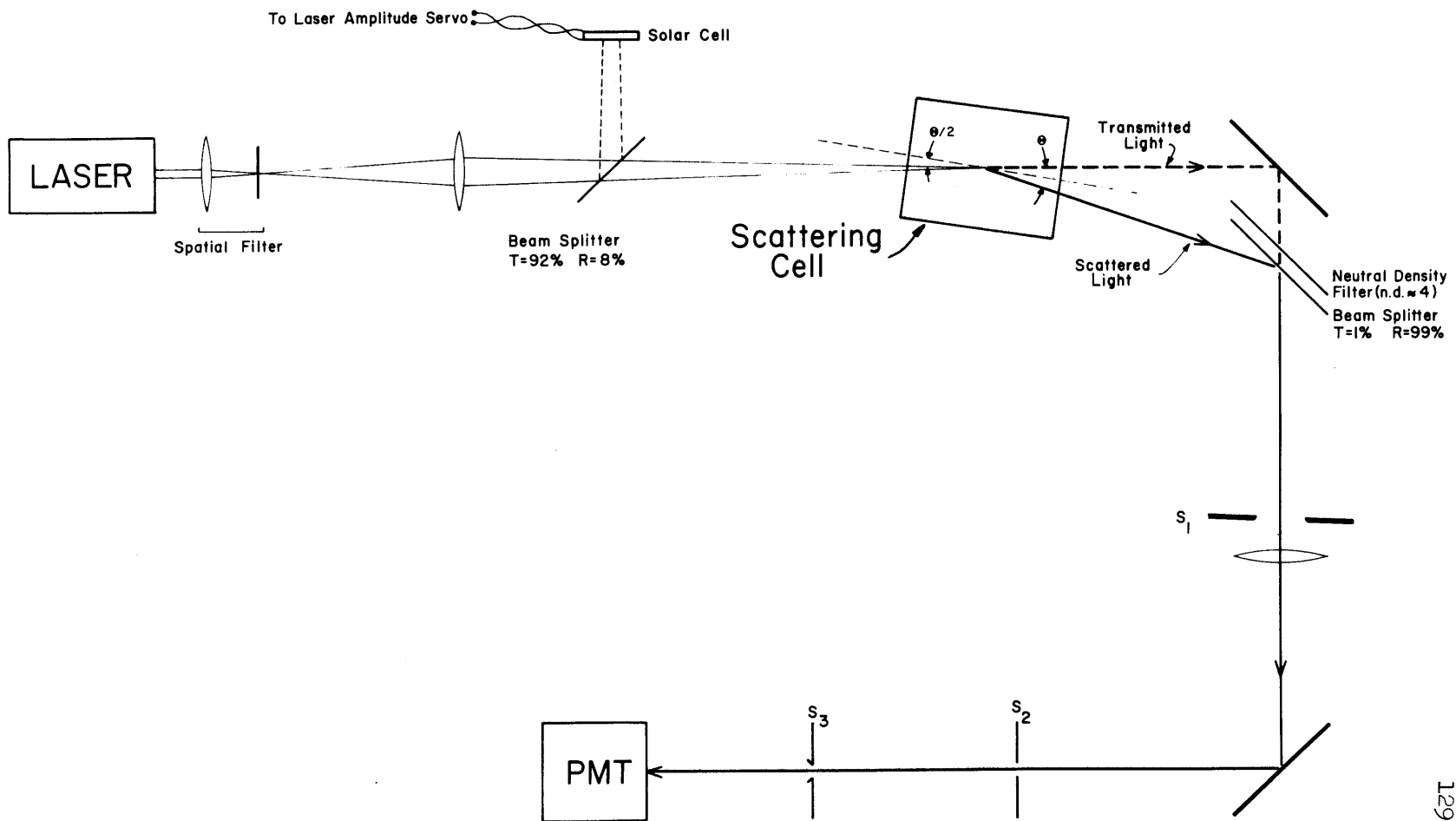


Fig. 3.8 The Optical System

passing through an 8% reflecting, 92% transmitting beam splitter, is focussed at the center of the sample chamber. As will be shown in Section III.G.2. the orientation of the sample chamber with respect to the direction of the incident beam determines the angle between the direction of the unscattered, transmitted light and the direction of the scattered light that is accepted by the collection optics. Light that is scattered by the sample is incident upon a beam splitter which is 1% transmitting and 99% reflecting. The transmitted beam emerges from the sample chamber and is deflected by a front surface mirror. This beam then passes through a neutral density filter which attenuates it by a factor of 10^4 . The attenuated beam then passes through the beam splitter and follows the same path as does the scattered light.

The composite beam then passes through a circular aperture, labelled S_1 in Fig. 3.8, which serves to limit the angular acceptance, $\Delta\theta$, of the scattered light about a mean scattering angle, θ . The beam then passes through a lens with a focal length of 40 cm. In the focal plane of this lens is a rectangular aperture, S_2 . We may note that all the light that passes through the aperture S_1 and which is incident upon the lens surface at some angle, θ' , is focussed at a particular point, P' , in the focal plane of the lens. Light incident at an angle θ'' is focussed at another point, P'' . Therefore, light that is scattered from the entire length of the sample chamber at some particular angle, θ' , is focussed at a particular point, P' , in the focal plane of the collecting lens. The position of the aperture S_2 thus selects the scattering angle, θ , of the light that is studied. The actual measurement of the scattering angle is described in the next section. The width of the aperture S_2

determines the angular spread, $\Delta\theta/\theta$, of the light that is studied. The area of the aperture determines the size of the solid angle, Ω , associated with the scattered light that is accepted for study. It was estimated that, for the scattering angle used in the experiments, $\Delta\theta/\theta = 0.1$.

The rectangular aperture S_3 is mounted in the image plane of the lens. At its image plane the lens forms a real image of the scattering region within the sample chamber. The width of aperture S_3 thus determines the length of the scattering region within the sample chamber from which light is accepted. The width of this aperture was always small enough to block the well-defined images of the spots caused by the beam passing through the entrance and exit windows of the sample chamber. The image of the scattering region was able to be observed by means of a moveable mirror and a telescope mounted immediately after the aperture S_3 .

Finally, light that has been scattered by the sample from a well-defined region in the sample chamber at a particular scattering angle, θ , with a well-defined angular spread, $\Delta\theta/\theta$, is allowed to fall on the photocathode of the photomultiplier tube. An RCA 7265 photomultiplier was used in the experiments.

Having discussed the optical system as such we shall next briefly describe the methods used to stabilize the intensity of the incident laser beam. It is known that the output optical power of the laser is a function of the plasma discharge current. Thus a convenient way to stabilize the laser power is through the stabilization of the plasma current. This was accomplished in the following way. As is shown in Fig. 3.8, 8% of the incident beam is reflected onto a silicon solar cell. The solar cell emits a current which is directly proportional to the

intensity of light incident on its surface. The output of the solar cell is compared with an adjustable reference voltage, and the difference is fed into a servo amplifier. The amplifier controls a resistor which sets the plasma current regulation point in the laser power supply. The response time of the system was adequate to servo slow laser power drifts and long-term stability of 1% was maintained during the experiments. Besides the slow drift in the laser power, additional intermittent instability in the laser output due to the spontaneous switching between the various allowed modes of oscillation in the laser cavity was observed. When the switching occurs coupling between the modes produces plasma oscillations of varying frequencies which modulate the laser output intensity. A 7 kilogauss magnet mounted next to the laser effectively suppressed the oscillations thus aiding in the overall stability of the laser output intensity.

2. Alignment of the Optics and the Determination of the Scattering Vector

Having described the components of the optical system, we shall next describe the procedures used to align the optical system so that light scattered at a particular angle is allowed to fall on the photomultiplier tube. We shall also calculate the scattering vector, q , used in the course of the experiments.

As was shown in Fig. 3.3 the sample chamber and its associated temperature control apparatus were mounted atop a multi-layered plexiglass base plate. This base plate was, in turn, mounted atop an aluminum base plate which was able to be levelled by means of three variable legs, and which

was able to be rotated to precisely known angles. The angles were determined by measuring the linear displacement of a portion of the base plate by means of a vernier caliper attached to the base plate at a known distance from the center of rotation.

The alignment procedure begins by setting the base plate to an angle of 0° . The sample chamber is then positioned atop the base plate so that (1) it is level with the ground as is the table upon which the components of the optical system are mounted, (2) it is of the proper height so that the focussed incident beam passes through the desired height in the sample and (3) the entrance window lies in the plane perpendicular to the direction of the incident beam. The proper positioning of the sample chamber is verified by noting that at 0° the beam reflected from the entrance window travels back along the incident beam. The sample chamber and associated apparatus is then fastened to the base plate.

Having determined the 0° position of the chamber one can rotate the unit to an angle θ_1 , defined as the angle between the direction of the normal to the entrance window and the direction of the incident beam. The magnitude of θ_1 may be determined from the vernier caliper reading. With the sample chamber in its rotated position the beam reflected from the entrance window travels back on an angle of reflection equal to the angle of incidence, θ_1 . In Fig. 3.9 is shown how use is made of this reflected beam in the alignment of the collection optics. The reflected beam strikes a spherical retro mirror and is sent back upon itself. Therefore, both the incident beam and the retro beam are incident upon the entrance window at an angle of incidence, θ_1 . Both beams are refracted

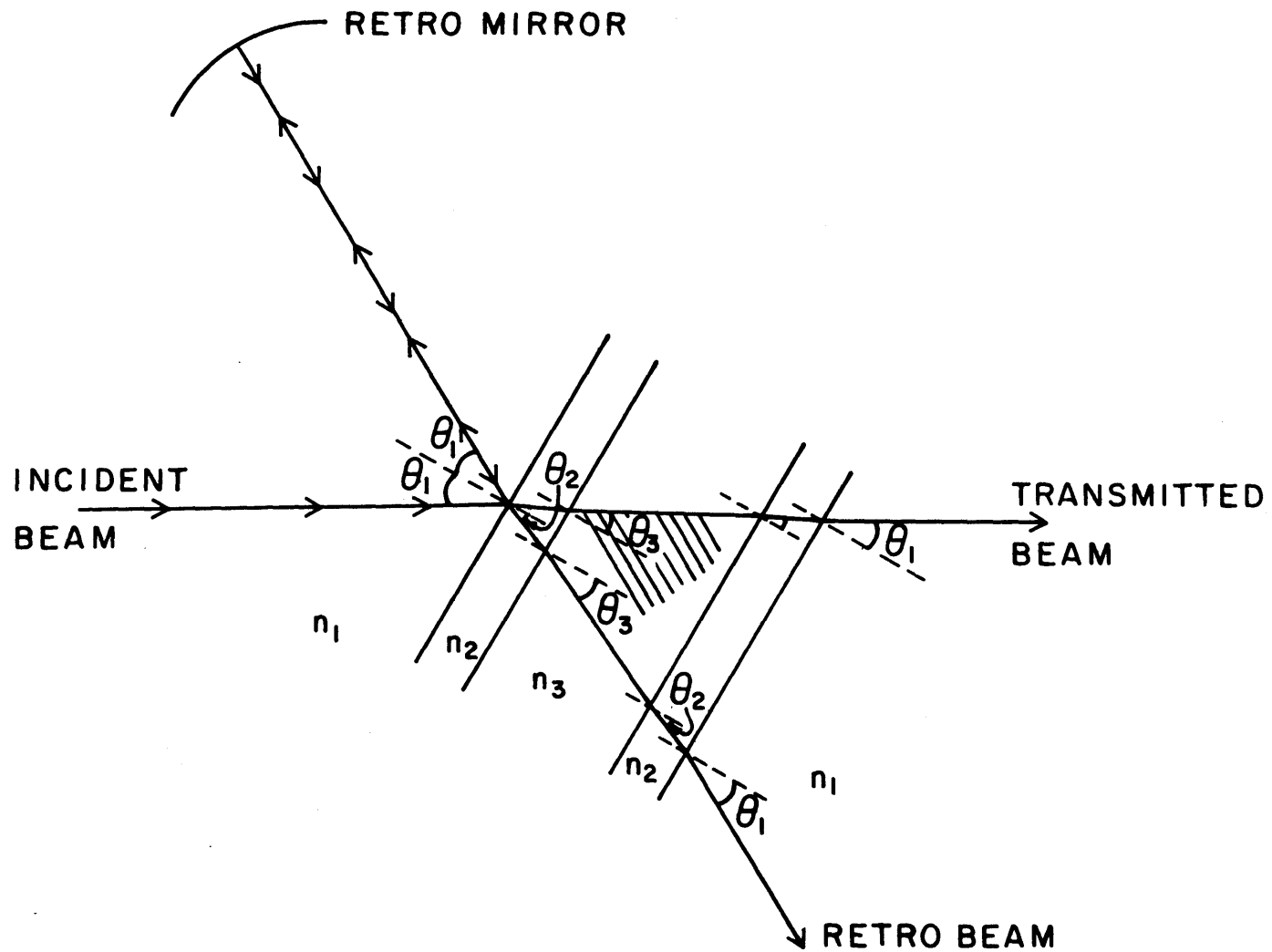


Fig. 3.9 Optical Alignment of the Sample Chamber

at an angle of refraction, θ_2 , in the glass window. Both beams then enter the SF_6 sample at an angle θ_3 with respect to the window normal. We note that the angle between the incident beam and the retro beam in the SF_6 sample is $2\theta_3$. The beams then enter the exit window and again are refracted at angle θ_2 . Finally, the two beams emerge from the exit window at an angle θ_1 with respect to the window normal.

The retro beam is used to align the collection optics. Referring to Fig. 3.8, the retro beam is reflected by the 99% reflecting beam splitter, passes through the circular aperture S_1 , and is focussed by the collecting lens. The position of the rectangular aperture S_2 in the focal plane of the lens is adjusted so that the focussed retro beam is centered on the aperture. Thus the position of aperture S_2 allows only that light which is incident upon the lens at the same angle as is the retro beam to pass through aperture S_3 and onto the photomultiplier. We note from Fig. 3.9 that light which is scattered by the SF_6 sample at an angle of $2\theta_3$ with respect to the transmitted beam is allowed to pass through aperture S_2 .

With the positioning of aperture S_2 completed, the retro mirror is blocked off and the reflected beam is dumped. The position and width of aperture S_3 is then adjusted so that only the light originating from the interior of the sample chamber is allowed to reach the photomultiplier.

We have shown that the alignment procedure is such that the scattered rays accepted by the collection optics make the same angle with the window normal as does the transmitted beam. This procedure ensures that the ratio of the intensity of the scattered light collected to the intensity

of the transmitted beam is independent of optical attenuation in the sample since the path lengths in the sample are identical. We shall next show that the alignment procedure ensures that the scattering vector, q , is independent of the index of refraction of the SF_6 sample.

The scattering vector is given by

$$q = \frac{4\pi n}{\lambda_0} \sin \frac{\theta}{2} , \quad (3.38)$$

where n is the refractive index of the sample, and θ is the scattering angle in the sample. From Fig. 3.9 we have $n = n_3$ and $\theta = 2\theta_3$. Therefore,

$$q = \frac{4\pi n_3}{\lambda_0} \sin \theta_3 . \quad (3.39)$$

However, from the laws of refraction,

$$n_1 \sin \theta_1 = n_2 \sin \theta_2 = n_3 \sin \theta_3 , \quad (3.40)$$

so that

$$\sin \theta_3 = \frac{n_1}{n_3} \sin \theta_1 . \quad (3.41)$$

We note that $n_1 = n_{\text{air}} \approx 1.00$, so that the scattering vector becomes

$$q = \frac{4\pi}{\lambda_0} \sin \theta_1 . \quad (3.42)$$

We see that the scattering vector is indeed independent of the index of refraction of the SF_6 .

In the experiments, the sample chamber was rotated to an angle $\theta_1 = 2.42^\circ$. Using $\lambda_0 = 6328\text{\AA}$, we find that the scattering vector operative throughout the course of the experiments was $q = 8382 \text{ cm}^{-1}$.

H. The Electronic Detection System

In the final section of the present chapter we shall discuss the electronic apparatus and the methods used to obtain measurements of the following quantities: (1) the ratio of the intensity of light scattered by the SF_6 sample to the intensity of the light incident upon the sample, $\frac{P_S}{P_I}$; (2) the frequency spectrum, $S_i(\nu)$, and (3) the time correlation function, $R_i(\tau)$, of the fluctuating photocurrent arising from the light scattered quasielastically from the thermally excited entropy fluctuations in the SF_6 sample. In Fig. 3.10 is shown a block diagram of the electronic detection apparatus.

Light that has passed through the optical system, Fig. 3.8, is incident on the photocathode of the RCA 7265 photomultiplier tube. Throughout the experiments the photomultiplier was operated at 1700 volts delivered by a Fluke 415B high voltage power supply. We have seen (Eq. (2.141)) that the instantaneous photocurrent emerging from the photomultiplier is proportional to the instantaneous power in the light beam incident upon its photocathode. When light scattered from fluctuations in the sample falls on the photocathode what emerges is a fluctuating photocurrent. We shall describe the techniques used to obtain (1) the frequency spectrum and (2) the time correlation function of the fluctuating photocurrent. We have also seen (Eqs. (2.97) and (2.141)) that the time average of the fluctuating photocurrent is proportional to the average power in the light beam incident upon the photocathode. In the next section we shall describe the technique used to obtain the quantity P_S/P_I from measurements of the average photocurrent.

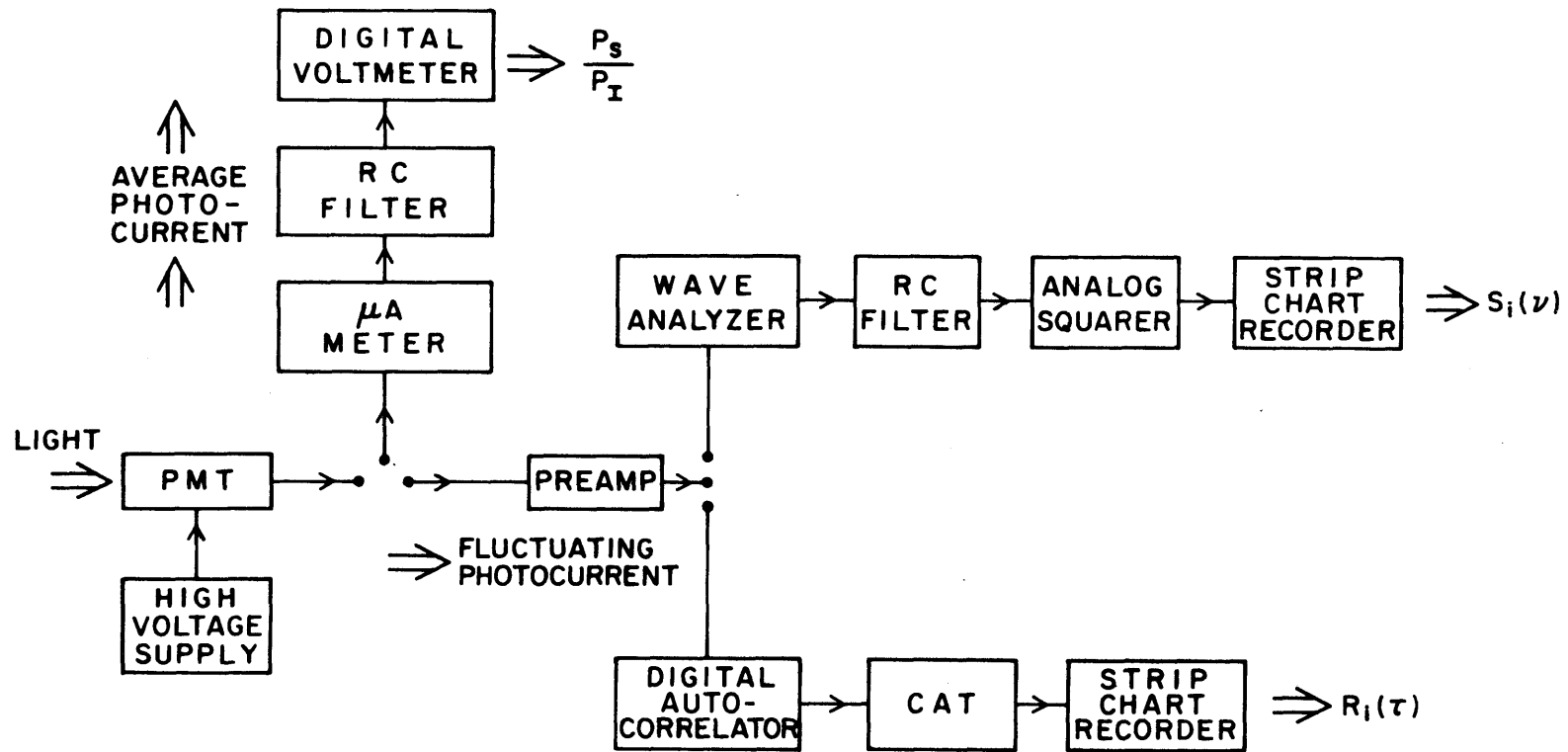


Fig. 3.10 The Electronic Detection System

1. Measurements of P_S/P_I

The average photocurrent was measured in the following way. The output of the photomultiplier was fed into a Keithley microammeter which provides a measurement of the time average photocurrent. The output of the microammeter was further averaged by an RC filter. The resulting averaged photocurrent was visually displayed on a digital voltmeter. When measuring the average photocurrent corresponding to the power in the scattered light, the transmitted light beam (see Fig. 3.8) was blocked after emerging from the sample chamber. Similarly, when measuring the average photocurrent corresponding to the power in the transmitted beam, the scattered light was blocked after emerging from the sample chamber.

As we have pointed out, the scattered light and the transmitted light travel through equal path lengths in the SF_6 sample. Therefore, even though what is measured is the ratio of scattered power to transmitted power, this measured ratio is identical to the ratio of scattered power to incident power, P_S/P_I .

We have shown (Eq. (2.120)) that

$$\frac{P_S}{P_I} = \frac{\pi^2 L \Omega}{4 \lambda_0} k_B T \left(\frac{\partial n^2}{\partial \rho} \right)_T^2 \rho^2 \kappa_T \frac{1}{(1 + q^2 \xi^2)} \quad (3.43)$$

We recall that L is the length of the scattering region accepted by the collection optics, Ω is the solid angle of collection, λ_0 is the vacuum wavelength of the incident light, k_B is Boltzmann's constant, q is the scattering vector, ξ is the Ornstein-Zernike long range correlation length, and κ_T is the isothermal compressibility. Throughout the course

of the experiments, the product of the square of the scattering vector and the square of the correlation length was always $\ll 1$. Therefore, in the experiments, the ratio of measured scattered power to measured transmitted power is proportional to $\rho^2 \kappa_T$ when corrections are made to account for the small changes in L and in $(\frac{\partial n^2}{\partial \rho})_T$ due to changes in the refractive index, n , of the sample as the sample density changes.

We must point out that a measurement of the absolute ratio of scattered power to transmitted power would have required a determination of the attenuation of the transmitted beam due to its passage through the neutral density filter and the 1% transmitting beam splitter shown in Fig. 3.8. This was not attempted. Thus, in the experiments, what was measured was the ratio of scattered power to attenuated transmitted power.

We may express the measured attenuated transmitted beam power as $(P_T)_{\text{meas.}} = P_T/A$, where P_T is the transmitted beam power that would be measured if the transmitted beam were to follow the same path in the optical collection system as does the scattered light, and A is the factor by which the transmitted beam is attenuated. We may express the coefficient in curly brackets in Eq. (3.43) as $B(\rho, T)$. We may then write

$$\frac{P_S}{P_I} = \frac{P_S}{P_T} = \frac{P_S}{A(P_T)_{\text{meas}}} = B(\rho, T) \rho^2 \kappa_T \quad . \quad (3.44)$$

Therefore the measured ratio of scattered power to transmitted power is

$$\left(\frac{P_S}{P_T}\right)_{\text{meas}} = A \cdot B(\rho, T) \rho^2 \kappa_T \quad . \quad (3.45)$$

In the experiments the magnitude of the quantity $A \cdot B(\rho, T)$ was determined by measuring both $(P_S/P_T)_{\text{meas}}$ and the pressure, P , at 23 points along a near critical isotherm of SF_6 over the density range $1.15 \leq \frac{\rho - \rho_C}{\rho_C} \leq 1.40$.⁽⁵⁾ The quantity $\rho^2 \kappa_T$ was determined by measuring the variation of P with density. We see that once the quantity $A \cdot B(\rho, T)$ has been determined from measurements **along** an isotherm, then it is known along the critical isochore and along the coexistence curve provided that the length of the scattering region accepted by the collection optics, L , and the solid angle of collection, Ω , remain unchanged.

We see then that from measurements of the ratio of scattered power to attenuated transmitted power we are able to determine the magnitude and temperature dependence of the quantity $\rho^2 \kappa_T$ as the critical point of the SF_6 sample is approached along either the critical isochore or the coexistence curve. We present these results in Chapter IV.

2. Measurement of $S_i(\nu)$

We shall next describe the techniques used to obtain the frequency spectrum, $S_i(\nu)$, of the fluctuating photocurrent. As is shown in Fig. 3.10 the first step in obtaining the power spectrum of the fluctuating photocurrent was to feed the output of the photomultiplier into a preamplifier. For measurements of the photocurrent spectrum the preamplifier used was a low impedance device of the type discussed by Lastovka.⁽¹⁰⁾ The low input and output impedances of the preamplifier allowed convenient cable lengths of several feet to be used at its input and output without causing a rolloff at high frequencies due to cable

capacitance. The preamplifier provided an extremely flat frequency response over the entire tuning range of the General Radio 1900A wave analyzer used in the experiments which was $0 \leq \nu \leq 60\text{kHz}$. In the course of the experiments the highest frequency examined was 15kHz so that essentially no rolloff was introduced by the preamplifier.

The next step in obtaining the photocurrent spectrum was to feed the output of the preamplifier into the GR 1900A wave analyzer. The wave analyzer acts as a narrow band tuned filter whose center frequency can be swept over the range of frequencies of interest in the photocurrent spectrum. The GR 1900A is equipped with selectable filter bandwidths of 3, 10, and 50 Hz. The proper selection of bandwidth prevents any measurable distortion of the spectral line shape by insuring that $S_1(\nu)$ is essentially constant over the bandwidth. Lastovka⁽¹⁰⁾ has shown that the measured half-width at half height of a Lorentzian spectrum, $\Delta\nu_{1/2}$, is broadened due to a finite filter bandwidth, ν_f . He finds that the true half-width is broadened by an amount $(\frac{\nu_f}{\Delta\nu_{1/2}})^2$. We see then that if the filter bandwidth is $\leq \frac{1}{10}$ of the half-width of the spectrum that the broadening is $\leq 1\%$.

In the experiments the 50 Hz bandwidth was used for half-widths greater than 500 Hz. The 10 Hz bandwidth was used for half widths between 200 Hz and 500 Hz. When the experimental half-widths became less than 200 Hz the wave analyzer was no longer employed. Instead, the time correlation function of the scattered light was determined.

In the experiments the filter bandwidth was swept over the desired frequency range by means of a variable speed stepping motor. An initial

sweep rate of either 600 Hz/hour or 300 Hz/hour was used depending on the half-width of the spectrum. Typically, the spectrum was measured out to a frequency of $5\Delta\nu_{1/2}$. A typical time for obtaining such a spectrum was 5 hours.

The detector incorporated in the GR 1900A wave analyzer is a linear full-wave rectifier. The rectifier produces a dc detector output voltage that is proportional to the root-mean-square current at its input. As a result the analyzer output is a dc voltage which is proportional to the square root of the total power passed to the detector by the narrow band filter. Thus as the filter frequency is swept over the desired range, the output of the wave analyzer generates a line shape proportional to the square root of the desired photocurrent spectrum.

In order to obtain a convenient plot of the photocurrent spectrum directly, the wave analyzer output voltage was first averaged by passing it through a double RC filter and then squared by a slow speed analog squaring machine prior to recording. Therefore, what is recorded on the Hewlett-Packard strip chart recorder using this technique is the power spectrum, $S_i(\nu)$, of the fluctuating photocurrent. The analog squarer used in the experiments is described by Lastovka.⁽¹⁰⁾ Typically, the time constant of the double RC filter was 10-15 seconds.

The complete system response (output amplitude versus frequency) of the phototube-preamplifier-wave analyzer-time averager-squarer-chart recorder units was calibrated by utilizing the fact that the shot noise spectrum is flat over the frequency range accessible to the wave analyzer. A shot noise spectrum was generated by illuminating the photomultiplier with a light bulb driven by a well-regulated power supply. The slightly

non-linear response of the system to the shot noise input was then recorded and the experimental traces of the photocurrent spectra arising from the light scattered by the entropy fluctuations in the SF₆ sample were corrected with the system calibration curve.

As we have shown (Eq. (2.158)), the photocurrent spectrum, $S_i(\nu)$, contains three terms: a baseline due to the shot noise, a delta function due to the average photocurrent, and a Lorentzian centered at zero frequency. The half-width at half height of the Lorentzian, $\Delta\nu_{1/2}$, is Γ/π Hz. We recall that Γ , the decay rate of the entropy fluctuations, is, in the hydrodynamic region, related to the thermal diffusivity, $\frac{\Lambda}{\rho C_P}$, by $\Gamma = \frac{\Lambda}{\rho C_P} q^2$. Therefore, from measurements of $\Delta\nu_{1/2}$ at a known scattering vector, q , one is able to determine the magnitude and temperature dependence of the thermal diffusivity of the SF₆ sample as the critical point is approached along either the critical isochore or the coexistence curve.

Each experimental spectrum was fit to a single Lorentzian using a three parameter, non-linear, least-squares fitting program. The program calculates the best fit for the amplitude at zero frequency, the baseline, and the half-width at half-height, $\Delta\nu_{1/2}$. The program also calculates the standard deviation associated with its best fit value for $\Delta\nu_{1/2}$.

We have seen that $\Delta\nu_{1/2}$ was broadened by $\leq 1\%$ due to a finite wave analyzer filter bandwidth. Similarly, Lastovka⁽¹⁰⁾ has shown that if light is collected from an acceptance angle $\Delta\theta$ about the mean angle θ then $\Delta\nu_{1/2}$ is broadened by an amount $(\frac{\Delta\theta}{\theta})^2$. Since $\Delta\theta/\theta \cong 0.1$ the broadening is 1%. Since the broadening due to these effects was small no

attempt was made to correct the best fit values of $\Delta\nu_{1/2}$. Typically, values of $\Delta\nu_{1/2}$ were obtained for each experimental spectrum with a precision of $\pm 3\%$. Repeated measurements at the same temperature and density of the sample allowed the determination of the magnitude of the thermal diffusivity at each temperature studied to an overall precision of 2% . We present these results in Chapter IV.

The fitting program was written in Fortran IV G and was executed on an IBM 370 Computer. A listing of the program appears in Appendix A.

3. Measurement of $R_i(\tau)$

We shall next describe the techniques used to obtain the time correlation function, $R_i(\tau)$, of the fluctuating photocurrent. As we have stated, when the experimental Lorentzian half-widths became less than 200 Hz, the technique of measuring $S_i(\nu)$ in order to obtain the thermal diffusivity of the SF_6 sample was no longer employed. Instead, an even more precise technique, the technique of measuring the time correlation function of the photocurrent, was employed to obtain the thermal diffusivity. As we have shown (Eq. (2.154)), the photocurrent correlation function arising from light scattered from the entropy fluctuations in the SF_6 sample contains three terms: a constant baseline due to the average photocurrent, a delta function at the origin due to the shot noise, and a decaying exponential with a decay time of $1/2\Gamma$. Now, since the Lorentzian half-width, $\Delta\nu_{1/2}$, is Γ/π Hz, we see that when $\Delta\nu_{1/2} = 200$ Hz we have $1/2\Gamma \approx 8 \times 10^{-4}$ sec. Decay time $\geq 8 \times 10^{-4}$ sec could be measured with extremely high accuracy with the digital autocorrelator used in the experiments.

As is shown in Fig. 3.10 the first step in obtaining the correlation function of the fluctuating photocurrent was to feed the output of the photomultiplier into a preamplifier. Now, the output of the photomultiplier actually consists of discrete pulses. The number of pulses in a given time interval is a fluctuating random variable. We have seen that for measurements of the power spectrum, the pulses were fed into a low impedance preamplifier which converted the discrete pulses into a continuous fluctuating current. For measurements of the correlation function, however, the discrete nature of the pulses was retained and the preamplifier used was a Keithley pulse amplifier with a gain of 1000.

The amplified pulses were then fed into a digital autocorrelator designed and constructed at M.I.T. by Dr. Joseph Lastovka and Dr. John Zollweg. The autocorrelator operates in conjunction with a Computer of Average Transients, CAT. When a pulse with an amplitude greater than a pre-set level enters the correlator, the process of computing the correlation function is initiated. The correlator determines the amount of correlation between the initial pulse and the number of pulses in succeeding discrete time intervals. When the computation is complete the result is stored in the memory of the CAT and the process is automatically re-initiated by another incoming pulse. The result of the second computation is added to the first and as the process continues, the correlation function, $\langle i(t)i(t + \tau) \rangle$, which is the average of many such computations, begins to "build up" in the memory of the CAT. The "growth" of the correlation function is able to be visually observed on the CRT output of the CAT. When it was decided that sufficient averaging

had occurred, usually after 1 to 1 1/2 hours, the correlator was halted and an output proportional to the content of each of the memory channels of the CAT was read out onto a Hewlett-Packard strip chart recorder.

The CAT is equipped with a maximum of 1024 memory channels. During the experiments, 256 memory channels were used. Typically, however, only the data stored in the first 120 channels were used in the determination of the correlation function. The CAT is equipped with four selectable values of the time interval per memory channel: 31.25×10^{-6} sec, 62.5×10^{-6} sec, 125×10^{-6} sec, and 250×10^{-6} sec. During the experiments either the 31.25 μ sec or the 62.5 μ sec interval was used depending on the value of the decay time. A single exponential decay decreases to approximately 2% of its initial amplitude at a time equal to four decay times. During the experiments, a sufficient number of memory channels was always used so that the correlation function was determined out to at least four decay times.

Each experimental correlation function was fit to a single exponential decay using a three parameter, non-linear, least squares fitting program. The program calculates the best fit for the amplitude at zero time, the baseline, and the decay time. The fitting program was written in Fortran IV G and was executed on an IBM 370 computer. A listing of the program appears in Appendix B.

Usually, the correlation function was measured three times at each temperature as the critical point of the SF₆ sample was approached. The decay time used to determine Γ was taken to be the average of the best

fit decay times for each of the runs. Best fit decay times from successive runs at the same sample temperature usually varied by no more than 1.5%. In the course of the experiments the measured decay times ranged from 7×10^{-4} sec to 7×10^{-3} sec. From the measurement of the average decay time, $1/2\Gamma$, at each temperature, the magnitude of the thermal diffusivity was determined. We present these results in Chapter IV.

References For Chapter III

1. J. D. Jackson, Classical Electrodynamics, John Wiley and Sons, Inc., New York (1962).
2. A. W. Francis, J. Chem. Eng. Data, 5, 534 (1960).
3. J. Otto and W. Thomas, Z. Phys. Chem., 23, 84 (1960).
4. M. Born and E. Wolf, Principles of Optics, Pergamon Press, New York (1959).
5. G. B. Benedek, J. B. Lastovka, M. Giglio and D. Cannell, in Critical Phenomena, edited by R. E. Mills and R. S. Jaffee, McGraw-Hill, New York, 1971.
6. L. D. Landau and E. M. Lifshitz, Statistical Physics, Addison-Wesley Publishing Co. Inc., Reading, Mass. (1958).
7. P. Schofield, J. D. Litster, and J. T. Ho, Phys. Rev. Letters 23, 1098 (1969).
8. I. W. Smith, private communication.
9. G. A. Hawkins, private communication.
10. J. B. Lastovka, Ph. D. Thesis, Department of Physics, M. I. T., 1967 (unpublished).

Chapter IV

EXPERIMENTAL RESULTS, ANALYSIS, AND DISCUSSION

A. Introduction

In this chapter we shall present the results of the measurements of the pressure, P , the ratio of scattered power to incident power, P_S/P_I , the half-width at half height of the photocurrent power spectrum, Γ/π , and the decay time of the photocurrent correlation function, $1/2\Gamma$, which were carried out on a sample of sulfur hexafluoride, SF_6 , along the critical isochore and along the coexistence curve. We shall analyze the results in order to determine the magnitude and temperature dependence of the isothermal compressibility, κ_T , and the critical part of the thermal diffusivity, D_C . We shall discuss the results in terms of the theoretical predictions of the scaling laws and of the mode-mode coupling theory.

In our presentation we shall first consider the measurements which were carried out along the critical isochore. These results have been reported.⁽¹⁾ We shall then turn our attention to the measurements which were carried out along the coexistence curve. These results have also been reported.⁽²⁾

B. The Critical Isochore

In this section we shall present, analyze and discuss the results of measurements carried out along the critical isochore of SF_6 over the temperature range $0.048^\circ K < (T - T_C) < 2.4^\circ K$. The SF_6 sample was brought to within 0.1% of critical density, ρ_C , using the technique

of meniscus height observation described in Section III.F.2. The critical temperature, T_C , was determined to be $318.707 \pm 0.002^\circ\text{K}$ by direct visual observation of the disappearance of the meniscus.

1. Measurements of Pressure

In Table 4.1 we present the results of the measurements of the pressure, P , as a function of temperature along the critical isochore. As was discussed in Section III.E. these measurements have been corrected for the time drift of the pressure transducer. The absolute magnitude of each of the measurements was adjusted so that when one extrapolates $P(T)$ to $P(T_C)$ one obtains $P(T_C) = 544.77$ psi which is critical pressure reported by MacCormack and Schneider. (3)

The $P(T)$ data were computer fit to the form

$$P(T) = P_C + A_1(T - T_C) + A_2(T - T_C)^2 \quad . \quad (4.1)$$

We see that

$$\left(\frac{\partial P}{\partial T}\right)_V = A_1 + 2A_2(T - T_C) \quad . \quad (4.2)$$

Using the values of A_1 and A_2 determined by the computer fit, we found that $\left(\frac{\partial P}{\partial T}\right)_V = [11.47 + 0.257(T - T_C)] \pm 0.15$ psi/ $^\circ\text{K}$. Converting to cgs units, we have

$$\left(\frac{\partial P}{\partial T}\right)_V = [7.91 + 0.18(T - T_C) \pm 0.1] \times 10^5 \text{ dyne/cm}^2 \text{ } ^\circ\text{K}$$

along the critical isochore. As will be shown later, the magnitude of $\left(\frac{\partial P}{\partial T}\right)_V$ plays an important role in the analysis of the light scattering measurement.

Table 4.1 Variation of Pressure with
Temperature along the
Critical Isochore

<u>T(°K)</u>	<u>P(psi)</u>
321.092	573.0
320.818	569.8
320.609	567.15
320.420	564.95
320.232	562.7
320.120	561.4
319.955	559.5
319.833	558.05
319.728	556.75
319.630	555.65
319.533	554.5
319.451	553.5
319.377	552.65
319.317	551.95
319.250	551.2
319.185	550.55
319.110	549.55
319.051	548.85
319.003	548.3
318.960	547.85
318.923	547.45
318.894	547.1
318.868	546.8
318.845	546.5
318.827	546.3
318.812	546.15
318.798	545.95
318.788	545.85
318.779	545.75
318.766	545.65
318.755	545.5

2. Measurements of κ_T

As we have previously shown (Eqs. (2.120) and (3.43)), the ratio of scattered power to incident power, P_S/P_I , is given by

$$\frac{P_S}{P_I} = \left[\frac{\pi^2 L \Omega}{\lambda_0^4} k_B T \left(\frac{\partial n^2}{\partial \rho} \right)^2 \right] \rho^2 \kappa_T \frac{1}{(1 + q^2 \xi^2)} \quad (4.3)$$

Since $q^2 \xi^2 \ll 1$ over the temperature range of the measurements, we see that, at constant density, the isothermal compressibility, κ_T , is proportional to $\left(\frac{P_S}{P_I} \right) \frac{1}{T}$. We have also shown (Eq. (3.44)) that the ratio P_S/P_I is proportional to the ratio of scattered power to attenuated transmitted power, $P_S/(P_T)_{\text{meas}}$. In Table 4.2 we present the results of measurements of the ratio of the scattered power to the measured attenuated transmitted power obtained by measurements of the average photocurrent arising from the light scattered by the SF_6 sample along the critical isochore. The measurements were obtained using a scattering vector $q = 8382 \text{ cm}^{-1}$. Each measurement has been normalized by the factor $\left(\frac{T}{T_C} \right)$ so that each measurement is directly proportional to the magnitude of κ_T .

The proportionality constant between the experimental quantity $\left(\frac{P_S}{P_T} \right)_{\text{meas}} \left(\frac{T}{T_C} \right)$ and κ_T was obtained by bringing the results into numerical agreement with the value of κ_T obtained from the PVT measurements of McCormack and Schneider⁽³⁾ at $T - T_C = 1.453^\circ \text{K}$. The proportionality constant obtained in this way is in agreement with the constant that was obtained using the method described in Section III.H.1. In Table 4.2 we thus present our deduced values of the isothermal compressibility along the critical isochore.

Table 4.2 κ_T along the Critical Isochore

$T(^{\circ}\text{K})$	$T-T_C(^{\circ}\text{K})$	$\frac{T-T_C}{T_C}$	$\left(\frac{P_S}{P_T}\right)^{\frac{T_C}{T}}$	$\kappa_T(\text{cm}^2/\text{dyne})$
321.092	2.385	7.483×10^{-3}	.7074	5.378×10^{-7}
320.818	2.111	6.624	.8130	6.181
320.609	1.902	5.968	.9267	7.046
320.420	1.713	5.375	1.044	7.938
320.232	1.525	4.785	1.210	9.200
320.120	1.413	4.434	1.325	1.007×10^{-6}
319.955	1.248	3.916	1.538	1.169
319.833	1.726	3.533	1.759	1.337
319.728	1.021	3.204	1.970	1.498
319.630	0.923	2.896	2.235	1.699
319.533	0.826	2.592	2.553	1.941
319.451	0.744	2.334	2.894	2.200
319.377	0.670	2.102	3.291	2.502
319.317	0.610	1.914	3.706	2.818
319.250	0.543	1.704	4.255	3.235
319.185	0.478	1.500	5.038	3.830
319.110	0.403	1.264	6.253	4.754
319.051	0.344	1.079	7.568	5.754
319.003	0.296	9.288×10^{-4}	9.127	6.939
318.960	0.253	7.938	11.36	8.637
318.923	0.216	6.777	13.53	1.029×10^{-5}
318.894	0.187	5.867	16.32	1.241
318.868	0.161	5.052	19.79	1.505
318.845	0.138	4.330	24.31	1.848
318.827	0.120	3.765	27.84	2.117
318.812	0.105	3.295	32.68	2.484

In Fig. 4.1 is shown a log-log plot of κ_T as a function of the reduced temperature, $(T/T_C - 1)$. We see that the isothermal compressibility accurately obeys the power law $\kappa_T = C_0(T/T_C - 1)^{-\gamma}$ with $C_0 = 1.26 \times 10^{-9} \text{ cm}^2/\text{dyne}$ and $\gamma = 1.235 \pm 0.015$.

Our measured value of γ is in good agreement with the results of Puglielli and Ford⁽⁴⁾ who obtained $\gamma = 1.225 \pm .02$ from turbidity measurements. It is interesting to note that the value of the critical exponent γ obtained for SF_6 is very close to the value of γ obtained for other fluids. For example, Lunacek and Cannell⁽⁵⁾ found that for CO_2 $\gamma = 1.219 \pm 0.01$. Also, Smith *et al.*⁽⁶⁾ found that for xenon $\gamma = 1.21 \pm 0.03$.

We may recall (Sec. II.D.) that the isothermal compressibility is indeed expected to diverge with a power law behavior as the critical point is approached along the critical isochore. We also recall that, according to the scaling law equation of state, if any two of the critical exponents are known then all the rest may be determined. In view of the excellent agreement between the value of γ obtained in this experiment and those values of γ obtained in other experiments we conclude that our value of γ is accurate and thus may be used in further analysis of the critical point properties of SF_6 .

3. Measurements of Γ/q^2

We next turn our attention to the measurements of the quantity Γ/q^2 , obtained from measurements of the half-width at half height of the photocurrent power spectrum, Γ/π , and the decay time of the photocurrent correlation function, $1/2\Gamma$, arising from the light scattered quasi-elastically from thermally excited entropy fluctuations in SF_6 along the critical isochore. These measurements were carried out over the temperature

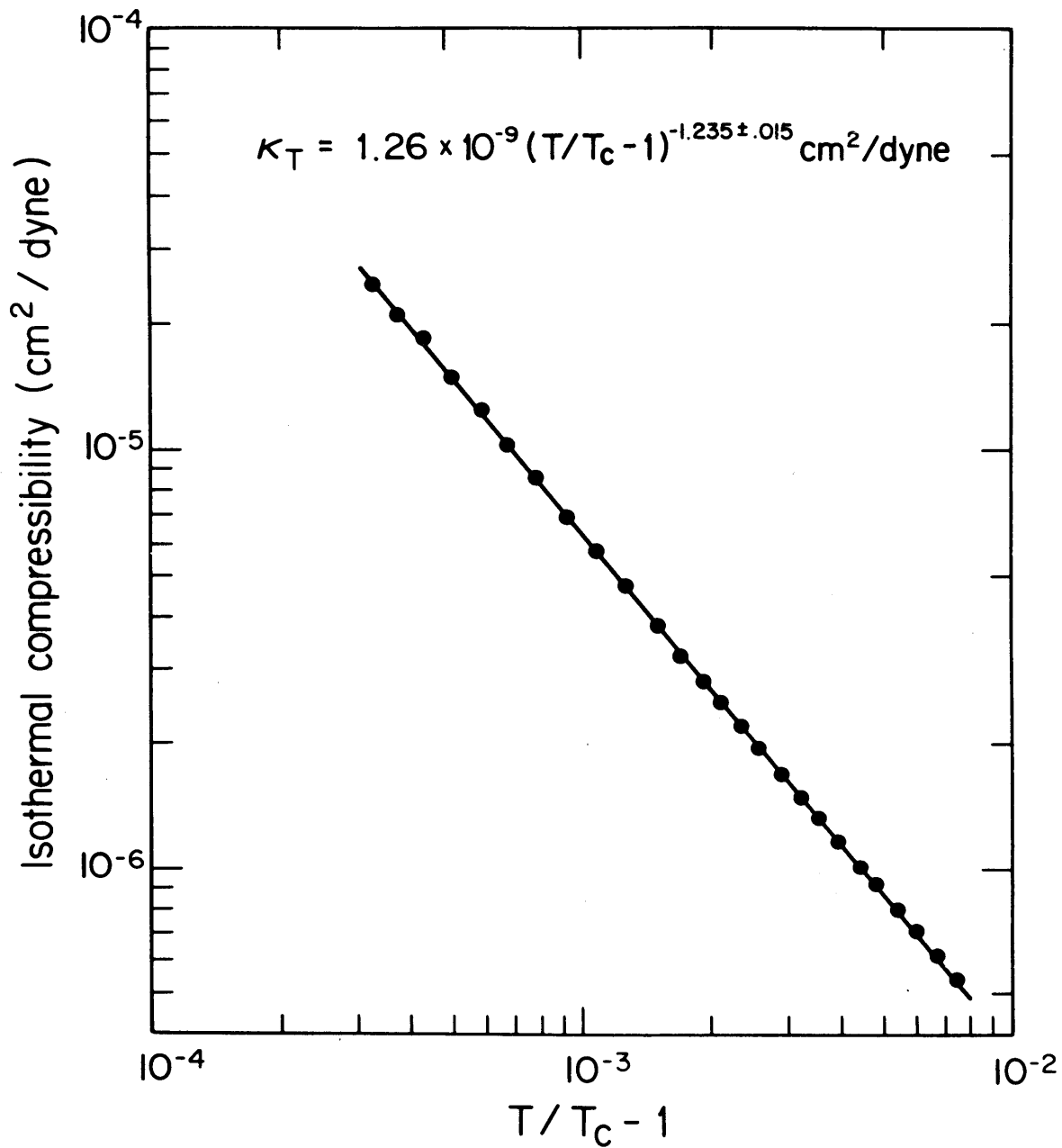


Fig. 4.1 Isothermal Compressibility, κ_T , along the Critical Isochore as a Function of the Reduced Temperature ($T/T_C - 1$)

range $0.048^\circ\text{K} < T - T_C < 2.4^\circ\text{K}$, and with a scattering vector $q = 8382 \text{ cm}^{-1}$.

In Table 4.3 we present our averaged experimental values of Γ/π and $1/2\Gamma$. We also present our results for Γ/q^2 using $q = 8382 \text{ cm}^{-1}$. We recall that, since $q^2\xi^2 \ll 1$ over the range of our measurements, the quantity $\Gamma/q^2 = \Lambda/\rho C_P$, the thermal diffusivity, where Λ is the thermal conductivity and C_P is the specific heat per unit mass at constant pressure.

In the upper portion of Fig. 4.2 are plotted the averaged results of the measurements of the thermal diffusivity as a function of $T - T_C$. The uncertainty of each point is approximately 2%. These results are larger at all temperatures and are different in curvature than results which were previously reported along the critical isochore of SF_6 by Saxman and Benedek,⁽⁷⁾ who found $\Lambda/\rho C_P = 1.26 \times 10^{-2}(T/T_C - 1)^{1.26} \text{ cm}^2/\text{sec}$ for $0.040^\circ\text{K} < T - T_C < 5^\circ\text{K}$. The data of Fig. 4.2 can be approximated by the formula $\Lambda/\rho C_P = 1.22 \times 10^{-3}(T/T_C - 1)^{0.78} \text{ cm}^2/\text{sec}$ in the temperature range $0.048^\circ\text{K} < T - T_C < 0.3^\circ\text{K}$. At temperatures higher than $T - T_C = 0.3^\circ\text{K}$ the data can no longer be adequately represented by a simple power law. To date there has been no convincing explanation for the discrepancy between the results presented here and those reported in Reference 7. Braun et al.⁽⁸⁾ have also reported measurements of the thermal diffusivity along the critical isochore of SF_6 . The results presented here are similar in curvature to those reported in Reference 8 but over the range of measurement are everywhere greater in magnitude by approximately 30%.

In Fig. 4.3 the data of Fig. 4.2 are re-plotted along with results obtained by Lim and Swinney and by Langley and Kachnowski.⁽⁹⁾ The good agreement between the results presented here and those reported in Reference 9 lends strong support to the belief that these results are indeed correct.

Table 4.3 $\Gamma/q^2 = \Lambda/\rho C_P$ along the Critical Isochore

$T(^{\circ}K)$	$T-T_C(^{\circ}K)$	$\Gamma/\pi(\text{Hz})$	$1/2\Gamma(\text{msec})$	$\Gamma/q^2(\text{cm}^2/\text{sec})$
321.092	2.385	753		33.51×10^{-6}
320.818	2.111	669		29.66
320.609	1.902	615		27.58
320.420	1.713	550		24.60
320.232	1.525	501		22.09
320.120	1.413	461		20.68
319.955	1.248	411		18.38
319.833	1.126	368		16.48
319.728	1.021	338		15.12
319.630	0.923	320		14.35
319.533	0.826	288		12.88
319.451	0.744	264		11.77
319.377	0.670	243		10.87
319.317	0.610	226		10.07
319.250	0.543	203		8.98
319.185	0.478	181		8.10
319.110	0.403		1.036	6.85
319.051	0.344		1.164	6.11
319.003	0.296		1.326	5.37
318.960	0.253		1.488	4.78
318.923	0.216		1.652	4.27
318.894	0.187		1.923	3.70
318.868	0.161		2.180	3.25
318.845	0.138		2.426	2.91
318.827	0.120		2.753	2.60
318.812	0.105		3.035	2.36
318.798	0.091		3.427	2.075
318.788	0.081		3.688	1.93
318.779	0.072		4.056	1.73
318.766	0.059		4.480	1.49
318.755	0.048		5.116	1.30

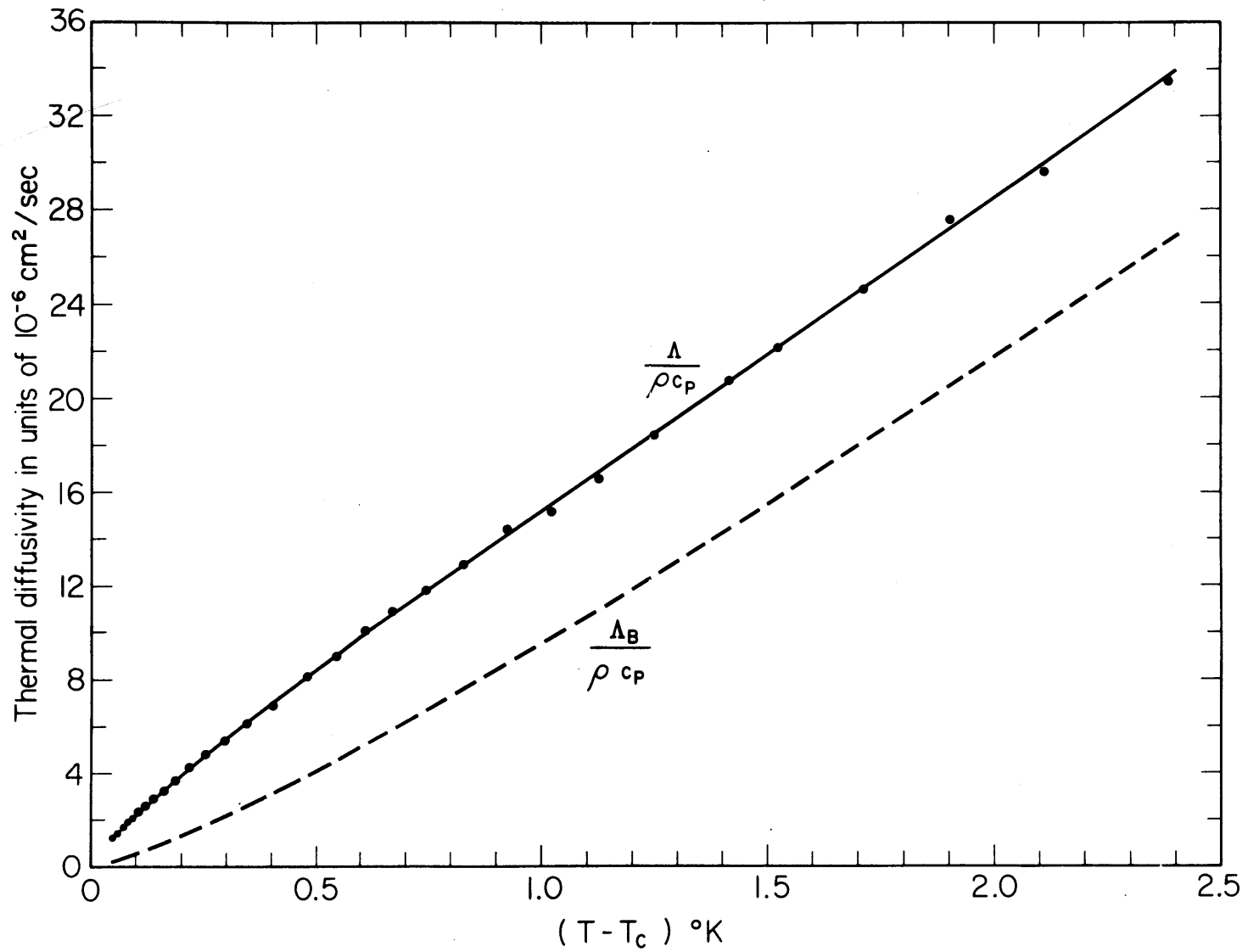


Fig. 4.2 Upper curve, data for the Thermal Diffusivity, $D = \Lambda/\rho C_p$, along the Critical Isochore. Lower curve, calculated Background Contribution to the Thermal Diffusivity, $\Lambda_B/\rho C_p$

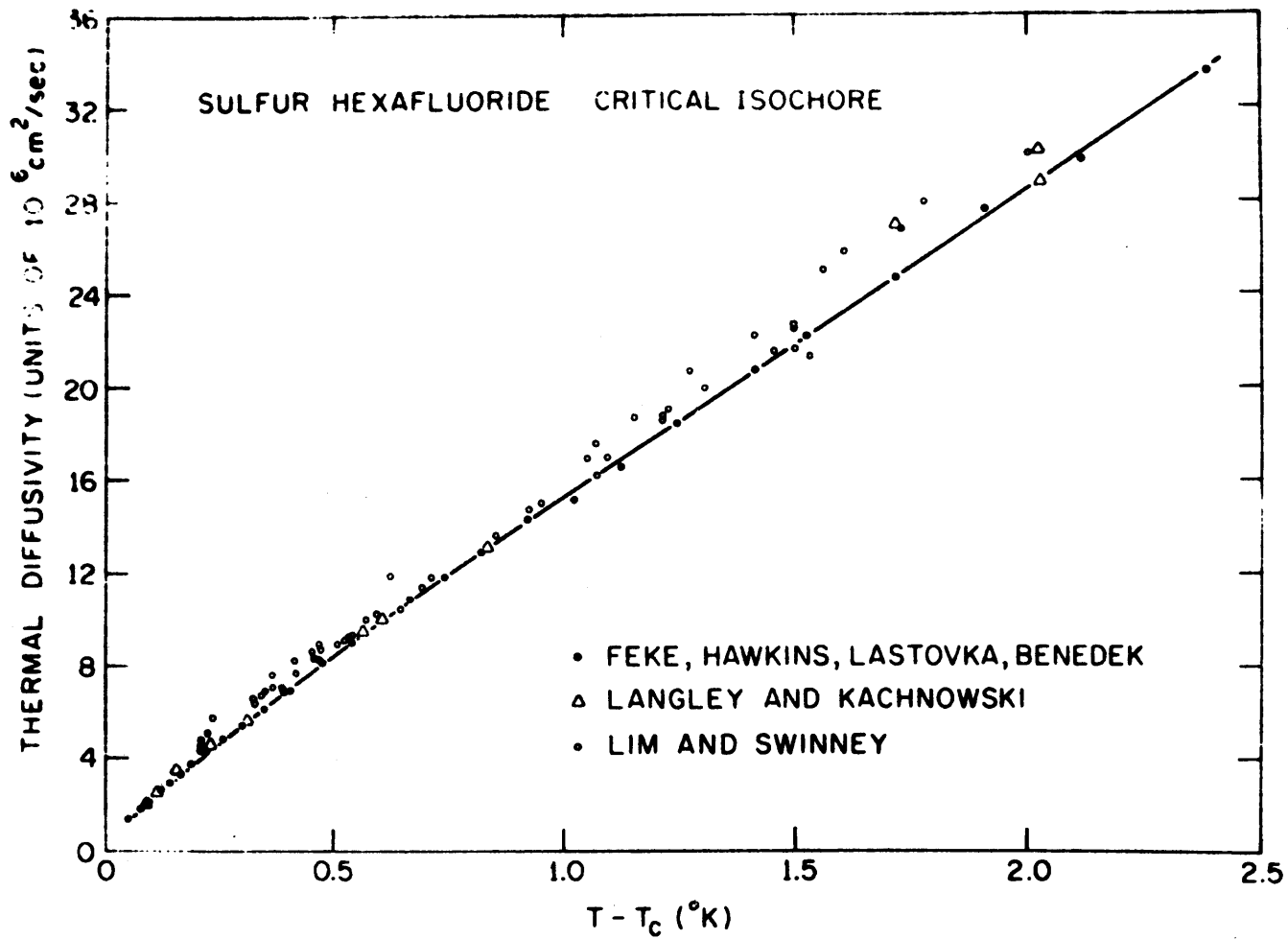


Fig. 4.3 Comparison of Experimental Thermal Diffusivities along the Critical Isochore

4. Analysis of Γ/q^2 Measurements

In order to properly analyze the measurements of $\Gamma/q^2 = \Lambda/\rho C_P$ it is necessary to recall that the mode-mode coupling theories predict the behavior of only the divergent or singular parts of the thermal conductivity and the thermal diffusivity. Specifically, we saw in Section II.E.3. that Kadanoff and Swift⁽¹⁰⁾ predict that in the hydrodynamic region the thermal conductivity of a fluid near its critical point contains a divergent component which has a temperature dependence which is essentially governed by the expression

$$\Lambda_S \sim \frac{k_B T \rho C_P}{\eta^* \xi} . \quad (4.4)$$

Further, we saw in Section II.E.4. that Kawasaki^{(11), (12)} predicts that the magnitude and temperature dependence of the critical part of the thermal diffusivity, $D_C = (\frac{\Lambda}{\rho C_P})_C$, in the hydrodynamic region is given by

$$D_C = \frac{k_B T}{6\pi\eta^* \xi} . \quad (4.5)$$

It becomes clear, then, that in order to analyze the data in terms of the mode-mode coupling theory one must take into account the background contribution to the thermal diffusivity which arises from the nondivergent part, Λ_B , of the thermal conductivity. Sengers and Keyes⁽¹³⁾ indicate that the thermal conductivity may be expressed as

$$\Lambda = \Lambda_B + \Lambda_S \quad (4.6)$$

where Λ_S is an ideal thermal conductivity in the absence of any critical

point anomaly. Empirically, the background Λ_B can only be estimated by extrapolating data away from the critical point into the critical region. As Sengers and Keyes indicate this extrapolation is simplified by noting that

$$\Lambda_B(\rho, T) = \Lambda_B(\rho) + \Lambda_B(\rho = 0, T) \quad . \quad (4.7)$$

We see then that an accurate estimate of Λ_B in the critical region may be obtained from measurements of $\Lambda_B(\rho = 0)$ at temperatures near T_C combined with measurements of $\Lambda_B(\rho)$ at densities near ρ_C but at temperatures away from T_C . While such data are readily available for CO_2 ⁽¹⁴⁾ and xenon,⁽¹⁵⁾ the determination of Λ_B for SF_6 required a more elaborate procedure.

Lis and Kellard⁽¹⁶⁾ have measured the thermal conductivity of SF_6 as a function of pressure along five supercritical isotherms and one subcritical isotherm. The densities corresponding to their measured pressures and temperatures range from $\rho = 0.030 \text{ gm/cm}^3$ to $\rho = 1.293 \text{ gm/cm}^3$. Further, Tauscher⁽¹⁷⁾ has measured the thermal conductivity of SF_6 at four points along the liquid side of the coexistence curve. The densities corresponding to these points range from $\rho = 1.55 \text{ gm/cm}^3$ to 1.83 gm/cm^3 . The densities corresponding to the measured temperatures and pressures of Lis and Kellard and Tauscher were determined by applying the SF_6 PVT data reported by Mears et al.,⁽¹⁸⁾ Otto and Thomas⁽¹⁹⁾ and Ulybin and Zherdev.⁽²⁰⁾

Having deduced $\Lambda(\rho, T)$ at a number of points from the measurements of Lis and Kellard and Tauscher, the next step was to obtain $\Lambda(\rho, T_C)$ from

these data. From the low density data of Lis and Kellard it was found that $\Lambda(\rho \rightarrow 0, T)$ varied linearly with temperature at a rate of 0.007×10^3 erg/sec·cm³K/°K. This variation of Λ with temperature was applied to each of the points, $\Lambda(\rho, T)$ in order to obtain a set of points, $\Lambda(\rho, T_C)$. In Fig. 4.4 are plotted each of these deduced points, $\Lambda(\rho, T_C)$. The symbols indicate the actual temperatures at which the measurements occurred but the plotted points have magnitudes which have been corrected to T_C .

The solid curve in Fig. 4.4 is an estimate of the background thermal conductivity, $\Lambda_B(\rho, T_C)$. This curve may be represented by a polynomial,

$$\Lambda_B(\rho, T_C) = A_0 + A_1\rho + A_2\rho^2 + A_3\rho^3 + A_4\rho^4 \quad (4.8)$$

where the coefficients have the following magnitudes:

$$\begin{aligned} A_0 &= 1.334 \\ A_1 &= 2.213 \\ A_2 &= 1.097 \\ A_3 &= -1.047 \\ A_4 &= 0.552 \end{aligned} \quad (4.9)$$

The coefficients have units of 10^3 erg/sec·cm³K and ρ is in units of gm/cm³.

Applying these results one finds that along the critical isochore the background thermal conductivity may be obtained from the expression

$$\Lambda_B(\rho_C, T) = (3.29 + 0.007(T - T_C) \pm 0.1) \times 10^3 \text{ erg/sec}\cdot\text{cm}^3\text{K} \quad (4.10)$$

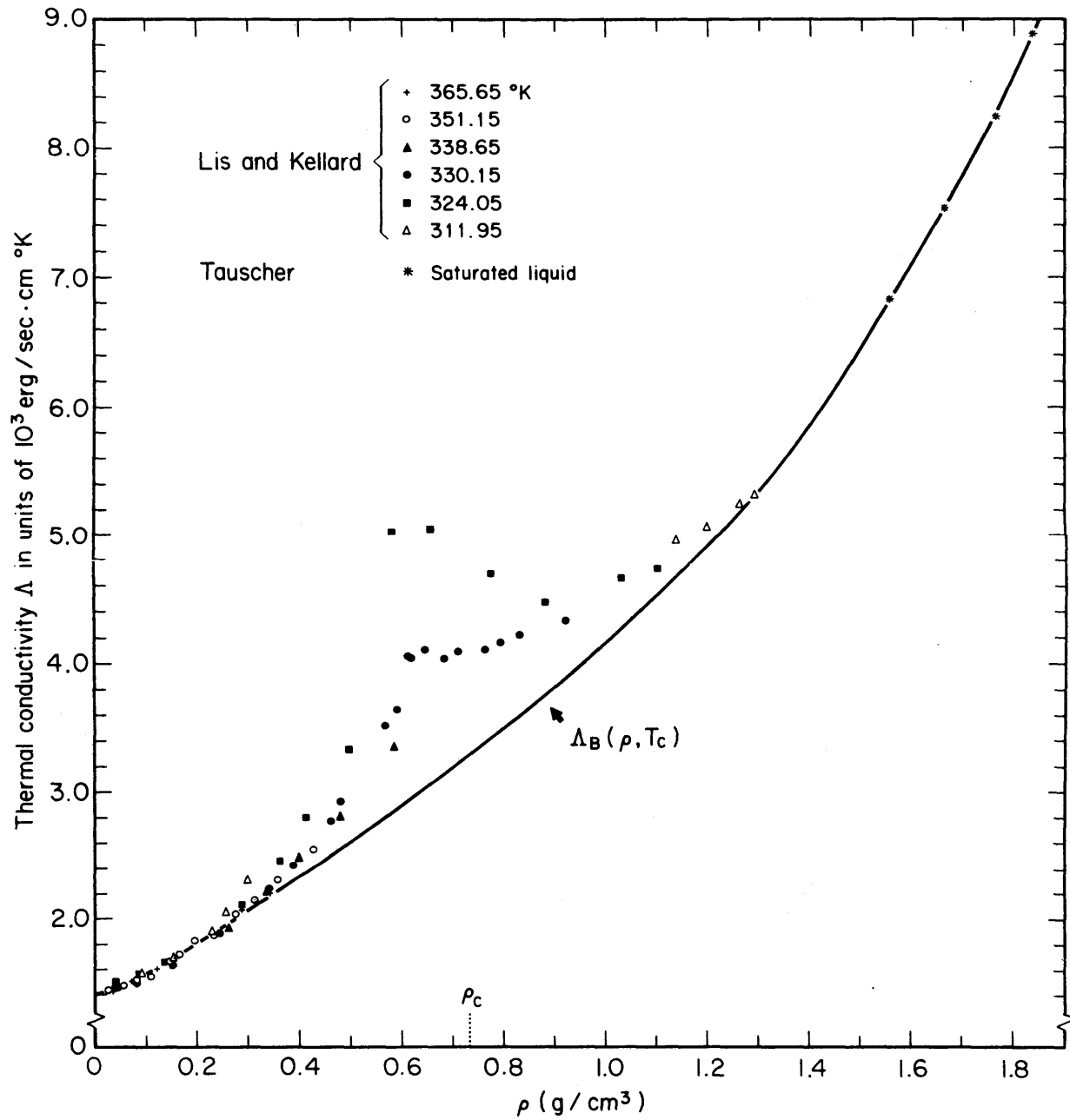


Fig. 4.4 Background Thermal Conductivity for SF_6

Having determined the background thermal conductivity, Λ_B , the next step in determining the background contribution to the thermal diffusivity, $\Lambda_B/\rho C_P$, is to calculate C_P . We recall from Eq. (2.61) that the specific heat per unit mass at constant pressure is given by:

$$C_P = C_V + \frac{T}{\rho} \kappa_T \left(\frac{\partial P}{\partial T} \right)_V^2 \quad (4.11)$$

where C_V is the specific heat per unit mass at constant volume. We recall from Eq. (2.66) that

$$\frac{C_P}{C_V} = \frac{\kappa_T}{\kappa_S} \quad (4.12)$$

where κ_S is the adiabatic compressibility. Now, κ_S is related to the low frequency sound speed, u , by

$$\kappa_S = \frac{1}{\rho u^2} . \quad (4.13)$$

Using Eqs. (4.11) - (4.13) we have the following expression for C_P :

$$C_P = \left[\frac{T}{\rho} \kappa_T \left(\frac{\partial P}{\partial T} \right)_V^2 \right] / \left[1 - \frac{1}{\rho u^2 \kappa_T} \right] . \quad (4.14)$$

Equation (4.14) was used to obtain the magnitude of C_P at each temperature along the critical isochore. In evaluating Eq. (4.14) the data presented in Section IV.B.1. for $\left(\frac{\partial P}{\partial T} \right)_V$ and in Section IV.B.2. for κ_T were used. For the low frequency sound speed, u , the measurements of Fritsch and Carome⁽²¹⁾ were used.

The dashed curve in the lower portion of Fig. 4.2 shows the background contribution to the thermal diffusivity, $\Lambda_B/\rho C_P$, as calculated from Eqs. (4.10) and (4.14). Due to uncertainties in the extrapolation of Λ_B

into the critical region and experimental uncertainties in the quantities entering into the expression for C_P , it is estimated that the uncertainty in $\Lambda_B/\rho C_P$ is approximately 10%.

We may thus obtain the critical part of the thermal diffusivity, D_C , from the light scattering data using the expression

$$D_C = \frac{\Lambda_S}{\rho C_{P_S}} = \left[\frac{\Lambda}{\rho C_P} - \frac{\Lambda_B}{\rho C_P} \right] \cdot \left[\frac{C_P}{C_{P_S}} \right]. \quad (4.15)$$

According to Sengers⁽²²⁾ the singular part of the specific heat, C_{P_S} , may be approximated by

$$C_{P_S} = C_P - C_V. \quad (4.16)$$

In Table 4.4 we present the averaged experimental values of $\Lambda/\rho C_P$, the calculated quantity $\Lambda_B/\rho C_P$, and the critical part of the thermal diffusivity obtained from Eqs. (4.15) and (4.16).

5. Discussion of the Results in Terms of the Mode-Mode Coupling Theory

Having obtained the critical part of the thermal diffusivity, $D_C = \Lambda_S/\rho C_{P_S}$, from the data, we shall examine these results in terms of the mode-mode coupling theory. The points comprising the upper solid curve in the logarithmic plot shown in Fig. 4.5 are the averaged results of the measurements of $\Gamma/q^2 = \Lambda/\rho C_P$. The open circles comprising the lower solid curve represent the point by point experimental deduction of the critical part of the thermal diffusivity, D_C , obtained using Eq. (4.15), which are listed in Table 4.4.

Table 4.4 $D_C = \frac{\Lambda_S}{\rho C_{P_S}}$ along the Critical Isochore

$T(^{\circ}K)$	$T-T_C(^{\circ}K)$	$\frac{\Lambda}{\rho C_P}(\text{cm}^2/\text{sec})$	$\frac{\Lambda_B}{\rho C_P}(\text{cm}^2/\text{sec})$	$\frac{\Lambda_S}{\rho C_{P_S}}(\text{cm}^2/\text{sec})$
321.092	2.385	33.51×10^{-6}	26.39×10^{-6}	7.51×10^{-6}
320.818	2.111	29.66	23.13	6.84
320.609	1.902	27.58	20.63	7.23
320.420	1.713	24.60	18.38	6.46
320.232	1.525	22.09	16.13	6.16
320.120	1.413	20.68	14.79	6.07
319.955	1.248	18.38	12.84	5.69
319.833	1.126	16.48	11.40	5.20
319.728	1.021	15.12	10.18	5.05
319.630	0.923	14.35	9.05	5.40
319.533	0.826	12.88	7.94	5.02
319.451	0.744	11.77	7.02	4.82
319.377	0.670	10.87	6.19	4.73
319.317	0.610	10.07	5.54	4.58
319.250	0.543	8.98	4.82	4.20
319.185	0.478	8.10	4.14	4.00
319.110	0.403	6.85	3.37	3.51
319.051	0.344	6.11	2.78	3.35
319.003	0.296	5.37	2.32	3.07
318.960	0.253	4.78	1.91	2.88
318.923	0.216	4.27	1.58	2.70
318.894	0.187	3.70	1.32	2.38
318.868	0.161	3.25	1.10	2.15
318.845	0.138	2.91	0.913	2.00
318.827	0.120	2.60	0.769	1.84
318.812	0.105	2.36	0.653	1.71
318.798	0.091	2.075	0.548	1.53
318.788	0.081	1.93	0.475	1.45
318.779	0.072	1.73	0.411	1.32
318.766	0.059	1.49	0.321	1.17
318.755	0.048	1.30	0.249	1.05

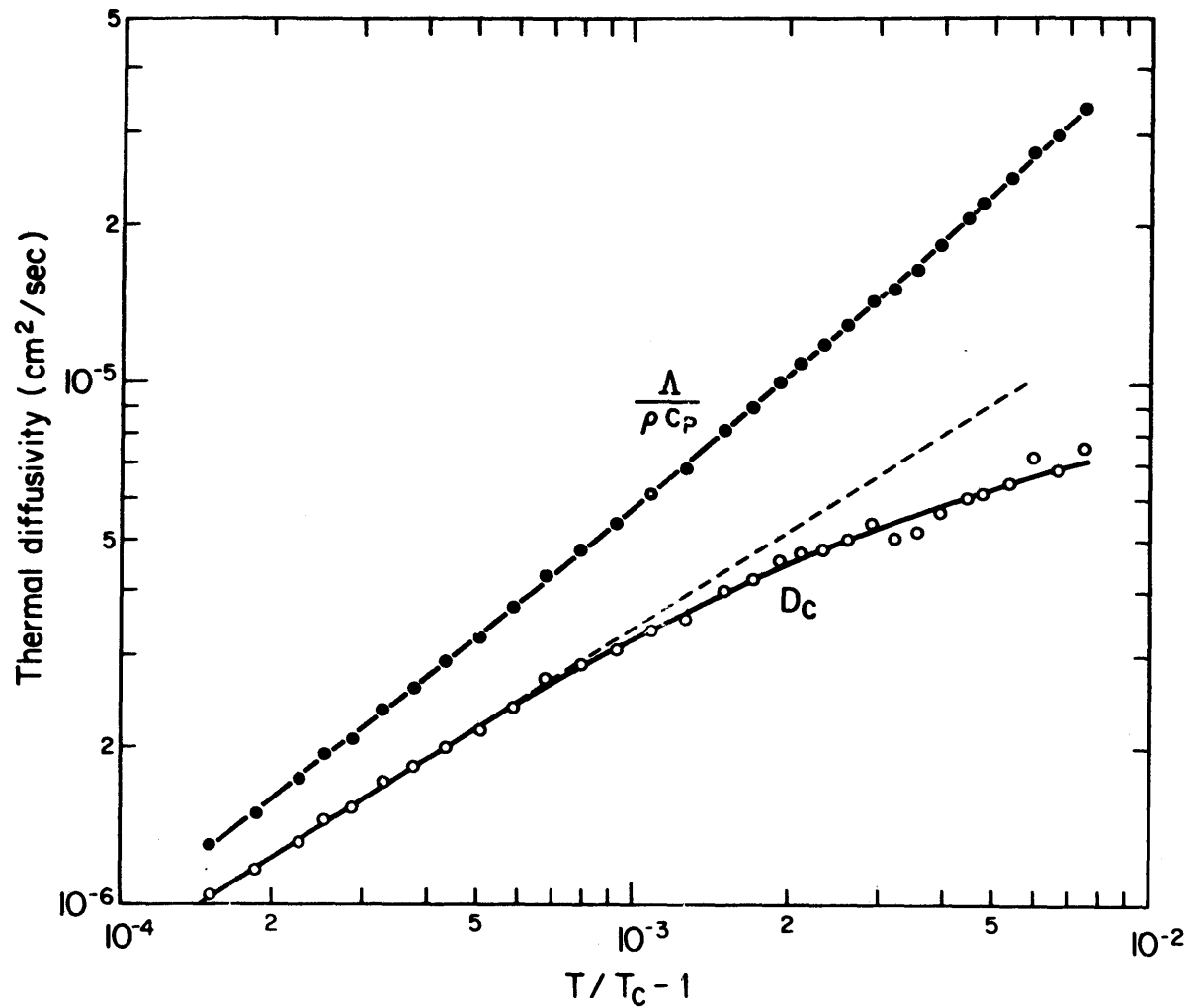


Fig. 4.5 Upper curve, data for the total Thermal Diffusivity, D . Lower curve, the deduced Critical Part of the Thermal Diffusivity. The straight (dashed) line represents $k_B T / 6\pi\eta^* \xi$ for the values of η^* and ξ discussed in the text.

We have seen that the mode-mode coupling theory predicts that $D_C = k_B T / 6\pi\eta^* \xi$. We have also seen in Section II.E.3. that the high frequency shear viscosity, η^* , is expected to be a slowly varying quantity. We see then that the temperature dependence of D_C is governed by the temperature dependence of the Ornstein-Zernike long range correlation length, ξ . We have seen (Eq. (2.56)) that ξ is predicted to diverge according to a simple power law with critical exponent ν . As can be seen in Fig. 4.5 the deduced values of D_C do in fact obey a simple power law behavior in the temperature range $0.048^\circ\text{K} < T - T_C < 0.5^\circ\text{K}$. The exponent describing the temperature dependence of D_C is estimated as 0.64 ± 0.04 . This value is consistent with the critical exponent ν for the temperature dependence of the correlation length, ξ , obtained by Puglielli and Ford⁽⁴⁾ from measurements at temperatures below $T - T_C = 0.5^\circ\text{K}$ ($\nu = 0.67 \pm 0.07$) as would be expected for a constant value of η^* .

If we use $\xi = (1.5 \pm 0.23)(T/T_C - 1)^{-0.67 \pm 0.07} \text{ \AA}$ as given in Reference 4, then the magnitude of η^* required to fit $k_B T / 6\pi\eta^* \xi$ to the data for D_C is approximately $400 \pm 50 \mu\text{P}$. The extrapolated straight dashed line in Fig. 4.5 thus represents $k_B T / 6\pi\eta^* \xi$ using these values of ξ and η^* .

Wu and Webb⁽²³⁾ have used the spectrum of light scattered from thermally excited surface waves to deduce the effective kinematic viscosity of the interface between the coexisting phases in SF_6 . They find that the average viscosity of the liquid and vapor phases is $\bar{\eta} = [425 + 14.5(T_C - T) \pm 15] \mu\text{P}$. Since the viscosities of the coexisting phases approach each other as $T \rightarrow T_C$, we may use their result to estimate η^* along the critical isochore. In Section II.E.4. we saw that the extended mode-mode coupling theory of Kawasaki and Lo⁽²⁴⁾ predicts that η^*

is 5.5% smaller than the measured hydrodynamic shear viscosity. We see then that if we use the data of Puglielli and Ford for ξ and the data of Wu and Webb to deduce η^* then indeed our deduced values of D_C agree extremely well with the calculated quantity $k_B T / 6\pi\eta^* \xi$ in the temperature range $0.048^\circ\text{K} < T - T_C < 0.5^\circ\text{K}$. As is seen in Fig. 4.5 there is a marked departure of the deduced values of D_C from a simple power law behavior at temperatures above $T - T_C = 0.5^\circ\text{K}$. This rapid departure is not characteristic of the fluids CO_2 ⁽⁵⁾ and xenon^{(6), (25), (26)} for which deduced values of D_C are observed to obey a simple power law behavior with magnitudes in agreement with the mode-mode coupling theory prediction at temperatures up to 3°K above T_C for xenon and 4.4°K above T_C for CO_2 .

It is important to note, however, that the measurements of ξ for SF_6 were carried out at temperatures below $T - T_C = 0.5^\circ\text{K}$. Thus there is no direct evidence that ξ continues to obey a simple power law behavior at higher temperatures.

We may conclude this section by reiterating that the magnitude and temperature dependence of the critical part of the thermal diffusivity, deduced from measurements of the photocurrent power spectrum and the photocurrent correlation function arising from light scattered quasi-elastically from SF_6 along the critical isochore, is in excellent agreement with the predictions of the mode-mode coupling theory over the temperature range where independent data exist allowing proper analysis. In the next section we shall turn our attention to the measurements which were carried out along the coexistence curve.

C. The Coexistence Curve

In this section we shall present, analyze, and discuss the results of measurements carried out along the liquid and vapor sides of the SF₆ coexistence curve over the temperature range $0.021^{\circ}\text{K} < (T_C - T) < 1.027^{\circ}\text{K}$. The measurements were carried out on the same sample of SF₆ that was used during the measurements along the critical isochore. The average density of the sample during these measurements was within 0.1% of ρ_C so that the meniscus remained near the mid height of the sample chamber over the entire temperature range investigated.

1. Measurements of Pressure

In Table 4.5 we present the results of the measurements of the pressure, P , as a function of the temperature below T_C . These data thus represent measurements of the SF₆ vapor pressure. Although pressure measurements at temperatures greater than 318.314°K were made, they are not presented since they could not be adequately corrected for the time drift of the pressure transducer (Section III.E.). The absolute magnitude of each of the presented measurements was adjusted so that when one extrapolates $P(T)$ to $P(T_C)$ one obtains $P(T_C) = 544.77$ psi which is the critical pressure reported by MacCormack and Schneider.⁽³⁾

The $P(T)$ data could be adequately represented by the form

$$P(T) = P_C + A_1(T - T_C) \quad , \quad (4.17)$$

so that the slope of the vapor pressure curve, $(\frac{\partial P}{\partial T})_{lv}$, is just A_1 . From a computer fit it was found that

$$\left(\frac{\partial P}{\partial T}\right)_{lv} = (7.94 \pm 0.1) \times 10^5 \text{ dyne/cm}^2 \text{ }^{\circ}\text{K} \quad .$$

Table 4.5 Variation of Pressure with Temperature along the Vapor Pressure Curve

<u>T(°K)</u>	<u>P(psi)</u>
317.682	533.95
317.781	534.1
317.875	535.2
317.959	536.2
318.036	537.05
318.103	537.8
318.166	538.5
318.222	539.2
318.268	539.7
318.314	540.2

As will be shown, the magnitude of $(\frac{\partial P}{\partial T})_{\rho, V}$ plays an important role in the analysis of the light scattering measurements.

2. Measurements of $(\frac{\partial \rho}{\partial \mu})_T$

As we have shown (Eqs. (2.120), (3.43) and (4.3)), the ratio of scattered power to incident power, P_S/P_I , is given by

$$\frac{P_S}{P_I} = \left[\frac{\pi^2 L \Omega}{4 \lambda_0} k_B T \left(\frac{\partial n^2}{\partial \rho} \right)^2 \right] \rho^2 \kappa_T \frac{1}{(1 + q^2 \xi^2)} \quad (4.18)$$

Since $q^2 \xi^2 \ll 1$ over the temperature range of the measurements, we see that the reduced compressibility, $\rho^2 \kappa_T = (\frac{\partial \rho}{\partial \mu})_T$, is proportional to

$(\frac{P_S}{P_I}) \frac{1}{T}$ when corrections are made to account for small changes in L , Ω , and $(\frac{\partial n^2}{\partial \rho})_T$ due to changes in n as ρ varies along the coexistence curve.

We have also shown (Eq. (3.44)) that the ratio P_S/P_I is proportional to the ratio of scattered power to attenuated transmitted power, $P_S/(P_T)_{\text{meas}}$.

We may account for the changes in L , Ω , and $(\frac{\partial n^2}{\partial \rho})_T$ in the following way. Referring to Figs. 3.8 and 3.9 and the discussion of Section III.G., we see that the width of aperture S_3 in Fig. 3.8 determines some length, $L(\theta)$, of the scattering region within the sample chamber from which light is accepted at a particular scattering angle, θ . For a fixed aperture width we may write

$$L(\theta) = \frac{L(\theta = 90^\circ)}{\sin \theta} \quad (4.19)$$

From Fig. 3.9 we see that the scattering angle is given by $\theta = 2\theta_3$.

According to Eq. (3.41),

$$\sin \theta_3 = \frac{n_1}{n_3} \sin \theta_1 \quad . \quad (4.20)$$

We see that since the scattering angle, θ , changes with the refractive index of the SF₆, n_3 , then the effective length viewed by the collection optics will also change. We may write

$$\sin 2\theta_3 = 2 \sin \theta_3 \cos \theta_3 \approx 2 \sin \theta_3 \quad (4.21)$$

since $\cos \theta_3 \approx 1$. Using this result in Eqs. (4.19) and (4.20), we have

$$L(\theta) = \frac{L(\theta = 90^\circ)}{2 \frac{n_1}{n_3} \sin \theta_1} \quad . \quad (4.22)$$

We see then that the change in L is directly proportional to the change in n_3 .

We now consider the change in Ω due to changes in n_3 . We saw that the area of aperture S_2 in Fig. 3.8 determines the size of the solid angle, Ω , associated with the scattered light that is accepted for study. In general we may write

$$d\Omega = d\theta_3 d\phi_3 \quad (4.23)$$

where $d\theta_3$ is the acceptance angle in the plane of Fig. 3.9 and $d\phi_3$ is the acceptance angle in the plane normal to that of Fig. 3.9. From Eq. (4.20) we have

$$\cos \theta_3 d\theta_3 = \frac{n_1}{n_3} \cos \theta_1 d\theta_1 \quad . \quad (4.24)$$

Since $\cos \theta_3 \approx \cos \theta_1 \approx 1$, we have

$$d\theta_3 \approx \frac{n_1}{n_3} d\theta_1 \quad (4.25)$$

Similarly,

$$d\phi_3 \approx \frac{n_1}{n_3} d\phi_1 \quad (4.26)$$

Therefore,

$$d\Omega \approx \left(\frac{n_1}{n_3}\right)^2 d\theta_1 d\phi_1 \quad (4.27)$$

We see then that the change in Ω is inversely proportional to the square of the change of the SF₆ refractive index, n_3 .

Finally, the change in the quantity $\left(\frac{\partial n^2}{\partial \rho}\right)_T$ as n and ρ vary along the coexistence curve was calculated using the Lorenz-Lorentz equation for SF₆ (Eq. (3.4)).

In Table 4.6 we present the results of measurements of the ratio of the scattered power to the measured attenuated transmitted power obtained by measurements of the average photocurrent arising from the light scattered by the SF₆ sample along the liquid side of the coexistence curve.

The measurements were obtained using a scattering vector $q = 8382 \text{ cm}^{-1}$.

Each measurement has been normalized by the factor

$$I_{\text{NORM}} = \frac{\left(\frac{\partial n^2}{\partial \rho}\right)_{\substack{\rho=\rho_C \\ T=T_C}}^2 \cdot T_C \cdot n_3}{\left(\frac{\partial n^2}{\partial \rho}\right)_T^2 \cdot T \cdot (n_3)_{\substack{\rho=\rho_C \\ T=T_C}}} \quad .$$

Each measurement then is directly proportional to the magnitude of $\left(\frac{\partial \rho}{\partial \mu}\right)_T$.

Table 4.6 $(\frac{\partial \rho}{\partial \mu})_T$ along the Liquid Side of the Coexistence Curve

$T(^{\circ}\text{K})$	$T_C - T(^{\circ}\text{K})$	$\frac{T_C - T}{T_C}$	$(\frac{P_S}{P_T}) \cdot I_{\text{NORM}}$	$(\frac{\partial \rho}{\partial \mu})_T (\text{g}^2 \text{erg}^{-1} \text{cm}^{-3})$
317.683	1.024	3.213×10^{-3}	.401	1.903×10^{-7}
317.781	0.926	2.905	.453	2.149
317.875	0.832	2.611	.518	2.458
317.959	0.748	2.347	.587	2.785
318.035	0.672	2.109	.667	3.165
318.103	0.604	1.895	.758	3.597
318.166	0.541	1.697	.865	4.104
318.222	0.485	1.522	.984	4.669
318.268	0.439	1.377	1.113	5.281
318.314	0.393	1.233	1.278	6.064
318.353	0.354	1.111	1.447	6.866
318.390	0.317	9.95×10^{-4}	1.663	7.891
318.423	0.284	8.91	1.910	9.063
318.453	0.254	7.97	2.174	1.032×10^{-6}
318.478	0.229	7.19	2.498	1.185
318.502	0.205	6.432	2.849	1.352
318.523	0.184	5.773	3.253	1.544
318.542	0.165	5.177	3.750	1.779
318.561	0.146	4.581	4.330	2.055
318.574	0.133	4.173	4.891	2.321
318.588	0.119	3.734	5.678	2.694
318.599	0.108	3.389	6.486	3.078
318.611	0.096	3.012	7.534	3.575
318.622	0.085	2.667	8.621	4.091

The proportionality constant between the experimental quantity $\left(\frac{P_S}{P_T}\right)_{\text{meas.}} \cdot I_{\text{NORM}}$ and $\left(\frac{\partial \rho}{\partial \mu}\right)_T$ was obtained using the method described in Section III.H.1. We recall that the proportionality constant was determined by measuring both $(P_S/P_T)_{\text{meas.}}$ and the pressure, P , at 23 points along a near critical isotherm over the density range $1.15 \leq \frac{\rho - \rho_C}{\rho_C} \leq 1.40$. The quantity $\rho^2 \kappa_T$ was then determined by measuring the variation of P with density. In Table 4.6 we thus present our deduced values of the reduced compressibility, $\left(\frac{\partial P}{\partial \mu}\right)_T$, along the liquid side of the coexistence curve.

In Fig. 4.6 is shown a log-log plot of $\left(\frac{\partial \rho}{\partial \mu}\right)_T$ as a function of the reduced temperature, $(1 - T/T_C)$. We see that the reduced compressibility accurately obeys the power law $\left(\frac{\partial \rho}{\partial \mu}\right)_T = C_0 (1 - T/T_C)^{-\gamma'}$ with $C_0 = 1.67 \times 10^{-10} \text{ g}^2 \text{ erg}^{-1} \text{ cm}^{-3}$, and $\gamma' = 1.225 \pm 0.015$.

We may recall that the measurements of the compressibility along the critical isochore indicated that $\gamma = 1.235 \pm 0.015$. Therefore the static scaling law prediction $\gamma = \gamma'$ (Eq. (2.69)), is indeed satisfied for SF_6 . We may note that the prediction $\gamma = \gamma'$ is also satisfied for xenon. (6)

We may also recall (Eq. (2.80)) that the parametric linear model equation of state⁽²⁷⁾ explicitly predicts the ratio of the magnitudes of the reduced compressibilities at equal temperature differences $|T - T_C|$ above T_C along the critical isochore and below T_C along the coexistence curve. The prediction is

$$\left(\frac{\partial \rho}{\partial \mu}\right)_{T > T_C} / \left(\frac{\partial \rho}{\partial \mu}\right)_{T < T_C} = \frac{\gamma}{\beta} [(1 - 2\beta)\gamma / 2\beta(\gamma - 1)]^{\gamma-1} .$$

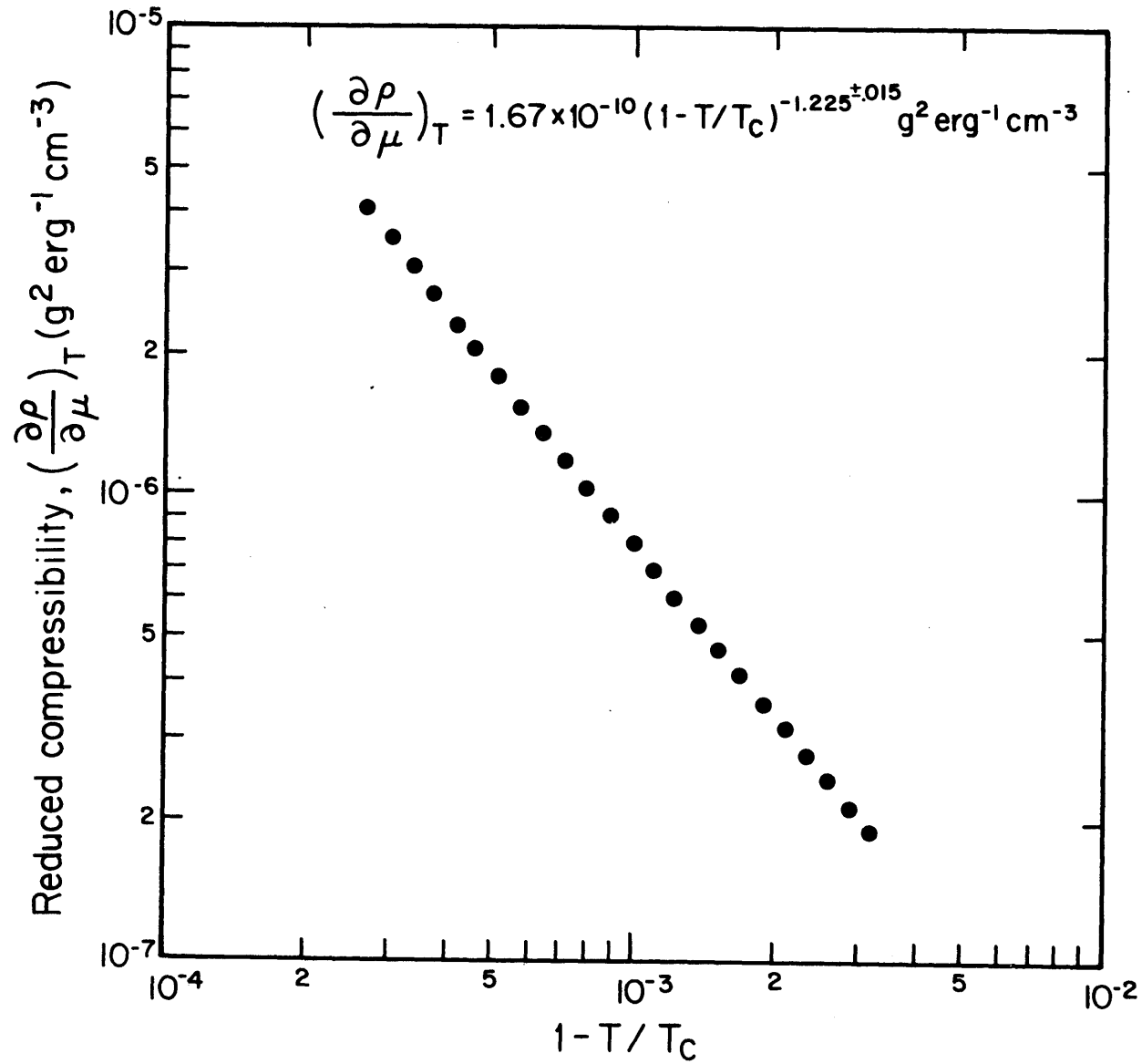


Fig. 4.6 Reduced Compressibility, $(\partial\rho/\partial\mu)_T$, along the Liquid Side of the Coexistence T Curve.

In this expression β is the critical exponent that describes the shape of the coexistence curve (Eq. (2.46)). The value $\beta = 0.33 \pm 0.01$ has been accurately determined.^{(7),(28)} Using this value of β and using $\gamma = 1.23 \pm 0.02$ we find that the linear model predicts $(\frac{\partial \rho}{\partial \mu})_{T > T_C} / (\frac{\partial \rho}{\partial \mu})_{T < T_C} = 4.6 \pm 0.2$. A direct calculation of the ratio of the magnitudes of the reduced compressibilities from the experimental results yields $(\frac{\partial \rho}{\partial \mu})_{T > T_C} / (\frac{\partial \rho}{\partial \mu})_{T < T_C} = 4.33 \pm 0.3$. We see that there is fair agreement with the predictions of the linear model.

Finally, we may recall from the discussion of Section II.D. that the scaling law equations of state predict that if any two of the critical exponents are known for a particular system then all the rest may be determined. Using $\gamma = 1.23 \pm 0.02$ and $\beta = 0.33 \pm 0.01$ we may determine the scaling law predictions for the other critical exponents for SF_6 . From Eq. (2.71) we have, for the critical exponent associated with the divergence of C_V , $\alpha = 0.11 \pm 0.04$. From Eq. (2.74) we have, for the critical exponent associated with the shape of the critical isotherm, $\delta = 4.73 \pm 0.18$. From Eq. (2.79) we have, for the critical exponent associated with the departure of the behavior of the pair correlation function from the prediction of the Ornstein-Zernike theory, $\eta_F = 0.05 \pm 0.03$. Finally, from Eq. (2.77) we have, for the critical exponent associated with the divergence of ξ , $\nu = 0.63 \pm 0.02$.

3. Measurements of Γ/q^2

We next turn our attention to the measurements of the quantity Γ/q^2 , obtained from measurements of the half-width at half height of the photocurrent power spectrum, Γ/π , and the decay time of the photocurrent

correlation function, $1/2\Gamma$, arising from the light scattered quasi-elastically from thermally excited entropy fluctuations in SF_6 along the liquid and vapor sides of the coexistence curve. These measurements were carried out over the temperature range $0.021^\circ K < T_C - T < 1.024^\circ K$, and with a scattering vector $q = 8382 \text{ cm}^{-1}$.

In Table 4.7 we present our averaged experimental values of Γ/π and $1/2\Gamma$. We also present our results for Γ/q^2 using $q = 8382 \text{ cm}^{-1}$. Since $q^2 \xi^2 \ll 1$ over the range of our measurements, the quantity $\Gamma/q^2 = \Lambda/\rho C_p$, the thermal diffusivity.

In Fig. 4.7 are plotted the averaged results of the measurements of the thermal diffusivity (open and closed circles) as a function of $T_C - T$. Also plotted in this figure are the results of Langley and Elterman⁽²⁾ (open and closed squares) obtained at U. of Mass. The U. of Mass. data were obtained using a scattering vector $q = 8.32 \times 10^4 \text{ cm}^{-1}$. From Fig. 4.7 we see that there is excellent agreement between the results of the two experiments even though the values of q^2 differ by two orders of magnitude.

The M. I. T. data and the hydrodynamic U. of Mass. data can be approximately represented by the empirical formulas $(\Gamma/q^2)_{\text{liquid}} = 9.02 \times 10^{-3} (1 - T/T_C)^{0.92} \text{ cm}^2/\text{sec.}$ and $(\Gamma/q^2)_{\text{vapor}} = 5.62 \times 10^{-3} (1 - T/T_C)^{0.86} \text{ cm}^2/\text{sec.}$ These formulas are shown as the dashed curves in Fig. 4.7.

The results presented in Fig. 4.7 are similar in curvature to those reported by Braun et al.⁽⁸⁾ but over the range of measurement are everywhere greater in magnitude by approximately 20%. The present results differ both in magnitude and in curvature from those previously reported

Table 4.7 $\frac{\Gamma}{q} = \frac{\Lambda}{\rho C_P}$ along the Coexistence Curve

LIQUID SIDE

$T(^{\circ}\text{K})$	$T_C - T(^{\circ}\text{K})$	$\Gamma/\pi(\text{Hz})$	$1/2\Gamma(\text{msec})$	$\Gamma/q^2(\text{cm}^2/\text{sec})$
317.683	1.024	985		44.04×10^{-6}
317.781	0.926	943		42.17
317.875	0.832	799		35.73
317.959	0.748	743		33.22
318.035	0.672	648		28.98
318.103	0.604	615		27.50
318.166	0.541	573		25.62
318.222	0.485	498		22.28
318.268	0.439	459		20.52
318.314	0.393	415		18.03
318.353	0.354	368		16.45
318.390	0.317	346		15.47
318.423	0.284	312		13.95
318.453	0.254	267		11.94
318.478	0.229	245		10.98
318.502	0.205		.6981	10.19
318.523	0.184		.7688	9.26
318.542	0.165		.8425	8.45
318.561	0.146		.9339	7.62
318.574	0.133		1.015	7.00
318.588	0.119		1.136	6.26

Table 4.7 (continued)

$T(^{\circ}\text{K})$	$T_c - T(^{\circ}\text{K})$	$\Gamma/\pi(\text{Hz})$	$1/2\Gamma(\text{msec})$	$\Gamma/q^2(\text{cm}^2/\text{sec})$
318.599	0.108		1.243	5.72
318.611	0.096		1.380	5.15
318.622	0.085		1.566	4.55
318.629	0.078		1.701	4.18×10^{-6}
318.638	0.069		1.868	3.81
318.647	0.060		2.107	3.39
318.652	0.055		2.350	3.08
318.661	0.046		2.695	2.64
318.667	0.040		3.105	2.29
318.674	0.033		3.778	1.89
318.679	0.028		4.577	1.55
318.686	0.021		5.973	1.19
VAPOR SIDE				
317.699	1.008	918		41.05×10^{-6}
318.234	0.473	446		19.94
318.464	0.243	253		11.29
318.598	0.109		1.235	5.76
318.648	0.059		2.156	3.30

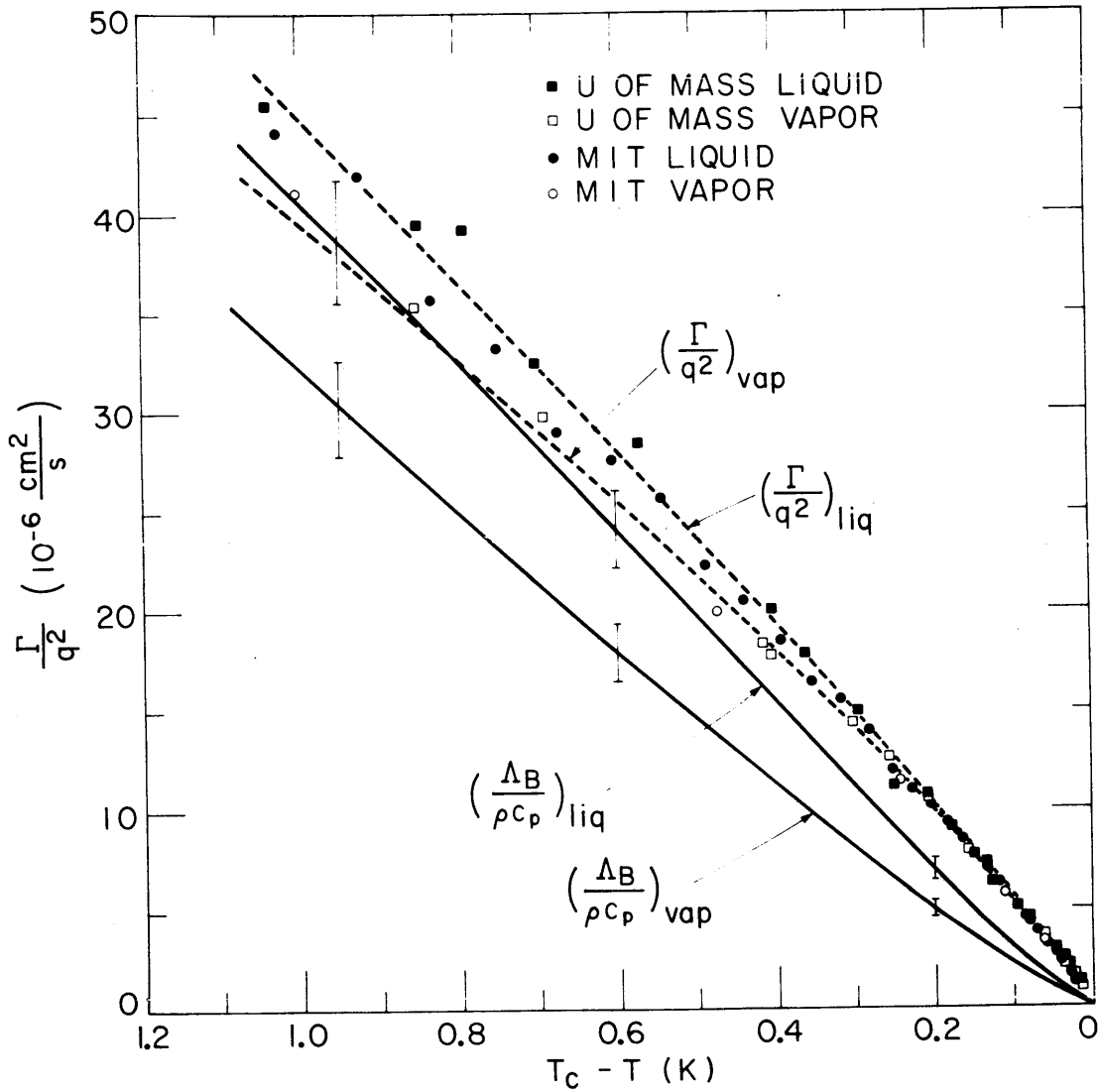


Fig. 4.7 Experimental values (squares and circles) for the Thermal Diffusivity for both sides of the Co-existence Curve. The solid lines represent the calculated Background Contribution to the Thermal Diffusivity, $\Lambda_B/\rho C_P$

by Saxman and Benedek⁽⁷⁾ who found $(\frac{\Lambda}{\rho C_P})_{\text{liquid}} = 1.75 \times 10^{-3} (1 - T/T_C)^{0.63} \text{ cm}^2/\text{sec}$ and $(\frac{\Lambda}{\rho C_P})_{\text{vapor}} = 1.79 \times 10^{-3} (1 - T/T_C)^{0.63} \text{ cm}^2/\text{sec}$.

To date there has been no convincing explanation for the discrepancy between the results presented here and those reported in Reference 7.

However, in view of the excellent agreement between the results of the two independent experiments shown in Fig. 4.7, it is believed that the present results are indeed correct.

4. Analysis of Γ/q^2 Measurements

As was discussed in Section IV.B.4., in order to properly analyze the measurements of $\Gamma/q^2 = \Lambda/\rho C_P$ it is necessary to deduce from the data the critical part of the thermal diffusivity. The critical part of the thermal diffusivity may be deduced by accounting for the background contribution to the measured thermal diffusivity which arises from the non-divergent part, Λ_B , of the thermal conductivity.

The background thermal conductivity, Λ_B , was calculated at each point along the coexistence curve where the thermal diffusivity was measured by using the formula

$$\Lambda_B(\rho, T) = [A_0 + A_1\rho + A_2\rho^2 + A_3\rho^3 + A_4\rho^4 + 0.007(T - T_C) \pm 0.1] \times 10^3 \text{ erg/sec. cm}^{\circ}\text{K} \quad (4.28)$$

where the magnitudes of the coefficients are given in Eqs. (4.9). As was discussed in Section IV.B.4., this formula was obtained from an interpolation of the thermal conductivity data of Lis and Kellard⁽¹⁶⁾ and Tauscher.⁽¹⁷⁾ The liquid and vapor densities corresponding to temperatures

along the coexistence curve were calculated from the expressions obtained by Saxman: (7)

$$\frac{\rho_l - \rho_g}{2\rho_C} = 1.81 \epsilon^{0.333} \quad (4.29)$$

$$\frac{\rho_l - \rho_g}{2\rho_C} = 1 + 0.60 \epsilon \quad (4.30)$$

where $\epsilon \equiv \left(\frac{T_C - T}{T_C}\right)$ and $\rho_C = 0.732 \text{ gm/cm}^3$.

Having determined the background thermal conductivity, Λ_B , the next step in determining the background contribution to the thermal diffusivity, $\Lambda_B/\rho C_P$, is to calculate C_P . We have seen that C_P may be obtained from the thermodynamic relation

$$C_P = C_V + \frac{T}{\rho} \left(\frac{\partial P}{\partial T}\right)_V^2 \left(\frac{\partial \rho}{\partial \mu}\right)_T \quad (4.31)$$

We have also seen, however, (Eq. (2.64)), that along the coexistence curve $\left(\frac{\partial P}{\partial T}\right)_V$ is not the slope of the vapor pressure curve $\left(\frac{\partial P}{\partial T}\right)_{lv}$, but is related to $\left(\frac{\partial P}{\partial T}\right)_{lv}$ through the formula

$$\left(\frac{\partial P}{\partial T}\right)_V = \left(\frac{\partial P}{\partial T}\right)_{lv} - \rho \left(\frac{\partial \mu}{\partial \rho}\right)_T \left(\frac{\partial \rho}{\partial T}\right)_{lv} \quad (4.32)$$

The final term in this formula changes markedly with temperature as $T \rightarrow T_C$ resulting in a marked temperature dependence in $\left(\frac{\partial P}{\partial T}\right)_V$. The explicit expression for C_P along the coexistence curve thus becomes

$$C_P = C_V + \frac{T}{\rho} \left[\left(\frac{\partial P}{\partial T}\right)_{lv} - \rho \left(\frac{\partial \mu}{\partial \rho}\right)_T \left(\frac{\partial \rho}{\partial T}\right)_{lv} \right]^2 \left(\frac{\partial \rho}{\partial \mu}\right)_T \quad (4.33)$$

The quantity C_P was calculated at each temperature along the coexistence curve using Eq. (4.33). In evaluating Eq. (4.33) the data presented in Section IV.C.1. for $\left(\frac{\partial P}{\partial T}\right)_{lv}$ and in Section IV.C.2. for $\left(\frac{\partial \rho}{\partial \mu}\right)_T$ were used.

The quantity $\left(\frac{\partial \rho}{\partial T}\right)_{\ell v}$ was obtained using Saxman's expression (Eq. (4.29)). The quantity C_V was obtained from the sound speed measurements of Schneider⁽²⁹⁾ in the manner indicated in Section IV.B.4.

The solid curves in Fig. 4.7 show the background contribution to the thermal diffusivity, $\Lambda_B/\rho C_P$, as calculated from Eqs. (4.28) and (4.33) for both the liquid and vapor sides of the coexistence curve. Due to uncertainties in the extrapolation of Λ_B into the critical region and experimental uncertainties in the quantities entering into the expression for C_P , it is estimated that $\Lambda_B/\rho C_P$ has been determined to $\pm 8\%$. This is indicated by the error bars in Fig. 4.7.

As was indicated in Section IV.B.4., we may obtain the critical part of the thermal diffusivity, D_C , from the light scattering data using the expression

$$D_C = \frac{\Lambda_S}{\rho C_{P_S}} = \left[\frac{\Lambda}{\rho C_P} - \frac{\Lambda_B}{\rho C_P} \right] \cdot \left[\frac{C_P}{C_{P_S}} \right] \quad (4.34)$$

where $C_{P_S} = C_P - C_V$.

In Table 4.8 we present the averaged experimental values of $\Lambda/\rho C_P$, the calculated quantity $\Lambda_B/\rho C_P$, and the critical part of the thermal diffusivity obtained from Eq. (4.34).

5. Discussion of the Results in Terms of the Mode-Mode Coupling

Theory

Having obtained the critical part of the thermal diffusivity, $D_C = \Lambda_S/\rho C_{P_S}$, from the data, we shall examine these results in terms of

Table 4.8 $D_C = \frac{\Lambda_S}{\rho C_{P_S}}$ along the Coexistence Curve

LIQUID SIDE				
$T(^{\circ}\text{K})$	$T_C - T(^{\circ}\text{K})$	$\frac{\Lambda}{\rho C_P} (\text{cm}^2/\text{sec})$	$\frac{\Lambda_B}{\rho C_P} (\text{cm}^2/\text{sec})$	$\frac{\Lambda_S}{\rho C_{P_S}} (\text{cm}^2/\text{sec})$
317.683	1.024	44.04×10^{-6}	41.54×10^{-6}	2.75×10^{-6}
317.781	0.926	42.17	37.67	4.91
317.875	0.832	35.73	33.84	2.04
317.959	0.748	33.22	30.33	3.10
318.035	0.672	28.98	27.12	1.98
318.103	0.604	27.50	24.23	3.46
318.166	0.541	25.62	21.52	4.31
318.222	0.485	22.28	19.11	3.31
318.268	0.439	20.52	17.13	3.52
318.314	0.393	18.03	15.19	3.43
318.353	0.354	16.45	13.47	3.07
318.390	0.317	15.47	11.89	3.68
318.423	0.284	13.95	10.48	3.55
318.453	0.254	11.94	9.20	2.80
318.478	0.229	10.98	8.16	2.87
318.502	0.205	10.19	7.17	3.07
318.523	0.184	9.26	6.31	2.99
318.542	0.165	8.45	5.55	2.94
318.561	0.146	7.62	4.78	2.87
318.574	0.133	7.00	4.28	2.75
318.588	0.119	6.26	3.75	2.53

Table 4.8 (continued)

$T(^{\circ}\text{K})$	$T_C - T(^{\circ}\text{K})$	$\frac{\Lambda}{\rho C_P}(\text{cm}^2/\text{sec})$	$\frac{\Lambda_B}{\rho C_P}(\text{cm}^2/\text{sec})$	$\frac{\Lambda_S}{\rho C_{P_S}}(\text{cm}^2/\text{sec})$
318.599	0.108	5.72	3.34	2.41
318.611	0.096	5.15	2.89	2.28
318.622	0.085	4.55	2.49	2.07
318.629	0.078	4.18	2.24	1.96
318.638	0.069	3.81	1.93	1.89
318.647	0.060	3.39	1.66	1.74
318.652	0.055	3.08	1.45	1.64
318.661	0.046	2.64	1.17	1.47
318.667	0.040	2.29	0.99	1.30
318.674	0.033	1.89	0.79	1.10
318.679	0.028	1.55	0.63	0.93
318.686	0.021	1.19	0.44	0.75
VAPOR SIDE				
317.699	1.008	41.05×10^{-6}	32.40×10^{-6}	9.11×10^{-6}
318.234	0.473	19.94	13.65	6.45
318.464	0.243	11.29	6.24	5.13
318.598	0.109	5.76	2.44	3.34
318.648	0.059	3.30	1.23	2.07

the mode-mode coupling theory. The open circles in Fig. 4.8 are the averaged results of the measurements of $\Gamma/q^2 = \Lambda/\rho C_P$ along the liquid side of the coexistence curve. The dashed line through these points represents the approximate empirical formula discussed earlier. The closed and open circles in Fig. 4.9 are the averaged results of the measurements of $\Gamma/q^2 = \Lambda/\rho C_P$ along the vapor side of the coexistence curve. The open circles are the U. of Mass. measurements reported in Reference 2. All of these results are again indicated by the solid symbols in the logarithmic plots shown in Figs. 4.10 and 4.11. The triangles in Fig. 4.10 are measurements far from T_C which were reported in Reference 7. Again, we see that the results from the two independent experiments (and, in the case of Fig. 4.10, from three experiments) are in excellent agreement. We observe from Fig. 4.10, however, that near T_C the U. of Mass. data are greater in magnitude than the M. I. T. data. This is expected since their data extend into the non-hydrodynamic region where the relation $q^2 \xi^2 \ll 1$ no longer holds. In general, one may write

$$\frac{\Gamma}{q^2} = \frac{\Lambda_B}{\rho C_P(q)} + \frac{\Lambda_S(q)}{\rho C_{PS}(q)} \cdot \frac{C_{PS}(q)}{C_P(q)} \quad (4.35)$$

It is when $q^2 \xi^2 \ll 1$ that C_P assumes its hydrodynamic value and $\Gamma/q^2 = \Lambda/\rho C_P$.

The open symbols in Figs. 4.10 and 4.11 represent the point by point experimental deduction of the critical part of the thermal diffusivity, D_C , in the hydrodynamic region obtained using Eq. (4.34). We have seen that the mode-mode coupling theory predicts that $D_C = k_B T / 6\pi\eta^* \xi$. The open symbols thus represent an experimental deduction of $k_B T / 6\pi\eta^* \xi$. Since, as we see from Figs. 4.7 - 4.9, the quantity $\Lambda_B/\rho C_P$ is a very substantial

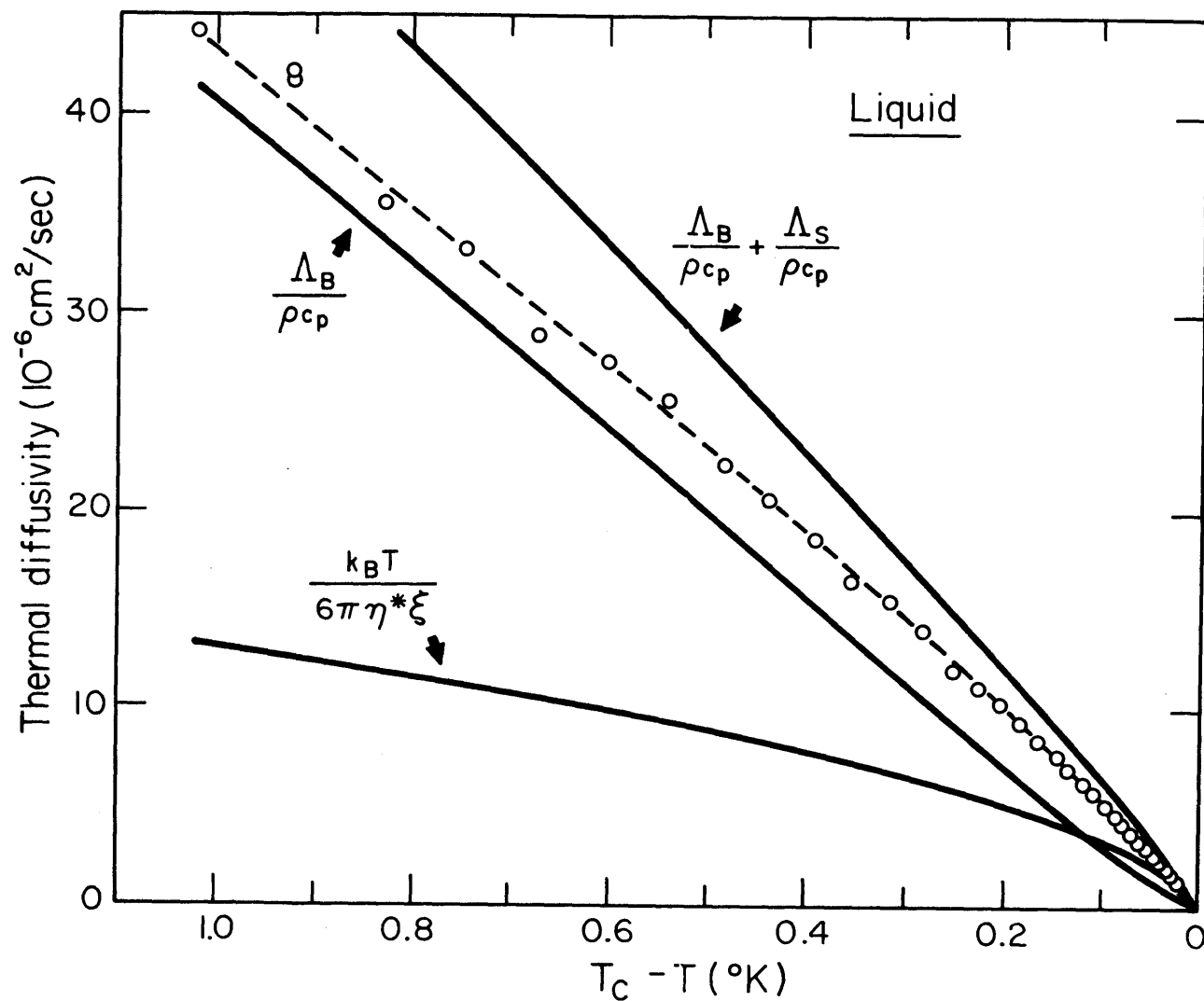


Fig. 4.8 Experimental values (circles) for the Thermal Diffusivity along the Liquid side of the Coexistence Curve. Lower curve represents $k_B T / 6\pi\eta^*\xi$ for the estimated values of η^* and ξ discussed in the text. Upper curve is the predicted total Thermal Diffusivity

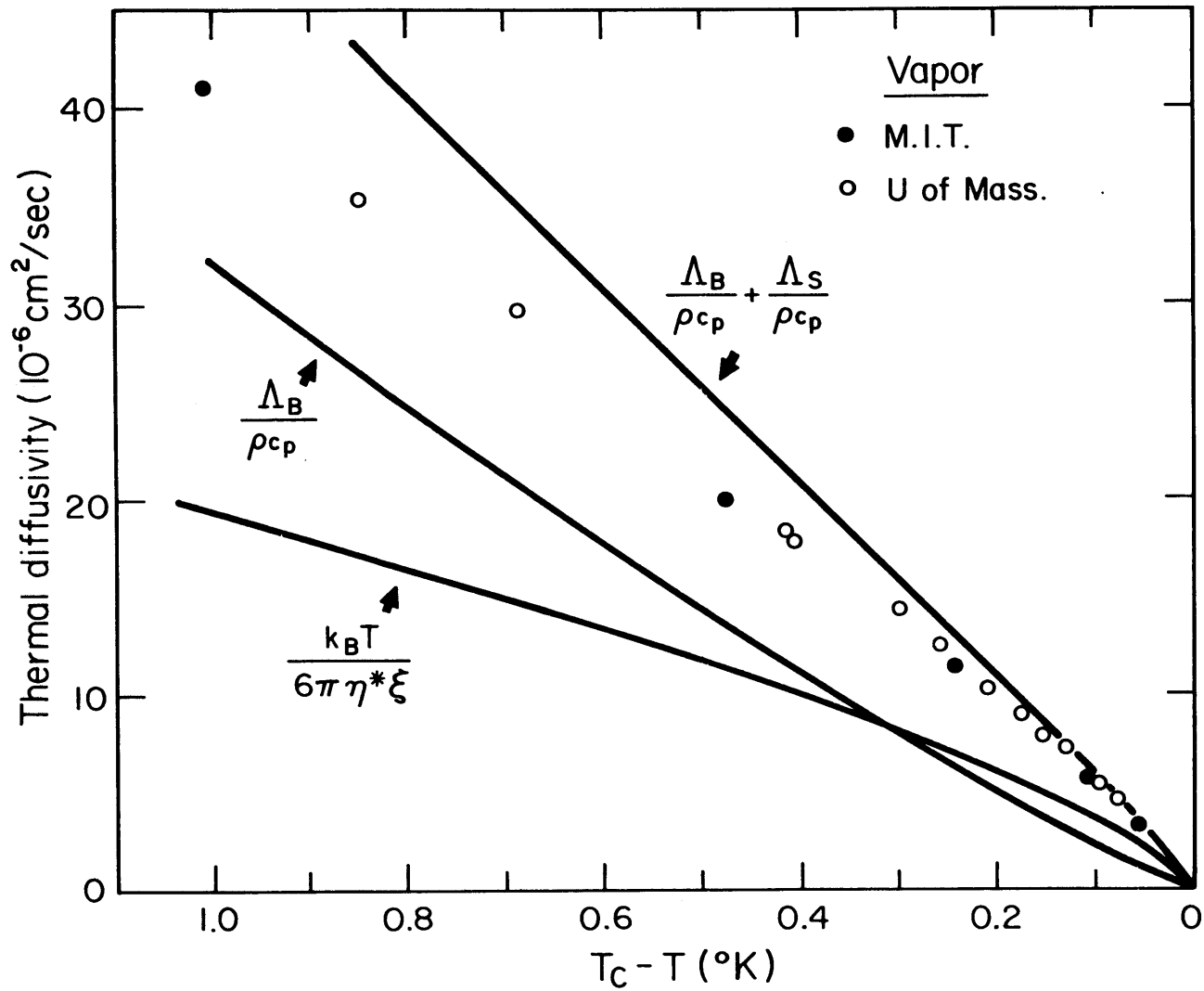


Fig. 4.9 Same as Fig. 4.8, showing Vapor Side

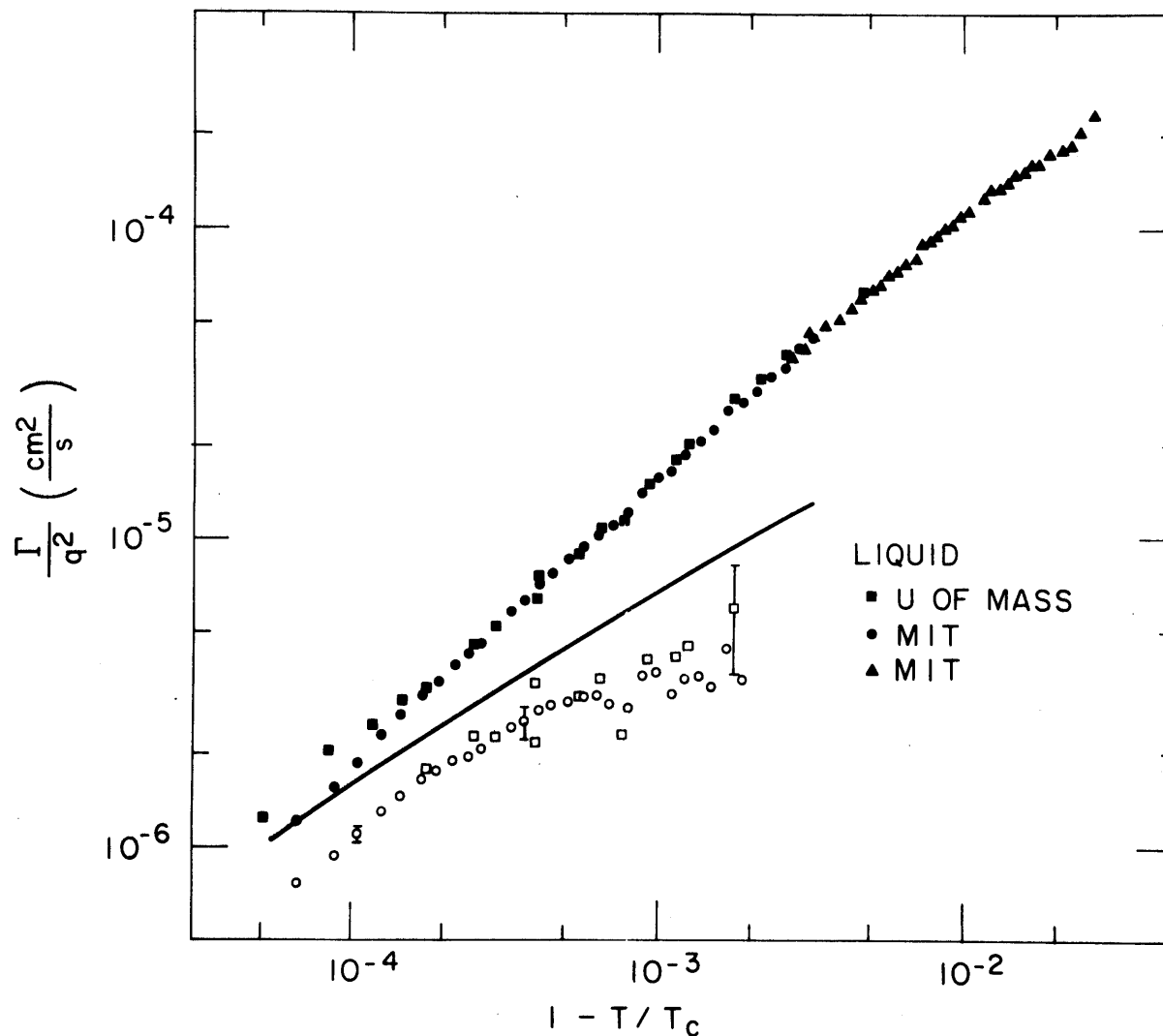


Fig. 4.10 Solid symbols: data for the Thermal Diffusivity. Open symbols: deduced values of the Critical Part of the Thermal Diffusivity. Solid curve represents $k_B T / 6\pi\eta^*\xi$ using estimated values of η^* and ξ discussed in the text

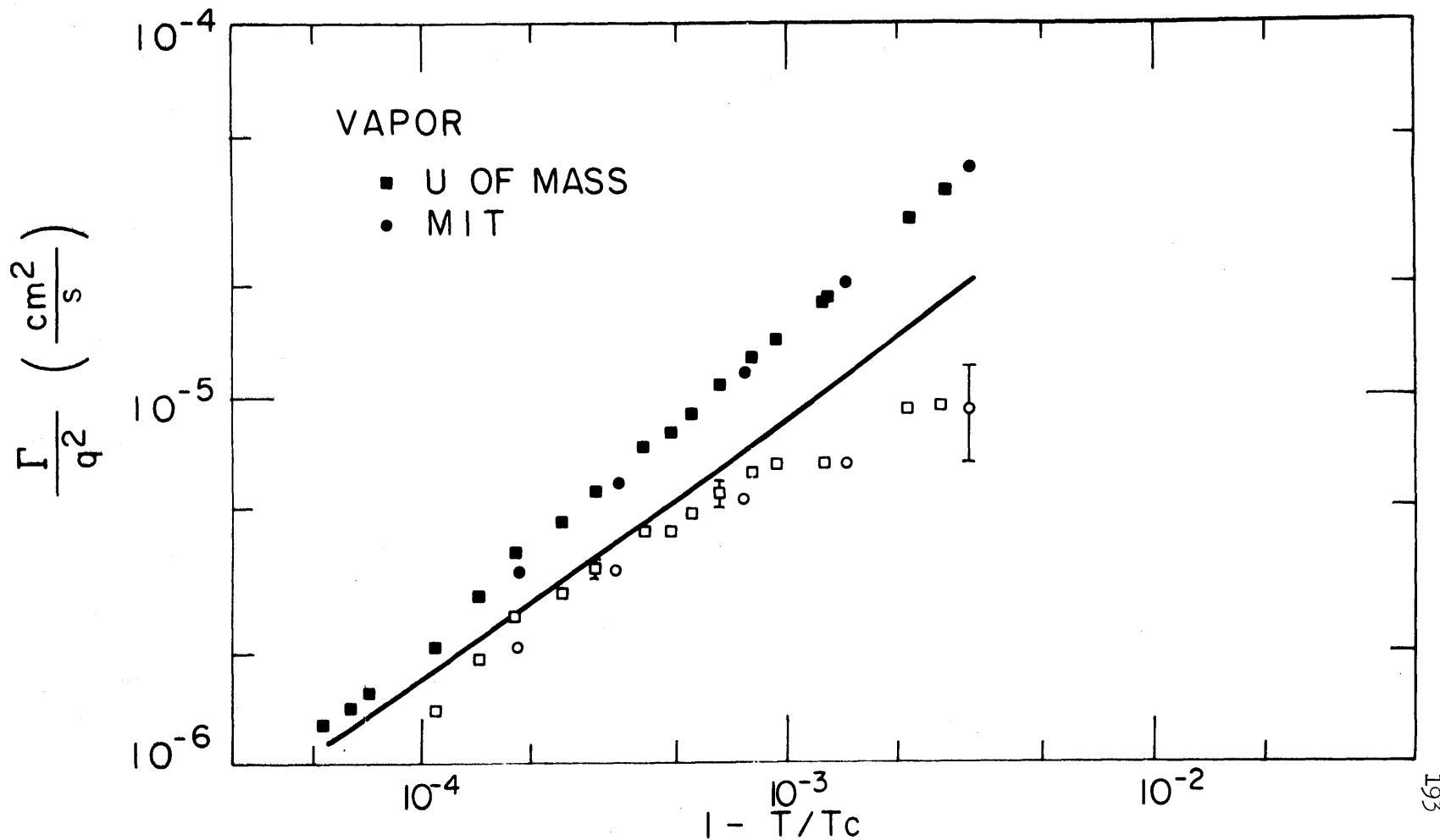


Fig. 4.11 Solid symbols: data for the Thermal Diffusivity. Open symbols: deduced values of the Critical Part of the Thermal Diffusivity. Solid curve represents $k T / 6\pi\eta^*\xi$ using estimated values of η^* and ξ discussed in the text

part of the total thermal diffusivity, errors in estimating this background term can result in substantial uncertainties (indicated by the vertical bars in Figs. 4.10 and 4.11) in the deduced values of $k_B T / 6\pi\eta^* \xi$.

To determine the validity of the mode-mode coupling theory prediction we must independently calculate $k_B T / 6\pi\eta^* \xi$ and compare the result with our experimentally deduced values. In the absence of direct measurements of the correlation range, ξ , along the coexistence curve, we may obtain an estimate for ξ in the following way. We recall from Section IV.C.2. that it was found that $(\frac{\partial \rho}{\partial \mu})_{T > T_C} / (\frac{\partial \rho}{\partial \mu})_{T < T_C} = 4.33 \pm 0.3$. We may also recall (Eq. (2.45)) that according to the Ornstein-Zernike theory the isothermal compressibility, κ_T , is related to the correlation range, ξ , by

$$\frac{\xi^2}{R^2} = \frac{\kappa_T}{\kappa_I} \quad (4.36)$$

where κ_I is the isothermal compressibility of an ideal gas at density ρ and temperature T , and R is the direct correlation range. We thus have the approximate prediction that

$$\begin{aligned} \xi_{T > T_C} / \xi_{T < T_C} &\cong \left[\left(\frac{\partial \rho}{\partial \mu} \right)_{T > T_C} / \left(\frac{\partial \rho}{\partial \mu} \right)_{T < T_C} \right]^{1/2} \\ &\cong (4.33 \pm 0.3)^{1/2} . \end{aligned} \quad (4.37)$$

We used this formula and the measurements of ξ along the critical isochore of SF_6 by Puglielli and Ford,⁽⁴⁾ who found $\xi_{T > T_C} = (1.5 \pm 0.23)(T/T_C - 1)^{-0.67 \pm 0.07} \text{ \AA}$, to determine ξ along the coexistence curve. We may note that this procedure of estimating $\xi_{T < T_C}$ has been checked by direct measurements in xenon and is verified to within the precision of the measurements which is $\pm 10\%$.⁽³⁰⁾

Experimental data for η^* as a function of density and temperature along each side of the coexistence curve is also unavailable. We have seen that Kawasaki and Lo⁽²⁴⁾ indicate that in the hydrodynamic region η^* differs from the macroscopically measured shear viscosity, η , by 5.5%. Therefore we estimated η^* by using the Lennert and Thodos⁽³¹⁾ semi-empirical formula for $\eta(\rho, T)$ which has been verified for a number of liquids and dense gases. Using parameters appropriate for SF₆, the Lennert and Thodos formula predicts $\eta(\rho, T) - \eta(0, T) = 1.13 \times 10^{-4} \left(\frac{\partial P}{\partial T}\right)_V^{1.075} \mu\text{P}$. We used the measurements of Kestin⁽³²⁾ who found $\eta(\rho \rightarrow 0, T = 25^\circ\text{C}) = 152.5 \mu\text{P}$ and $\Delta\eta/\Delta T = 0.45 \mu\text{P}/^\circ\text{C}$ to determine $\eta(0, T)$, and the expression for $\left(\frac{\partial P}{\partial T}\right)_V$ given in Eq. (4.32) in order to obtain $\eta(\rho, T)$ along the liquid and vapor sides of the coexistence curve. We find that as $T_C - T$ changes from 0.020°K to 1.00°K , η_{vapor} decreases from 400 to 350 μP and η_{liquid} increases from 419 to 514 μP .

We may note that the Lennert and Thodos formula predicts that $\eta(\rho = \rho_C, T = T_C) = 408 \mu\text{P}$. We recall from Section IV.B.5. that Wu and Webb⁽²³⁾ estimate from their measurements of the average viscosity of the liquid and vapor phases in SF₆ that $\eta(\rho_C, T_C) = 425 \pm 15 \mu\text{P}$. The Lennert and Thodos prediction is thus in excellent agreement with their estimate. We further recall that if we use $\eta = 400 \mu\text{P}$ along the critical isochore then the deduced values of D_C presented in Section IV.B.4. are in excellent agreement with the predictions of the mode-mode coupling theory and was discussed in Section IV.3.5.

When applied to xenon the Lennert and Thodos formula agrees well with measurements of the effective kinematic viscosity,

$\bar{\nu} = (\eta_{\text{vapor}} + \eta_{\text{liquid}})/(\rho_{\text{vapor}} + \rho_{\text{liquid}})$, in xenon by light scattering from surface waves.⁽³³⁾ The formula disagrees, however, with the recent measurements of Strumpf and Pings⁽³⁴⁾ who found a weak logarithmic divergence in the shear viscosity in xenon along the coexistence curve. They obtained viscosities that were greater in magnitude by about 20% in the liquid phase and by about 10% in the vapor phase than those predicted by Lennert and Thodos.

Recently Moeller and Carome⁽³⁵⁾ have also carried out studies which determine the viscosity of SF₆ near the critical point. Their results indicate a strong divergence in the shear viscosity and hence are markedly different from the results obtained in other experiments and from the predicted viscosities of the Lennert and Thodos formula which were used in our calculations.

The solid lines in Figs. 4.10 and 4.11 represent our calculation of $k_B T / 6\pi\eta^* \xi$ for the liquid and for the vapor using the means discussed above for estimating ξ and η^* . Linear plots of $k_B T / 6\pi\eta^* \xi$ for the liquid and for the vapor are shown in Figs. 4.8 and 4.9. In Figs. 4.8 and 4.9 are also shown plots of the background thermal diffusivity, $\Lambda_B / \rho C_P$. The upper solid curves in Figs. 4.8 and 4.9 represent the predicted total thermal diffusivities:

$$\frac{\Lambda}{\rho C_P} = \frac{\Lambda_B}{\rho C_P} + \frac{\Lambda_S}{\rho C_P} = \frac{\Lambda_B}{\rho C_P} + \frac{k_B T}{6\pi\eta^* \xi} \cdot \frac{C_{P_S}}{C_P} \quad (4.38)$$

From Figs. 4.8 and 4.9 we see that the comparison between the predicted total thermal diffusivities and the experimentally measured thermal diffusivities is not good. Similarly, from Figs. 4.10 and 4.11 we see that

the comparison between the solid lines, $k_B T / 6\pi\eta^* \xi$, and the experimentally deduced values of the critical part of the thermal diffusivity is also not good. In considering these differences one must keep in mind that neither ξ nor η^* have been directly measured and that our estimates for these quantities involve substantial uncertainties. Larger values of ξ or η^* would bring the mode-mode coupling theory prediction into better agreement with the experimental results.

Since the mode-mode coupling theory is in excellent agreement with the results of the experiments carried out along the critical isochore of SF_6 over the temperature range where independent data exist allowing proper analysis, we feel that direct independent measurements of the correlation range, ξ , and the viscosity, η , along the SF_6 coexistence curve will provide the information for the proper analysis of the results of this study and, hopefully, will lead to agreement between our results and the predictions of the mode-mode coupling theory.

References For Chapter IV

1. G. T. Feke, G. A. Hawkins, J. B. Lastovka, and G. B. Benedek, *Phys. Rev. Lett.* 27, 1780 (1971).
2. G. T. Feke, J. B. Lastovka, and G. B. Benedek, and K. H. Langley and P. B. Elterman, *Optics Communications* 7, 13 (1973).
3. K. E. MacCormack and W. G. Schneider, *Can. J. Chem.* 29, 699 (1951).
4. V. G. Puglielli and N. C. Ford, Jr., *Phys. Rev. Lett.* 25, 143 (1970).
5. J. H. Lunacek and D. S. Cannell, *Phys. Rev. Lett.* 27, 841 (1971).
6. I. W. Smith, M. Giglio, and G. B. Benedek, *Phys. Rev. Lett.* 27, 1556 (1971).
7. G. B. Benedek, J. B. Lastovka, M. Giglio, and D. Cannell, in Critical Phenomena, edited by R. E. Mills and R. I. Jaffee (McGraw-Hill, New York, 1971).
8. P. Braun, D. Hammer, W. Tscharnuter, and P. Weinzierl, *Phys. Lett.* 32A, 390 (1970).
9. T. K. Lim and H. L. Swinney and K. H. Langley and T. A. Kachnowski, *Phys. Rev. Lett.* 27, 1776 (1971).
10. L. P. Kadanoff and J. Swift, *Phys. Rev.* 166, 89 (1968).
11. K. Kawasaki, *Ann. Phys.* 61, 1 (1970).
12. K. Kawasaki, *Phys. Rev. A* 1, 1750 (1970).
13. J. V. Sengers and P. H. Keyes, *Phys. Rev. Lett.* 26, 70 (1971).
14. B. LeNeindre, P. Bury, R. Tufeu, P. Johannin, and B. Vodar, in Proceedings of the Ninth Thermal Conductivity Conference, edited by N. R. Shanks (U. S. A. E. C., Division of Technical Information Extension, Oak Ridge, Tenn., 1970).
15. R. Tufeu, B. LeNeindre and P. Bury, *Compt. Rend. Acad. Sci. (Paris)* B273, 113 (1971).
16. J. Lis and P. O. Kellard, *Brit. J. Appl. Phys.* 16, 1099 (1965).
17. W. Tauscher, *Kältetechn. Klim.* 20, 287 (1968).
18. W. H. Mears, E. Rosenthal, and J. V. Sinka, *J. Phys. Chem.* 73, 2254 (1969).

19. J. Otto and W. Thomas, Z. Phys. Chem. 23, 84 (1960).
20. S. A. Ulybin and E. P. Zherdev, Soviet Physics-Doklady 15, 306 (1970).
21. K. Fritsch and E. F. Carome, NASA Report No. CR-1670, 1970 (unpublished).
22. J. V. Sengers, Ber. Bunsenges. Physik. Chem. 76, 234 (1972).
23. E. S. Wu and W. W. Webb, Phys. Rev. A 8, 2077 (1973).
24. K. Kawasaki and S. Lo, Phys. Rev. Lett. 29, 48 (1972).
25. H. L. Swinney, D. L. Henry and H. Z. Cummins, J. Phys. (Paris) 33 Suppl. C1, 81 (1972).
26. J. Zollweg, G. Hawkins, I. W. Smith, M. Giglio and G. B. Benedek, J. Phys. (Paris) 33 Suppl. C1, 135 (1972).
27. P. Schofield, J. D. Litster, and J. T. Ho, Phys. Rev. Lett. 23, 1098 (1969).
28. E. S. Wu and W. W. Webb, Phys. Rev. A 8, 2065 (1973).
29. W. G. Schneider, Can. J. Chem. 29, 243 (1951); J. Chem. Phys. 20, 759 (1952).
30. I. W. Smith, private communication.
31. D. A. Lennert and G. Thodos, Am. Inst. Chem. Eng. J. 11, 155 (1965).
32. J. Kestin, private communication.
33. J. Zollweg, G. Hawkins, and G. B. Benedek, Phys. Rev. Lett. 27, 1182 (1971).
34. H. J. Strumpf and C. J. Pings, to be published.
35. R. P. Moeller and E. F. Carome, to be published.

Appendix A

3 PARAMETER SINGLE LORENTZIAN FITTING PROGRAM

```

0001      IMPLICIT REAL*8(A-H,O-Z)
0002      DIMENSION QZ(400),T(400),D(200),VALUE(200),ANORM(200),DATA(200),
          CFREQ(20)
0003      1000 FORMAT(I10,2F10.1)
0004      1010 FORMAT(6F11.1)
0005      1020 FORMAT(6F11.0)
0006      91  FORMAT(I10,F10.1)
0007      102  FORMAT(1H1,5X,12H HALF WIDTH ,15X,8H HEIGHT ,15X,12H SHOT LEVEL ,
          C15X,12H DERIVATIVE ,15X,10H FUNCTION //)
0008      103  FORMAT(1H ,7X,F8.2,16X,E10.4,15X,E10.4,14X,E15.8,10X,E15.8)
0009      104  FORMAT(1H0.43X,3H + ,F8.2)
0010      105  FORMAT(1H ,20X,13H HALF WIDTH= ,F8.2)
0011      106  FORMAT(1H ,43X,3H - ,F8.2)
0012      107  FORMAT(1H1,15X,11H FREQUENCY ,15X,6H DATA ,15X,5H FIT ,15X,
          C10H RESIDUAL //)
0013      108  FORMAT(1H ,15X,F11.0,13X,F11.2,9X,F11.2,12X,F11.2)
0014      READ(5,1000) MN,QQ,AQ
0015      READ(5,1010) (QZ(J),J=1,MN)
0016      READ(5,1020) (T(J),J=1,MN)
0017      DO 9915 J=1,MN
0018      QZ(J)=(QQ+AQ)/(QZ(J)+AQ)
0019      9915 CONTINUE
0020      READ(5,91) N,A
0021      READ(5,1010) (D(I),I=1,N)
0022      READ(5,1020) (VALUE(I),I=1,N)
0023      IF(T(1) .GT. VALUE(1) .OR. T(MN) .LT. VALUE(N)) GO TO 325
0024      DO 9990 I=1,N
0025      DO 9960 J=1,MN
0026      IF(T(J) ,GT. VALUE(I)) GO TO 9970
0027      9960 CONTINUE
0028      9970 ANORM(I)=(QZ(J-1)*(T(J)-VALUE(I))+QZ(J)*(VALUE(I)-T(J-1)))/
          C(T(J)-T(J-1))
0029      DATA(I)=(D(I)+A)*ANORM(I)

```



```

0030      9990 CONTINUE
0031      HAFHT=(DATA(1)-DATA(N))/2.0+DATA(N)
0032      DO 40 I=1,N
0033      IF(DATA(I) .LT. HAFHT) GO TO 50
0034      40 CONTINUE
0035      50 FFREQ=VALUE(I)
0036      FREQ1=FFREQ-0.1*FFREQ
0037      FREQ2=FFREQ+0.1*FFREQ
0038      TAU1=1.0/FREQ1
0039      TAU2=1.0/FREQ2
0040      WRITE(6,102)
0041      J=1
0042      FREQ(1)=0.0
0043      D1=0.0
0044      D2=0.0
0045      D3=0.0
0046      S0=0.0
0047      S1=0.0
0048      S2=0.0
0049      DSQ=0.0
0050      DO 20 I=1,N
0051      BORC=1.0/(1.0+(VALUE(I)*TAU1)**2)
0052      D1=D1+BORC
0053      D2=D2+BORC**2
0054      D3=D3+BORC**3
0055      S0=S0+DATA(I)
0056      S1=S1+DATA(I)*BORC
0057      S2=S2+DATA(I)*(BORC**2)
0058      DSQ=DSQ+DATA(I)**2
0059      20 CONTINUE
0060      EN=N
0061      ACDEF=(EN*S1-D1*S0)/(EN*D2-D1**2)
0062      BCDEF=(D2*S0-D1*S1)/(EN*D2-D1**2)
0063      DFDTC1=(ACDEF*(S1-S2)-(ACDEF**2)*(D2-D3)-ACDEF*BCDEF*(D1-D2))/
CTAU1
0064      FUNC1=DSQ-ACDEF*S1-BCDEF*S0
0065      WRITE(6,103) FREQ1,ACDEF,BCDEF,DFDTC1,FUNC1

```

```

0066      D1=0.0
0067      D2=0.0
0068      D3=0.0
0069      S0=0.0
0070      S1=0.0
0071      S2=0.0
0072      DSQ=0.0
0073      DO 10 I=1,N
0074      BORC=1.0/(1.0+(VALUE(I)*TAU2)**2)
0075      D1=D1+BORC
0076      D2=D2+BORC**2
0077      D3=D3+BORC**3
0078      S0=S0+DATA(I)
0079      S1=S1+DATA(I)*BORC
0080      S2=S2+DATA(I)*(BORC**2)
0081      DSQ=DSQ+DATA(I)**2
0082  10    CONTINUE
0083      EN=N
0084      ACDEF=(EN*S1-D1*S0)/(EN*D2-D1**2)
0085      BCDEF=(D2*S0-D1*S1)/(EN*D2-D1**2)
0086      DFDTC2=(ACDEF*(S1-S2)-(ACDEF**2)*(D2-D3)-ACDEF*BCDEF*(D1-D2))/
CTAU2
0087      FUNC2=DSQ-ACDEF*S0-BCDEF*S0
0088      WRITE(6,103) FREQ2,ACDEF,BCDEF,DFDTC2,FUNC2
0089  11    SLOPE=(DFDTC1-DFDTC2)/(TAU1-TAU2)
0090      YCEPT=DFDTC1-SLOPE*TAU1
0091      TAUQ=YCEPT/SLOPE
0092      D1=0.0
0093      D2=0.0
0094      D3=0.0
0095      S0=0.0
0096      S1=0.0
0097      S2=0.0
0098      DSQ=0.0
0099      DO 30 I=1,N
0100      BORC=1.0/(1.0+(VALUE(I)*TAU0)**2)
0101      D1=D1+BORC
0102      D2=D2+BORC**2

```

```

0103      D3=D3+BORC**3
0104      SO=SO+DATA(I)
0105      S1=S1+DATA(I)*BORC
0106      S2=S2+DATA(I)*(BORC**2)
0107      DSQ=DSQ+DATA(I)**2
0108      30  CONTINUE
0109      EN=N
0110      ACDEFO=(EN*S1-D1*SO)/(EN*D2-D1**2)
0111      BCDEFO=(D2*SO-D1*S1)/(EN*D2-D1**2)
0112      DFDTCO=(ACDEFO*(S1-S2)-(ACDEFO**2)*(D2-D3)-ACDEFO*BCDEFO*(D1-D2))/
CTAUO
0113      FUNCO=DSQ-ACDEFO*S1-BCDEFO*SO
0114      FREQO=1.0/TAUO
0115      WRITE(6,103) FREQO,ACDEFO,BCDEFO,DFDTCO,FUNCO
0116      BLATZ1=DABS(DFDTC1-DFDTCO)
0117      BLATZ=DABS(DFDTC2-DFDTCO)
0118      IF(BLATZ2 .GT. BLATZ1) GO TO 280
0119      TAU1=TAUO
0120      DFDTC1=DFDTCO
0121      GO TO 97
0122      280 TAU2=TAUO
0123      DFDTC2=DFDTCO
0124      97  J=J+1
0125      IF(J .GT. 20) GO TO 325
0126      FREQ(J)=FREQO
0127      RATIO=(DABS(FREQ(J)-FREQ(J-1)))/(FREQ(J)+FREQ(J-1))
0128      IF(RATIO .LT. 0.00001) GO TO 324
0129      GO TO 11
0130      324 CONTINUE
0131      A1=((FUNC1-FUNCO)*FREQO*FREQ1)/((FREQ1-FREQO)**2)
0132      A2=((FUNC2-FUNCO)*FREQO*FREQ2)/((FREQ2-FREQO)**2)
0133      AV=(A1+A2)/2.0
0134      B=-(2.0*AV*FREQO+FREQO*FUNCO)
0135      C=AV*(FREQO**2)
0136      FHI=(-B+((B**2)-4.0*AV*C)**0.51)/(2.0*AV)
0137      FLO=(-B-((B**2)-4.0*AV*C)**0.5)/(2.0*AV)

```

```
0138      PORK=FHI-FREQO
0139      DORK=FREQO-FLO
0140      WRITE(6,104) PORK
0141      WRITE(6,105) FREQO
0142      WRITE(6,106) DORK
0143      WRITE(6,107)
0144      DO 60 I=1,N
0145      SPEC=(ACDEFO*(FREQO**2)/VALUE(I)**2+FREQO**2)+BCDEFO
0146      RESID=DATA(I)-SPEC
0147      WRITE(6,108) VALUE(I),DATA(I),SPEC,RESID
0148      60  CONTINUE
0149      325 CONTINUE
0150      CALL EXIT
0151      END
```

Appendix B

3 PARAMETER SINGLE EXPONENTIAL DECAY FITTING PROGRAM

```

0001     DIMENSION Y(256),G(3),DI(256),ERR(256)
0002     READ (5,1) N,TC
0003     1   FORMAT(I10,F10.2)
0004     READ(5,20) (Y(I),I=1,N)
0005     20  FORMAT(6F11.1)
0006         E=10.
0007         DO 2 J=1,3
0008             M=5*J
0009             K=M+30
0010             L=M+60
0011     2   G(J)=(Y(K)*Y(K)-Y(M)*Y(L))/(Y(M)+Y(L)-2*Y(K))
0012         C=-(G(1)+G(2)+G(3))/3.
0013         EN=N
0014         B=(ALOG(Y(N)-C)-ALOG(Y(1)-C))/(EN-1.0)
0015     102  FORMAT(1H1,15X,6H DATA ,15X,5H FIT , 15X,10H RESIDUAL //)
0016     8   CONTINUE
0017         IN=0
0018         IUT=0
0019         IF(.1-ABS(E)) 3,100,100
0020     3   UB=0.
0021         UA=0.
0022         UC=0.
0023         UN=0.
0024         RLA=0.
0025         DO 5 J=1,N
0026             UB=EXP(J*B)+UB
0027             UA=Y(J)*EXP(J*B)+ UA
0028             UC=UC+Y(J)
0029             UN=Y(J)*Y(J)+UN
0030     5   RLA=EXP(2.*J*B)+RLA
0031         EN=N
0032         A=(EN*UA-UC*UB)/(EN*RLA-UB*UB)
0033         C=(UC-A*UB)/EN
0034         S=SQRT(UN-C*UC-A*UA)/EN
0035         IF(IN.EQ.1.OR.IUT.EQ.1) GO TO 15

```

```

0036      SQ=S
0037      BC=B
0038      AR=A
0039      CR=C
0040      15      CONTINUE
0041      IF (IN.EQ.1) GO TO 6
0042      B=(1+E/100)*BO
0043      IN=1
0044      GO TO 3
0045      6      IF (IUT.EQ.1) GO TO 7
0046      SU=S
0047      B=(1-E/100)*BO
0048      IUT*1
0049      GO TO 3
0050      7      SL=S
0051      UM=(SU-SL)/(2.*(SU+SL-2.*SO))
0052      B=BO*(1.-UM*E/100. )
0053      E=ABS(UM*E)
0054      IF(E.GE.100) GO TO 10
0055      GO TO 8
0056      100     WRITE(6,102)
0057      DO 10 J=1,N
0058      FU=CR+AR*EXP(B*J)
0059      DI(J)=Y(J)-FU
0060      ERR(J)=DI(J)**2
0061      WRITE(6,11) Y(J),FU,DI(J)
0062      11     FORMAT(1H ,15X,F6,2,15X,F6,2,17X,F6.2)
0063      10     CONTINUE
0064      SUM=0.0
0065      DO 40 J=1,N
0066      SUM=ERR(J)+SUM
0067      40     CONTINUE
0068      EN=N
0069      RMS=(SUM/EN)**0.5
0070      WRITE(6,106) RMS
0071      106     FORMAT(1H0,20X,12H RMS ERROR= ,F10.4)
0072      D=-TC/BO
0073      WRITE(6,105) D
0074      105     FORMAT(1H0,20X,13H DECAY TIME = ,F10.2,2X,14H MICROSECONDS //)
0075      CALL EXIT
0076      END

```

Biographical Note

Gilbert Thomas Feke was born in Cleveland, Ohio on February 12, 1945. He received his primary and secondary school education at St. Gregory the Great parochial school and St. Joseph High School. From 1963 to 1967 he attended John Carroll University in University Heights, Ohio, majoring in physics. He was graduated summa cum laude in 1967 with the degree of Bachelor of Science. He received the degree of Master of Science from John Carroll University in 1969. He and Carol Harriet Schildkret were married on October 7, 1972. Their son Gilbert David was born on November 4, 1973.

Acknowledgments

My most sincere thanks go to Professor George Benedek, my advisor throughout my years at M. I. T., who made it possible for me to come to M. I. T., who provided the financial support that allowed me to remain at M. I. T., and who, most importantly, provided the personal support and encouragement which allowed me to bring my work at M. I. T. to a fruitful completion.

My thanks go also to my many associates at M. I. T. to whom I am indebted for their friendship and for their help in my work. I especially wish to thank Dr. Joseph Lastovka, Gilbert Hawkins and Irl Smith.

I am grateful to Mrs. Louise Capra for her expert typing of the thesis manuscript.

Finally, I acknowledge my wife, Carol. She has provided loving encouragement throughout the writing of this thesis. She has taught me the meaning of patience. She is the mother of our new son.